Synthesis and Characterisation of a Novel Di-carbazole-dihtienophenazine Dye Sensitiser for the Application in Dye Sensitised Solar Cells

Master Thesis

Masterarbeit

A report submitted in fulfillment of the requirements of the Degree of Master of Science, Graz University of Technology.

zur Erlangung des akademischen Grades eines Diplom-Ingenieurs der Studienrichtung Technische Chemie, Technische Universität Graz

Manuel Wieser

Dezember 2011

Supervisor: Assoc. Prof. Dr. Gregor Trimmel

ICTM - Institute for Chemistry and Technology of Materials

Graz University of Technology (TUG)

Supervisor: Dr. Shih-Chun (Lawrence) Lo

COPE - Centre for Organic Photonics & Electronics

The Universtiy of Queensland (UQ)

Abstract

With the projected rise of the global energy consumption to 30 TW (~946 EJ) by 2050 and the present ecological situation of CO_2 related climate change, the increase in demand has to be compensated by transition to renewable and CO_2-free energy generation. In this context photovoltaic energy generation presents itself as the most promising and technically most feasible way of clean and reneable energy production.

The aim of this project is to prepare a novel metal-free dye, 2,5-bis(3,6-bis(4-(2-ethylhexyloxy)phenyl)-9H-carbazol-9-yl)dithieno[2,3-a:3',2'-c]phenazine-9-carboxylic acid and investigate its potential use in dye sensitised solar cell applications. The dye structure was based on a D-π-A motif, where carbazole units are incorporated for electron donation (D), a benzodithiophene-phenazine compound is used as the π-conjugated system and the electron accepting moiety (A) is represented by a carboxylic acid. The key reaction step in the synthesis, was a Buchwald-Hartwig crosscoupling reaction to build the electron donors to the π-conjugated bridge, involved, which was proved to be the most challenging step. Further, it was demonstrated that the dye and all of its intermediates, with the exception of compounds related to the aforementioned coupling reaction, can be synthesised in good yields.

Investigation of the photophysical properties of the target compound revealed a strong absorption peak in the visible region of the solar spectrum which can be attributed to intra molecular charge transfer (ICT) processes. Electrochemistry using cyclic voltammetry confirmed HOMO and LUMO energy levels that are well positioned with respect to those of TiO_2 photoanode and the redox mediator. Uptake of the dye onto TiO_2 substrates showed that sufficient amounts of the dye can be adsorbed onto the mesoporose semiconducting metal oxide which in turn allowed for efficient light harvesting. Preliminary, photovoltaic devices were constructed using the synthesised dye as the sensitising molecule and were characterised in relation to photovoltaic parameters, yielding promising results.

Future work can focus on optimising parameters for cell assembly in order to achieve optimal device performance as well as the modification of the synthesised dye system with respect to improvement of its molar extinction coefficient and the enhancement of its electron withdrawing abilities for a further red-shifted ICT band.

Kurzfassung

Mit dem geschätztem Anstieg des globalen Energieverbrauchs auf 30 TW (~946 EJ) bis 2050 und der derzeitigen ökologischen Situation des CO_2 bedingtem Klimawandels, muss die steigende Nachfrage durch einen Übergang zu sowohl erneuerbaren als auch CO_2-neutralen Energiequellen gedeckt werden. In diesem Zusammenhang stellt die Energiegewinnung durch photovoltaische Systeme die vielversprechendste als auch technisch relevanteste Möglichkeit dar.

Diese Arbeit befasst sich mit der Herstellung des neuartigen Metall-freien Farbstoffs *2,5-Bis(3,6-bis(4-(2-ethylhexyloxy)phenyl)-9H-carbazole-9-yl)dithieno[2,3-a:3',2'-c]phenazine-9-carboxylic acid* und dessen Anwendung in Farbstoff-sensibilisierten Solarzellen. Die Struktur basiert auf einem D-D-π-A Konzept, welches Carbazol als Elektronendonor (D), eine Benzodithiophen-phenazin Verbindung als π-konjugiertes System und eine Karbonsäure Funktionalität als Elektronenakzeptor (A) verwendet. Die Verbindung des Elektronendonors mit dem π-konjugiertem System mittels Buchwald-Hartwig-Kopplung stellte hierbei den synthetischen Schlüsselschritt dar und erwies sich als schwer kontrollierbar. Zusätzlich wurde im Rahmen dieser Arbeit gezeigt, dass der Farbstoff so wie alle Intermediate, mit Ausnahme von Produkten der zuvor erwähnten Kopplungsreaktion, in hohen Ausbeuten synthetisiert werden können.

Untersuchung der fotophysikalischen Eigenschaften der Zielverbindung zeigte eine starke Absorptionsbande im sichtbaren Bereich des Sonnenspektrums, welche auf einen intramolekularen Ladungstransfer (ICT) zurückzuführen ist. Elektrochemische Untersuchungen bestätigten die vorteilhafte Lage von HOMO und LUMO Energiezuständen im Verhältnis zu TiO_2 Photoanode und Redox-Vermittler. Durch Experimente zur Adsoprtionskinetik des Farbstoffes auf TiO_2 Substrate konnte eine ausreichende Menge an adsorbierte Zielverbindung festgestellt werden um Licht effektive zu absorbieren. Der letze Schritt beinhaltete die Herstellung photovoltaischer Zellen unter Verwendung des synthetisierten Farbstoffes.

Zukünftige Arbeit sollte einerseits die Optimierung des Zellenbaus mit Hinsicht auf verbesserte Leistung und andererseits eine Modifizierung der Struktur des Farbstoffmoleküls, mit dem Ziel eines gesteigerten molaren Extinktionskoeffizienten und der Verbesserung 0der Eigenschaften des Elektronenakzeptors für eine bathochrome Verschiebung der ICT Absorptionsbande, anstreben.

Table of Contents

Acknowledgements

First and foremost I would like to thank my two supervisors Lawrence and Gregor for accepting me as a master student and making this thesis possible. Special thanks go to Lawrence for enduring numerous discussions about why certain things just would not work while always providing motivation, constructive feedback and leading me into the right direction.

I would like to show my gratitude to all my colleagues at COPE for creating a good workplace atmosphere, especially to Simon, Rob and Ross who were unfortunate enough to work in the same bay and hence occasionally had to withstand an overwhelming amount of questions. Not only were they of great help when dealing with chemical problems but also did they make time in the lab less serious and more enjoyable.

Furthermore, I would like to thank all the other people who have contributed to the content of this thesis by giving me the training and skills necessary to successfully complete this task. Without all their help it would not have been possible.

Last but not least I would like to express my gratitude to my family who always supported me.

Lastly I want to thank Rumantha for all the encouragement, enthusiasm and distraction from chemistry during this year.

Statutory Declaration

I declare that I have authored this thesis independently, that I have not used other than the declared sources / resources, and that I have explicitly marked all material which has been quoted either literally or by content from the used sources.

………………………………   ……………………………………………..

        date   (signature)

Abbreviations

°C	Degree Celsius	NHE	Normal hydrogen electrode
AcOH	Acetic Acid		
AM	Air mass	nm	Nanometers
Argon (g)	Argon gas	NMR	Nuclear magnetic resonance
a.u.	Absorption units		
CB	Conduction band	ppm	parts per million
CV	Cyclic voltammetry	P_{max}	Point of maximum power
Da	Dalton		
DCM	Dichloromethane	r.t.	Room temperature
DHB	Dihydroxybenzoic acid	re	Reduction
Dith	Dithranol	s	Seconds
DMSO	Dimethyl sulfoxide	sh	Shoulder
EJ	Exajoule	TW	Terra watt
ESI	Electro spray ionisation	THF	Tetrahydrofuran
EtOH	Ethanol	TLC	Thin layer chromtatography
$E_{1/2}$	Half-wave potential		
eV	Electron Volt	UV-Vis	Ultraviolet-Visible
Fc^+/Fc	Ferricenium/Ferrocene	V_{OC}	Open circuit voltage
g	Grams		
h	Hours	ε	Molar extinction coefficient
HOMO	Highest occupied molecular orbital		
		ε_r	Dielectric constant
$h\nu$	Light	δ	Chemical shift
ICT	Intra molecular charge transfer	λ	Wavelength
LUMO	Lowest unoccupied molecular orbital		
M+	Molecular ion		
MALDI-TOF MS	Matrix-assisted laser desorption-ionisation time-of-flight mass spectrometry		
mg	Milligrams		
MHz	Megahertz		
ml	Milliliters		
mp	Melting point		
mV	Millivolts		

Chapter 1- Introduction

Continuous energy supply has become one of the most viable economical factors determining the growth of a global sustainable society. For the last centuries mankind has relied on the generation of energy from fossil fuels such as oil, coal and gas. However, the decreasing amount of deposited non-renewable resources coupled with their negative impact on the ecosystem through combustion have rendered the search for sources of renewable clean energy an urgent task for the 21st century.[1] The mean global energy consumption was estimated to be about 15 TW (~ 473 EJ) in 2010. Optimistic but reasonable projections predict the global energy demand to reach 30 TW (~946 EJ) by 2050 under the assumption of a steady growth in population. Hence, the additional 15 TW of preferably renewable CO_2-neutral energy is needed to contribute to the stabilisation of the already existing atmospheric carbon dioxide levels by mid-century. Although photovoltaic (PV) energy costs are not yet price competitive, the abundance of solar energy, with approximately 170.000 TW (53.611.20 EJ) every year, which strikes the earth's surface makes it extremely attractive for use as a source of renewable energy. Harnessing 600 of these > 10^5 TW trough PV technology was estimated to be technically feasible.[2,3] Figure 1 shows a schematic representation of incident solar energy represented by the orange cube in relation to the annual world consumption of primary energy and the estimated amounts of remaining fossil fuel deposits.

Remaining gas deposits (7714 EJ)

Remaining petroleum deposits (3429 EJ)

Remaining coal deposits (34286 EJ)

Remaining uranium deposits (2571 EJ)

Solar energy that annually strikes the earth's surface (5361120 EJ)

Annual world-energy consumption in 2010 (473 EJ)
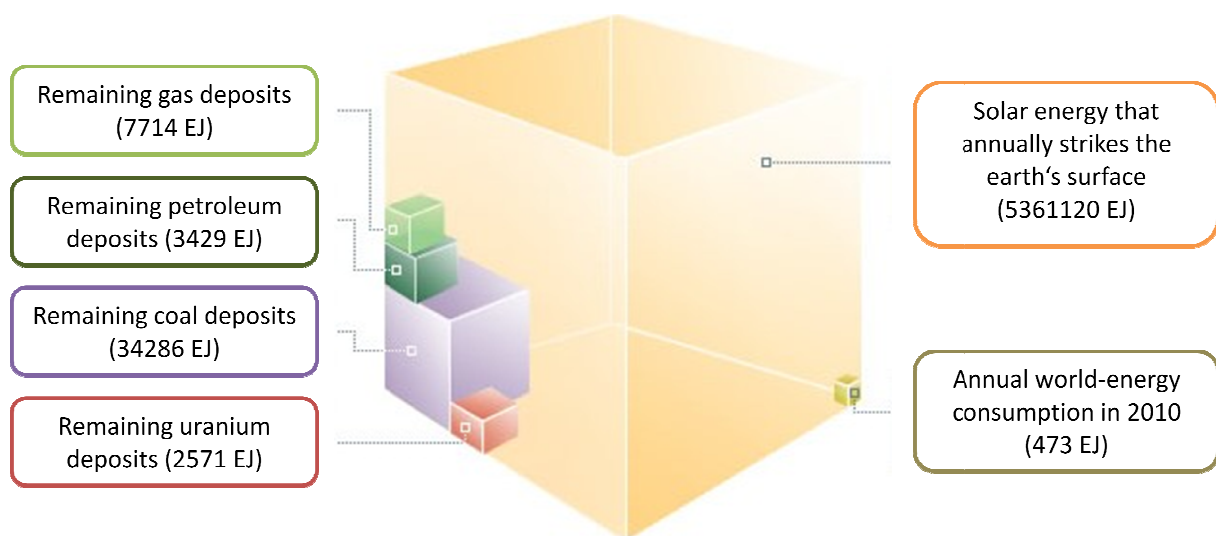
Figure 1: Energy cube (values are given in exajoule).[4,5]

However, the most realistic scenario of finding a way towards a suitable transition to renewable fuels is one in which a mix of different energy sources is applied such as photovoltaic, other renewables and nuclear power for electricity generation, hydrogen for transportation and fossil fuels for residential and industrial heating.[6] According to projections made by the International Energy Agency (IEA), renewables and nuclear power are going to account for more than 50% of the globally installed power capacity added until 2035 as illustrated in Figure 2.[7]
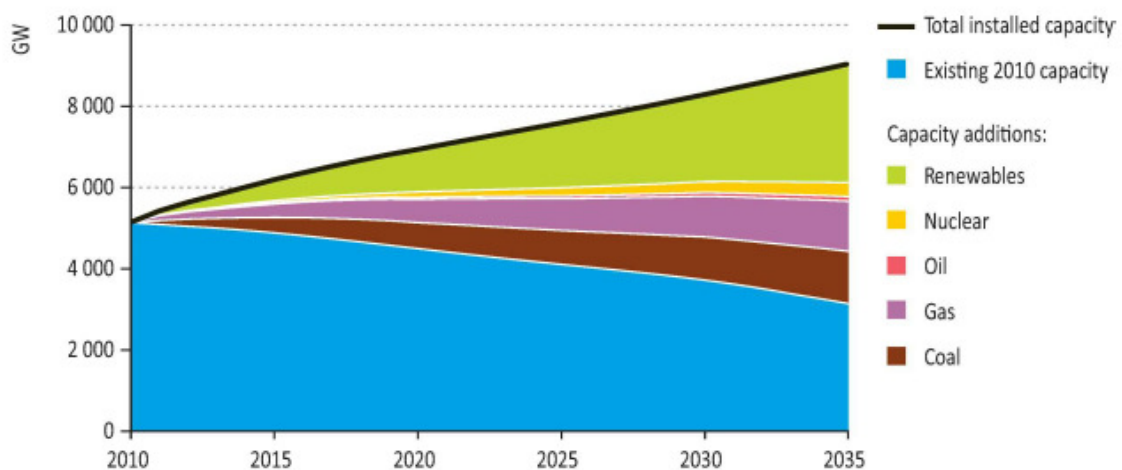
Figure 2: Additions to globally installed power capacity until 2035 (adapted from International Energy Agency 2011).[7]

While currently renewable resources account for 13% of all energy production, photovoltaics only contribute 0.04%. This value is expected to grow by 25 to 30% for the next decades on an annual basis.[8]

Light-harvesting concepts, however, have only been translated into technological advances recently.[9] The first photovoltaic device was developed at Bell Laboratories in 1954 by Chaplin and co-workers which was based on a silicon single p-n junction design, showing an overall efficiency of 6%.[10] This discovery ultimately led to the first generation photovoltaics consisting of crystalline silicon assemblies, which are highly efficient (with a maximum theoretical solar power conversion efficiency of 33%) but expensive due to an inherently costly production process.[11] Shortly thereafter, a second generation of solar cells (*e.g.* group II-VI semiconductors) emerged during the past 10 years using thin layers of semiconductor materials applied to a backing material which is referred to as thin film technology. Their most successful designs incorporate materials such as copper,

indium, gallium diselenide [Cu(InGa)Se$_2$] and cadmium telluride (CdTe) combined with amorphous, micromorphous or crystalline silicon. Due to cheap manufacturing processes and the use of minimal materials, these types of solar cells possess high cost reduction potential at high production volumes.[12] As shown in Figure 3 the current market is still dominated by polycrystalline silicon solar cells while the shares of monocrystalline and cadmium telluride devices have been steadily rising. The major reason for the success of silicon in the PV market lies in its natural abundance, low toxicity, well established processing technologies and the vast amounts of rejected material from the high-tech semiconductor industry that can be used for the production of PV devices.[8,13]
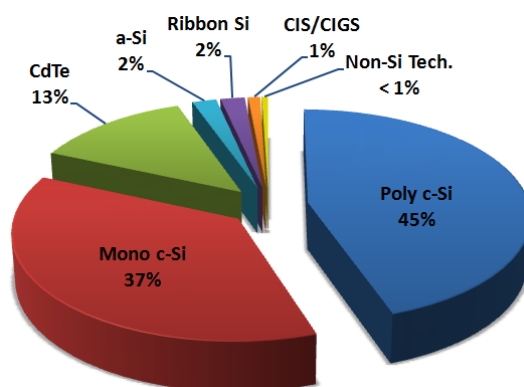
Figure 3: Market size and share held by relative technologies in 2009 (adapted from Wolden *et al.*).[2]

Over the last two decades research on organic semiconducting materials has increased rapidly leading to a whole range of new OPV device designs where at least one organic material is incorporated into the light absorbing layer. This organic based approach and those which are not related to a single p-n junction are classified as third generation devices.[11] This section comprises multijunction cells derived from group IV and III-V semiconductors,[14] hybrid solar cells (HSCs) which combine the advantages of both organic and inorganic semiconducting materials,[15] more elaborate hybrids, where inorganic quantum dots are doped into a semiconducting polymer matrix,[16] all-organic solid state donor-acceptor based heterojunction solar cells [17] and finally dye sensitised solar cells (DSSCs), which have been pioneered by Grätzel and co-workers.[18] In this context, a short overview containing cell components, operating principals and recent developments in the field of DSSCs will be given.

1.1 Dye sensitised solar cells (DSSCs)

Ever since their first demonstration, dye-sensitised solar cells have attracted considerable attention due to the fact that they offer a low-cost alternative to the conventional silicon solar cell systems for the generation of photovoltaic energy, with efficiencies over 11%.[18] Compared to silicon cells one of the major differences in the operating principle is that light absorption and electron/hole transport is not performed by the same material resulting in a more complex operational mechanism.

Within these cells a dye is used for light absorption, nanocrystalline metal oxides for electron and electrolytes for hole transportation.[19] The components of a DSSC comprise (i) a glass substrate coated with a transparent conductive oxide layer, (ii) a nanocrystalline thin film semiconductor acting as the photoanode, (iii) a dye-sensitiser, (iv) an electrolyte (redox-mediator) and (v) a metal-coated glass substrate acting as the photoinert counterelectrode (cathode).[20] A schematic illustration of the device structure is displayed in Figure 4.
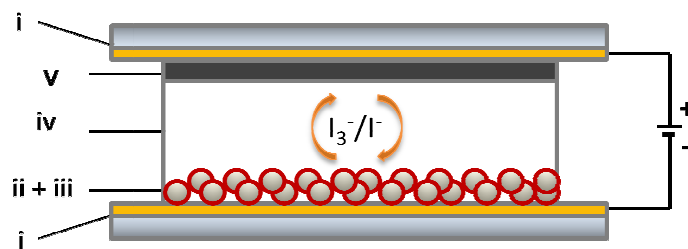
Figure 4: Schematic representation of the cell components.

Prior to device assembly the dye has to be adsorbed to the mesoporose metal oxide in a sensitisation step. It was suggested that the carboxy groups in the dye can form ester linkages with the semiconductor surface and efficiently enable electronic communication between dye and inorganic semiconductor.[20]

The operational principle of this type of cell can be explained by the underlying electrochemical processes that occur upon light absorption as shown by the schematic representation in Figure 5. The photosensitisation, redox and charge transfer reactions are summarised in Scheme 1 which follows:
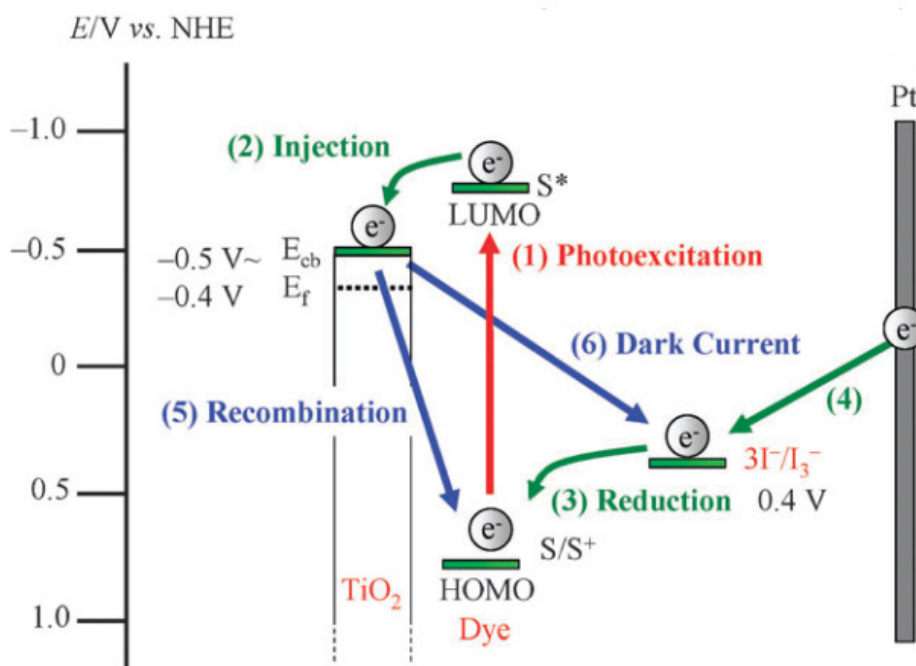
Figure 5: Scheme of electron transfer reactions in DSSCs (adapted from Ooyama & Harima)[20].

Photoexcitation:

S (on TiO_2) + hν $\longrightarrow$ S*　　　　　　　(1)

Dye oxidation and electron injection:

S* (on TiO_2) $\longrightarrow$ S$^+$ (on TiO_2) + e$^-$ (TiO_2)　　(2)

Dye neutralisation:

2S$^+$ (on TiO_2) + 3I$^-$ $\longrightarrow$ 2S (on TiO_2) + I$_3^-$　　(3)
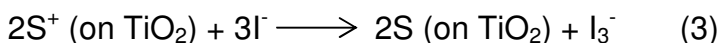
Electrolyte regeneration:

I$_3^-$ + 2e$^-$ (Pt) $\longrightarrow$ 3I$^-$　　　　　　　(4)

Charge recombination with dye:

S$^+$ (on TiO_2) + e$^-$ (TiO_2) $\longrightarrow$ S (on TiO_2)　　(5)
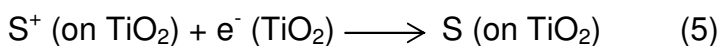
Charge recombination with electrolyte:

I$_3^-$ + 2e$^-$ (TiO_2) $\longrightarrow$ 3I$^-$　　　　　　(6)

Scheme 1: Summary of photosensitisation, redox and charge transfer reactions.

The initial step in this electrochemical cascade is the absorption of a photon by the sensitising molecule S, which is anchored to the surface of the TiO_2 nanocrystals, inducing the photoexcited state S* (equation 1). From the photoexcited state the dye injects an electron into the conduction band of the photoanode which occurs on a subpico to femto second (10^{-12}-10^{-15} s) time scale.[3,19] The difference in the energy levels of the LUMO (lowest unoccupied molecular orbital, *i.e* conduction band, E_{CB}) edge of the metal oxide and the dye's LUMO represents the driving force of the electron injection which occurs more rapidly with a larger value of E_{CB}-E_{LUMO} (equation 2).[20, 21] Subsequently the oxidised dye accepts an electron from the I^- ions of the electrolyte, which thereby gets regenerated (dye gets neutralised) and returns to its ground state S (equation 3). Following injection, the electrons percolate through the thin film of interconnected metaloxide nanoparticles to the transparent conductive oxide (TCO) and are channeled through an external circuit to the counterelectrode. At the cathode's metal surface, the redox mediator I^- ion is regenerated by a two electron reduction process of the triiodide ion I_3^-, hence completing the electrical circuit (equation 4).

However, during this electrochemical cycle two undesired side processes may occur and reduce device efficiency. In some instances, electrons injected into the CB (conduction band) of the semiconductor may recombine with the dye in its oxidised state (equation 5). The second process relates to recombination of electrons with the electrolyte (I_3^-) at the TiO_2/dye interphase accounting for the dark current (equation 6). The latter process can be influenced by the dye structure. Dyes that either form a compact monolayer on the TiO_2 or contain long alkyl chains can prevent the oxidised electrolyte from approaching the semiconductor's surface and therefore effectively suppress dark current generation. These processes of charge recombination exhibit rather slow reaction kinetics with timescales ranging from milli- to mircoseconds (10^{-3}-10^{-6} s).[19] For efficient device performance, electron injection as well as dye regeneration (equations 1 and 2), have to be kinetically favoured over competing processes of charge recombination (equations 5 and 6).[20]

1.1.1 Metal oxide anode

One of the most important factors in determining the performance of a DSSC is the semiconducting metal oxide.[22] In the sensitisation process a layer of dye molecules is adsorbed onto the porose metal oxide film, which collects injected electrons coming from the LUMO level of the dye. Specific prerequisites such as a high surface area in order to adsorb a maximum amount of dye to subsequently create a maximum amount of charge carriers as well as high electron mobility and chemical stability were found to be crucial for device performance.[22]

According to O'Regan and Grätzel the breakthrough for DSSCs was the use of mesoporose TiO_2 as the semiconductor material for the photoanode.[23] The porosity of the semiconducting TiO_2 improves device performance for two reasons. Firstly the internal surface area of the metal oxide is increased by a factor of 1000 thus allowing an overall larger amount of dye to be adsorbed. Secondly the degree of porosity is responsible for interconnecting the particles and therefore directly influences the percolation path length of the charge carriers. Accordingly, high porosity in TiO_2 films leads to an extended percolation path length and hence a decrease in light harvesting efficiency can be observed. Therefore, a porosity of 50-60% was found to be the optimum.[24]

TiO_2 offers several advantages including: stability, non-toxicity, limited absorbance to below 388 nm, wide availability and cheapness, and suitable conduction band energies, which has resulted in solar cells constructed with TiO_2 achieving superior efficiencies compared to devices using other metal oxides such as ZnO, SnO_2 an Nb_2O_5 as the photoanode material[3,25.] This can directly be attributed to inferior chemical stability, unsuitably located conduction band energies and smaller band gaps of the aforementioned materials.[3]

1.1.2 Dye sensitiser

The dye sensitiser's properties are critical for the generation of the electron-hole pair. Additionally, the dye molecule possesses the biggest degree of tailorability within this photovoltaic system, which allows for a wide range of modifications. Nevertheless, certain requirements for an efficient dye have to be satisfied [22]:

(1)   For optimal light absorption the dye's absorption spectrum should match with solar sunlight spectrum, *i.e* covering all visible light region to the near IR region of the solar spectrum with an absorption peak in the visible region as this region contributes the majority of solar sunlight spectrum. Additionally the dye sensitiser should have a high molar extinction coefficient.[22]

(2)   The energy levels of the dye should show correct alignment with those of the metal oxide and the electrolyte. For efficient electron injection into the photoanode, the LUMO of the dye should be localised near the anchoring group and above the conduction band edge of the photoanode. The HOMO level of the sensitiser should be localised below the energy level of the electrolyte to allow for efficient regeneration of the oxidised dye.[22,26]

(3)   In order to minimise charge recombination between injected electrons and the oxidised dye, electrons have to be quickly separated from holes. A well defined D-A character is therefore required for providing directionality of the electron flow towards the injection site.[22]

(4)   Sensitising materials should exhibit a strong link to the semiconductor surface to minimise interface resistance by forming ester linkages through carboxy groups on the dye molecule.[20,22]

(5)   The outer regions of the dye molecule should be hydrophobic to decrease contact of electrolyte and anode, which could result in water induced desorption of the dye.[26]

(6)   Aggregation of the dye on the metal oxide surface would lead to non-radiative decay and ultimately to a decreasing power conversion efficiency.[27]

(7)   For a dye to be economically viable, it has to display superior oxidative and reductive stability, in order to endure 10^8 turnovers (complete reduction and oxidation cycles) under sunlight which correlates to a lifetime of 20 years.[22]

As mentioned above, broad absorption throughout the visible and near infrared region in order to yield an optimum overlap with the solar spectrum accounts for one of the most important requirements related to dye sensitisers. The solar spectrum comprises wavelengths ranging from the ultraviolet over the visible to the infrared region.[19] The spectrum with its peak in the visible region resembles the one emitted by a blackbody at 5760 K. Dips in the spectrum at 900, 1100, 1400, 1900 nm and at 1800 and 2600 nm are contributions from atmospheric absorption of H_2O and

CO_2, while ultra violet light is filtered out by O_3, respectively (Figure 6). In accordance to Figure 7 it becomes clear that increasing photo-currents can be obtained upon red-shifting the absorption spectrum of the sensitising materials by aiming at a theoretical optimum λ_{max} of 920 nm.[3,22]
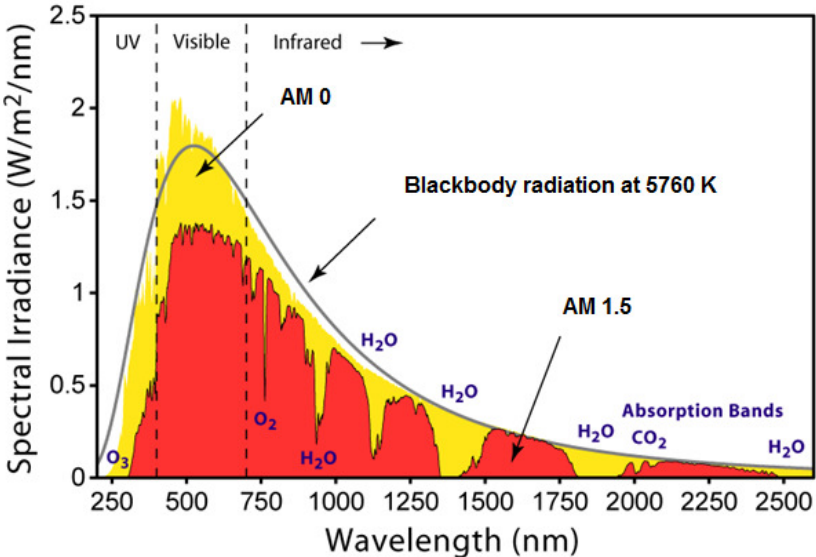
Figure 6: Blackbody radiation and solar radiant energy of the AM 0 and the AM 1.5 G spectrum (adapted from Lund *et al.*).[28]
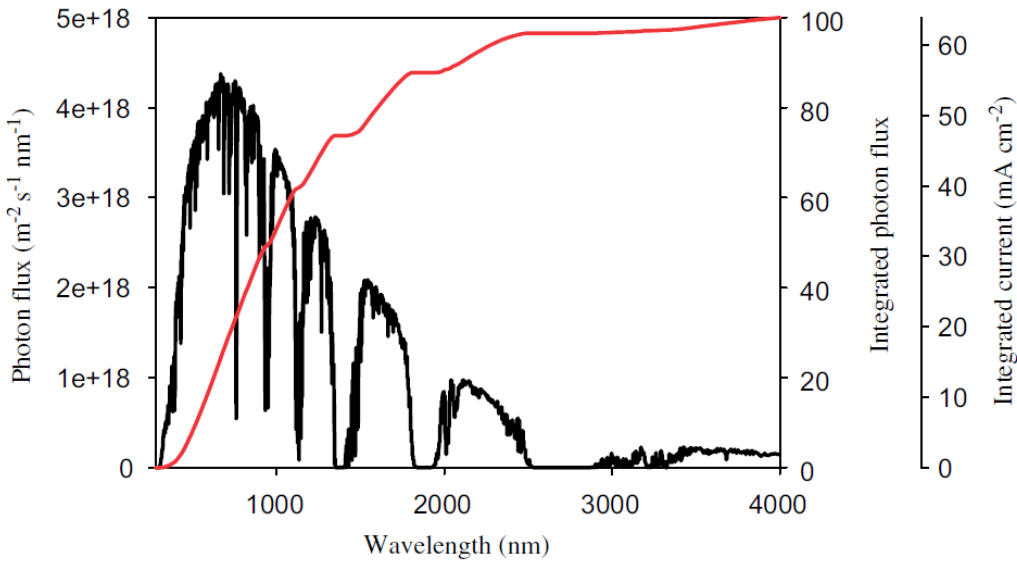
Figure 7: Photon flux of the sun AM 1.5 spectrum, the total number of photons and obtainable photocurrent (adapted from Bundgard & Krebs).[29]

Solar radiation that hits the earth's surface has the shortest path length with the sun being directly overhead (i.e. normal to the earth's surface). The path length is

called the air mass (AM) and correlates to the angle (φ) of the sun's elevation with AM 0 being the extraterrestrial irradiance spectrum, respectively. The path length can be approximated by AM= $1/\cos(\varphi)$, where φ is the angel for the incident solar radiation relative to the normal to the earth's surface. Efficiency measurements are commonly conducted using spectral irradiance for an air mass of 1.5 G (global) where the number denotes the angle of elevation which is 48° for standardised reference spectra.[3]

However, the synthesis of a panchromatic single sensitiser proved to be challenging, as red-shifting the absorption spectrum towards higher wavelength and therefore lower energy photons, would require the dye to possess a sufficiently narrow band gap. Consequently this could have a negative effect on electrochemical properties such as HOMO and LUMO energies that have to be efficiently tuned for correct alignment with the conduction band edge of TiO_2 and the energy level of the redox mediator.[19]

A new approach towards panchromatic absorption is the co-sensitisation of the photoanode with dyes that exhibit complementary spectral responses. Although devices built on this principle generally show improved light harvesting, their overall efficiencies are usually inferior to solar cells incorporating only one of the dyes. The main problems of this strategy is related to the finite amount of TiO_2 anchoring sites as well as the occurrence of energy and electron transfers between dyes leading to deactivation of the excited state and preventing electron injection.[8,19]

1.1.3 Redox mediator and electrolyte

Presently electrolytes can be grouped into solvent-based liquid ones, solvent-free liquid ones, quasi-solid state and solid state ones. The organic solvent-based liquid ones are most commonly used for device fabrication related to research activities whereas solid state electrolytes present and ideal form for commercialisation due to negligible solvent loss during continuous operating conditions.

The organic solvent in this group of electrolytes usually contains nitrile and ester compounds, where recently mixtures of valeronitirle and acetonitrile have become popular. The most important constituent of the electrolyte is represented by

the redox couple which is responsible for the regeneration of the oxidised dye subsequently to electron injection. So far, best performing devices are associated with the redox couple iodide/triiodide (I^-/I_3^-). In this system the oxidised dye is neutralised by I^-, which itself is then regenerated to I_3^- by a slow but catalytically efficient two electron transfer process that occurs at the counterelectrode. With fast diffusion of I^- and I_3^- towards the respective electrodes, these kinetically controlled processes cause only preferred reactions at cathode and anode to occur and hence are responsible for the superior functionality of this redox-mediator.[22]

1.2 Types of dye molecules

DSSCs can generally be divided into two major groups: cells that use functional ruthenium complexes as the dye sensitising and light harvesting molecule and metal-free organic donor-acceptor (D-A) dyes.

1.2.1 Ruthenium complexes

Highest efficiencies of 10.5 % in the field of DSSCs were obtained with dyes based on heteroleptic ruthenium complexes.[8] In 1993 Nazeerudin *et al.* reported the first high performing polypyridyl complex N3 [(4,4′-dicarboxylic acid-2,2′-bipyridine) ruthenium(II)] which became the standard reference.[30] Shortly thereafter N3 was surpassed by a dye with similar architectural features, the black dye introduced in 1997.[31] Addition of the coadsorbing agent guanidinium thiocyanate, put N3 back on the first rank by increasing the cells V_{OC} (as N719) (Figure 8).[32]

In order to compensate for some of the major drawbacks of ruthenium dyes, structures were modified to incorporate long alkyl chains, which affects their long term stability (Z 907) introduced by Zakeeruddin and co-workers.[33] More recent synthetic efforts try to focus on the development and improvement of their molar extinction coefficients by the use of thiophenes and phenylenevinylenes in the structure of their ancillary bipyridyl ligands reaching ε (molar extinction coefficient) values of 24 200 $M^{-1}cm^{-1}$.[19]

To date ruthenium complexes are the only dyes to achieve efficiencies over 10% in DSSCs.[8] Their superior performance can be accredited to a wide absorption range from the visible to the near infrared (NIR) part of the solar spectrum with high molar extinction coefficients. It was found that at the heart of their functioning stands a metal to ligand charge transfer (MCLT), in which electrons are effectively channeled to the carboxylate electron accepting moieties followed by ultrafast injection into the conduction band of TiO_2. The essential use of ruthenium dyes, however, can also be seen as their downside since the scarcity and high costs of this resource reduces their economical value. In this context, the synthesis of compounds free from ruthenium was pursued in order to give rise to metal-free organic dyes.[26]
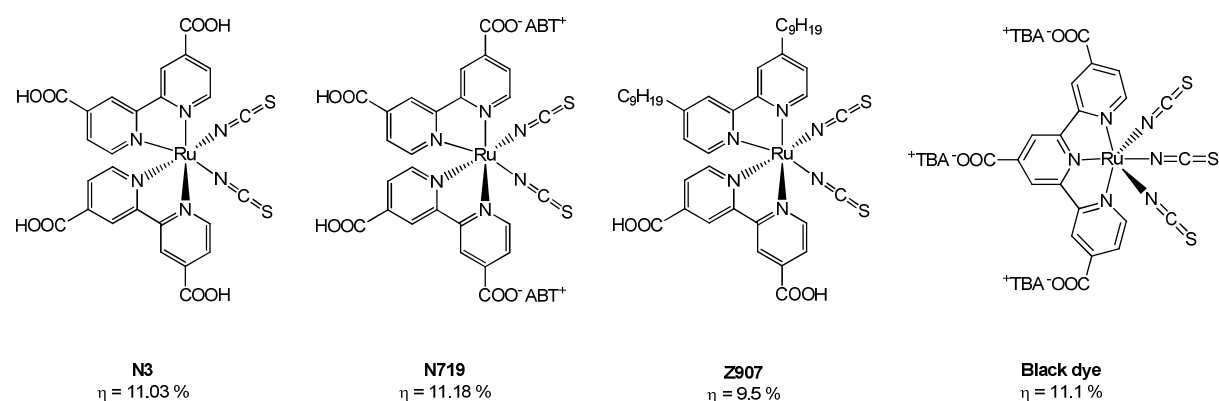
Figure 8: Chemical structures of Ru-complexes N3,[30] N719,[32] Z907 [33] and the black dye.[31]

1.2.2 Metal free organic dyes

The major advantages of metal-free dyes are larger molar extinction coefficients, relatively inexpensive preparation in accordance to existing architectural strategies and the inherent possibility to tune their absorption as well as electrochemical properties such as HOMO and LUMO levels and hence achievable V_{OC} (open-circuit voltage) in PV devices.[26] The design of metal-free sensitisers follows a simple structural D-π-A concept which is shown in Figure 9. Donor-acceptor π-conjugated dyes incorporate three different functional areas where the viable parts are an electron-donating unit and an electron accepting moiety linked by a π-

conjugated bridge. Tertiary amines such as triphenylamine, carbazole or dialkylamines were found to donate electrons effectively while carboxylic acid, cyanoacrylic acid or rhodanine-3-acetic acid take on the role of the electron acceptor and anchoring group due to their strong electron withdrawing properties. A number of dyes featuring a great variety in the design of the π-conjugated spacer have been developed where basic building blocks are represented by vinylene, conjugated or fused thiophenes and perylene moieties.[20]
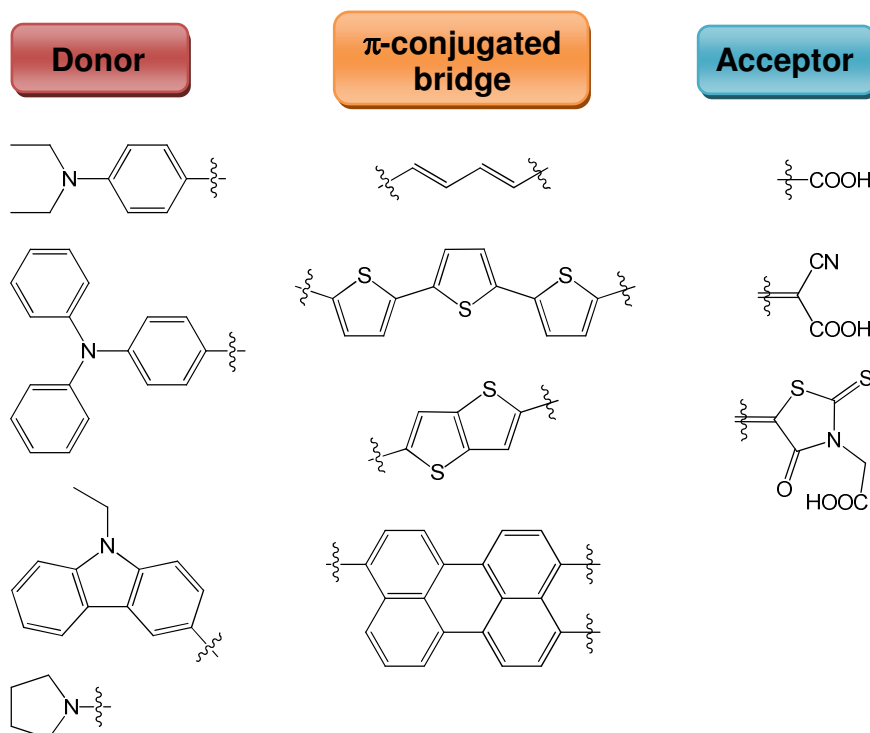
Figure 9: Commonly used building blocks for metal free dye sensitisers.

Although metal-free dyes may tend to be less stable and less efficient compared with Ru-containing dyes, enormous progress has been made over the past years.[8] In accordance with the requirements for dye sensitiser molecules stated under point 1.1.2, a range of dyes was synthesised including cyanine, merocyanine, porphyrine indoline, coumarin, perylene, polyene, triphenylamine, trithiophene, anthraquinone dyes and others.[8]

Investigation of structure-property relationships of the broad spectrum of available dyes made it possible to deduce some general trends. First, the highest occupied molecular orbitals (HOMOs) of the D-π-A dyes are delocalised over the π-bridge, centered at the electron donating part of the molecule while LUMOs are

delocalised over the electron accepting part.[20] The electron transfer from the dye into the TiO$_2$ electrode can therefore effectively occur via intramolecular-charge-transfer (ICT) through the preceding step of electron-excitation from the HOMO into the LUMO of the organic dye. Furthermore, the length of the π-conjugated bridge as well as the presence of electron-donating and -accepting groups on the dye skeleton can influence and shift energy levels of HOMOs and LUMOs. Both, the extension of the π-conjugated system and the substitution of the dye structure with additional electron donating or accepting units have demonstrated shifts to lower LUMO energies, thereby reducing the dye's band gap while at the same time red-shifting its absorption spectrum.[20] Additionally it was found that electron lifetime in metal-free dyes containing more than one donor moiety is increased, due to an increase in steric hindrance on the semiconductor surface, by decreasing recombination effects of the electrolyte with the injected electrons [34].

In this context, vinyl moieties (-CH=CH-) are often used to extend the range of π-conjugation and to induce bathochromic shifts in absorption spectra. This approach often proved to be disadvantageous since the vinyl unit destabilises the organic molecule through rotation and cis/trans isomerisation about the central vinyl double bond, thereby interrupting the charge transfer over the π-conjugated bridge.[20] Increased tendencies towards π-aggregation can also be attributed to the incorporation of vinyl units into the dye backbone. The use of phenylene units in attempts to create an extended π-conjugated system, increases stability and the molar extinction coefficient which was successfully demonsrated by Hwang *et. al.*[35] The remarkably simply structured triphenylamine dye using a phenylenevinylene π-conjugated bridging unit and cyanoacrylic acid as the electron withdrawing group gave efficiencies of 9.1% (Figure 10 (A)). Another group of compounds that is widely used for building blocks in dye sensitising molecules is represented by thiophene fused thiophene and oligothiophene compounds due their high chemical stability and strong light absorption properties.[20]

π-Stacked aggregation of dye molecules on the TiO$_2$ surface generally leads to intermolecular energy transfer and hence decreases the amount of injected electrons resulting in low photon conversion efficiencies.[36] To prevent dyes from aggregating deoxycholic acid (DCA) was used as a co-adsorbent. Coumarine dyes reaching efficiencies of 5% were reported in 2007 by Hara *et al.*[37] After addition of DCA as a co-adsorbent the cell performance significantly improved to give a device

efficiency of 8.2% as a direct result of the reduction in aggregation of the dye molecules due to strong π-π interactions (Figure 10 (D)). Although the co-adsorption of DCA presents a viable way of simultaneously improving a cells photocurrent and photovoltage, it also accounts for a significant loss in dye adsorption which ultimately limits photovoltaic performance. However, another way to effectively reduce intermolecular interaction and dye aggregation was found to be the incorporation of long alkyl chains into the dye skeleton. For instance, the introduction of a sterically hindered n-octyl substituent onto the rhodanine ring of an indoline dye demonstrated effectively the suppression of aggregation as well as charge recombination (dark current) (Figure 10 (H)). To date, this indoline dye, synthesised by Grätzel and co-workers, is the best performing metal free dye yielding power conversion efficienies of 9.5%.[38] As discussed earlier, the presence of at least one carboxy group in the dye structure is necessary for electronic communication between dye and semiconductor. Hence, development of new dyes is limited and improvements on the acceptor part of the molecule have to be aimed at creating well combined π-bridge acceptor systems that show strong interaction with TiO$_2$. Dyes with high efficiencies and promising structural design are displayed in Figure 10.

In summary, photophysical, electrochemical and related charge transfer properties of D-π-A dyes are strongly interconnected with the abilities of D and A to donate and withdraw electrons as well as electronic properties of the π-bridge. In order to develop efficient dyes properties of each of the components D, A and π-bridge must be selectively tuned through chemical modifications.[20,26]
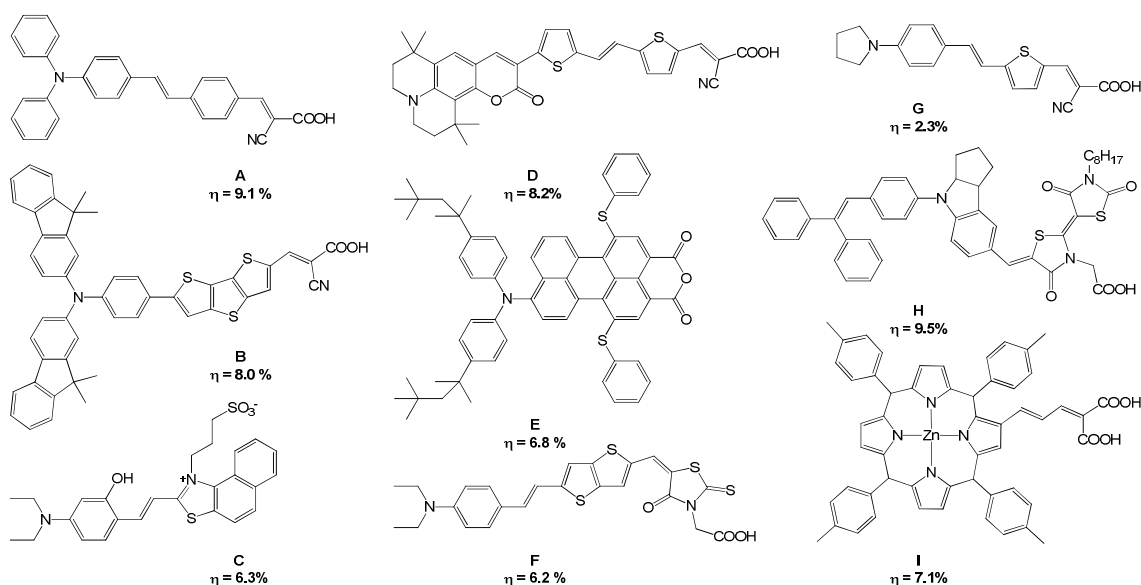
Figure 10: Chemical structures of metal-free dyes, with their corresponding efficiencies.[26]

1.4 Device Performance characteristics

The performance of a DSSC can be evaluated by measurement of the photocurrent density (J) as a function of various voltages (V) and plotting a J-V curve. Related to a cell's performance, four key factors can be identified: the open-circuit voltage (V_{OC}), the short-circuit photocurrent density (J_{SC}), the fill factor (ff), and the solar energy-to-electricity conversion efficiency (η).[20] A typical curve is depicted in Figure 11.
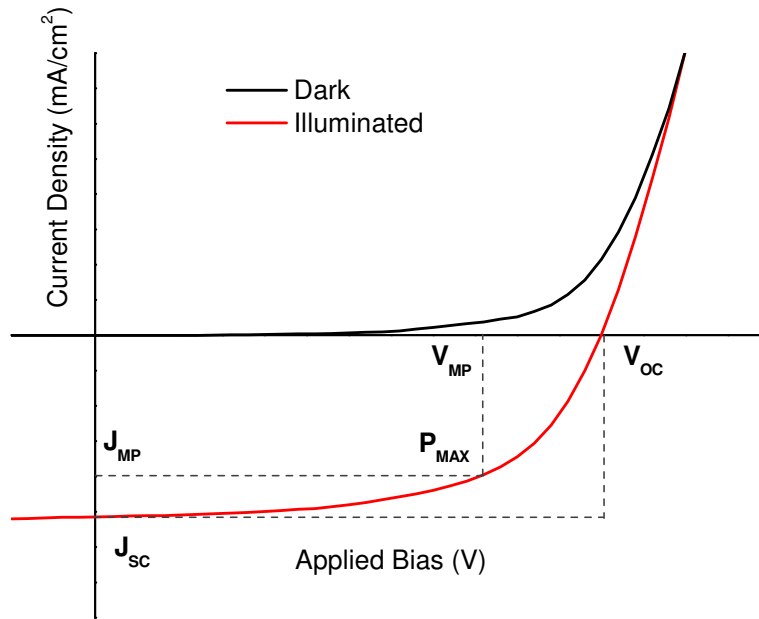
Figure 11: J-V characteristics.

V_{OC} is defined as the difference in electrical potential between two terminals of a cell under illumination when the circuit is open with the maximum V_{OC} in a DSSC corresponding to difference between the energy level of the CB of TiO_2 and the redox potential of the electrolyte. J_{SC} is the photocurrent per unit area when a DSSC under irradiation is short-circuited and is related to the interaction between TiO_2, the dye and its absorption coefficient. The fill factor is defined as the maximum power output ($J_{MP}*V_{MP}$) divided by the product of J_{SC} and V_{OC} (overlapping rectangles in Figure11). The η value is defined as the ratio of the maximum power (P_{max}) of the cell to the energy of the incident sunlight (P_0) and is therefore determined by J_{SC}, V_{OC}, ff and P_0.

$$ff = (J_{MP}V_{MP})/(J_{SC}V_{OC}) \qquad \eta(\%) = \frac{P_{max}}{P_0} = \frac{Jsc*Voc*ff}{P_0}$$

1.5 Aim of thesis

The aim of this project is to design and synthesise a novel dye **14** (Figure 12) and the investigation of its potential application for the use in metal-free DSSCs. In the process, recent findings on structure-property relationships will be implemented into the dyes structural architechture which is based on a D-π-A concept. In order to improve existing dye systems, important features such as a high molar extinction coefficient for effective light harvesting, absorption of the longer wave length region (> 600 nm), oxidative stability, strong donor-acceptor properties and consequently a narrow band gap, have to be addressed.
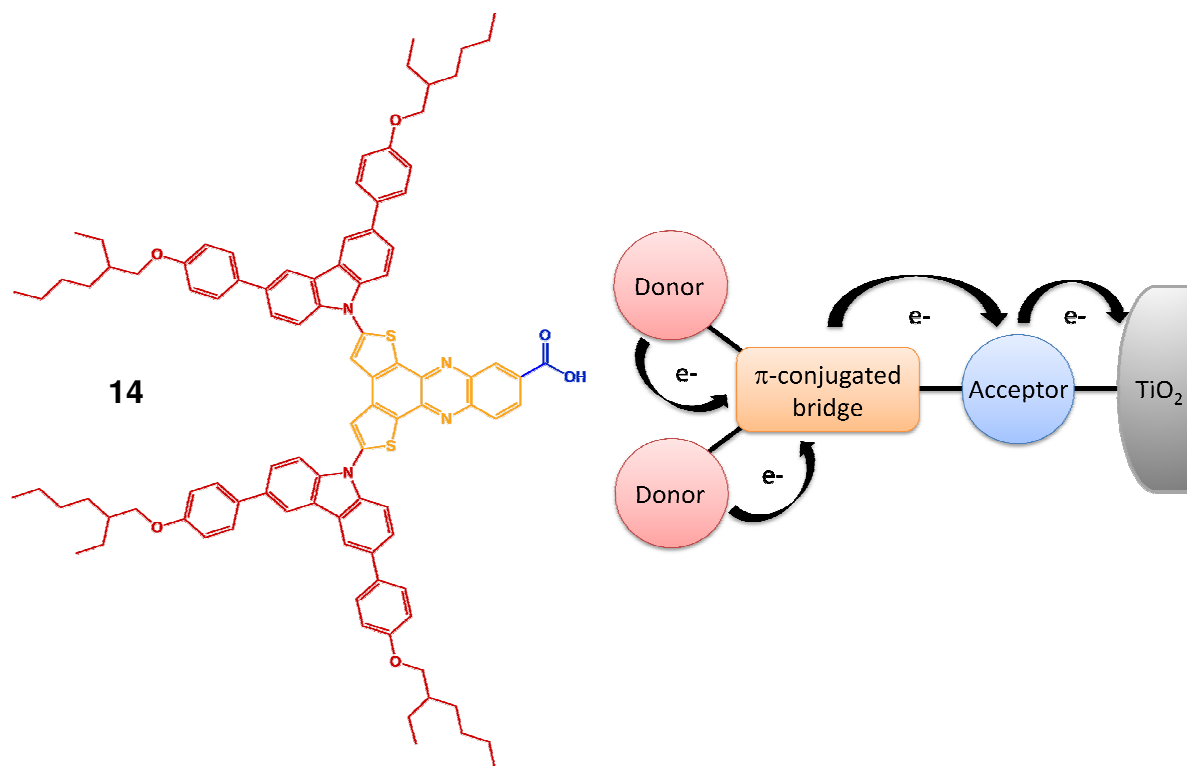
Figure 12: Dye **14** structure and schematic ICT process.

Previous works have demonstrated the inherent donor-acceptor character of benzodithiophene-phenazine compounds with the thiophene units acting as the electron rich and the phenazine moiety as the electron deficient part of the molecule.[39] In addition to the enforced planarity and the resulting increased π-π overlap that fused thiopene ringsystems provide, the rigidity and the intrinsic donor-acceptor properties of the aforementioned phenazine compound are hoped to be beneficial when used as the π-conjugated bridge moiety in this new dye system.

Only a few compounds used in DSSCs incorporate carbazole which was found to exhibit excellent absorption properties in the blue region of the solar spectrum.[40] The electron rich nitrogen of this tricyclic fully aromatic system, its insusceptibility to oxidation of the 9-postion, stable radical cation formation, excellent thermal and photochemical stability as well as relatively high charge mobility renders carbazole perfectly suitable for the role of the electron donating group in a dye molecule.[41] The introduction of 2-ethyl-hexyloxy-phenyl sidechains to the carbazole has several necessary functions: (i) to act as a solubilising group, (ii) to create a hydrophobic environment to prevent the oxidised electrolyte from approaching the anode followed by subsequent leakage of injected electrons (dark current), (iii) to provide steric hindrance among dye molecules so to minimise π-π aggregation on the TiO_2 surface, and (iv) to increase the electron density on the carbazole nitrogen.

Finally, the introduction of a carboxylic acid to the phenazine ring system is intended to induce and promote directionality of the electron flow towards the electron withdrawing region of the compound, supported by the donor effect of the dye's core. Within this work, the target dye **14** will be synthesised in accordance to the aforementioned structural components to produce the desired properties. Ultimately, dye sensitised solar cells will be fabricated and their performance will be evaluated using the new dye as the sensitising material.

Chapter 2 - Synthesis: Results and Discussion

2.1 Introduction

The synthetic strategies employed to prepare the novel organic dye for the use in metal-free dye sensitised solar cells will be discussed and evaluated. Two routes (A and B) to obtain the dye molecule were proposed and examined. The retrosynthetic analysis of route A and B is displayed below in Scheme 2 and 3. The preparation of this material will be displayed in three separate parts: the synthesis of the electron donating unit of the molecule (2.2), the build up of the π-conjugated core (2.3) and the preparation of the actual dye (2.5 and 2.6). Briefly, e^--donor and core material along with the e^--accepting carboxylic acid moiety were synthesised independently and coupled together in the second last step. The structures of all new materials were fully characterised with ^{1}H NMR spectroscopy, MALDI TOF as well as FT-IR. Experimental data used to support the success of conducted synthetic work are presented along with their interpretation.
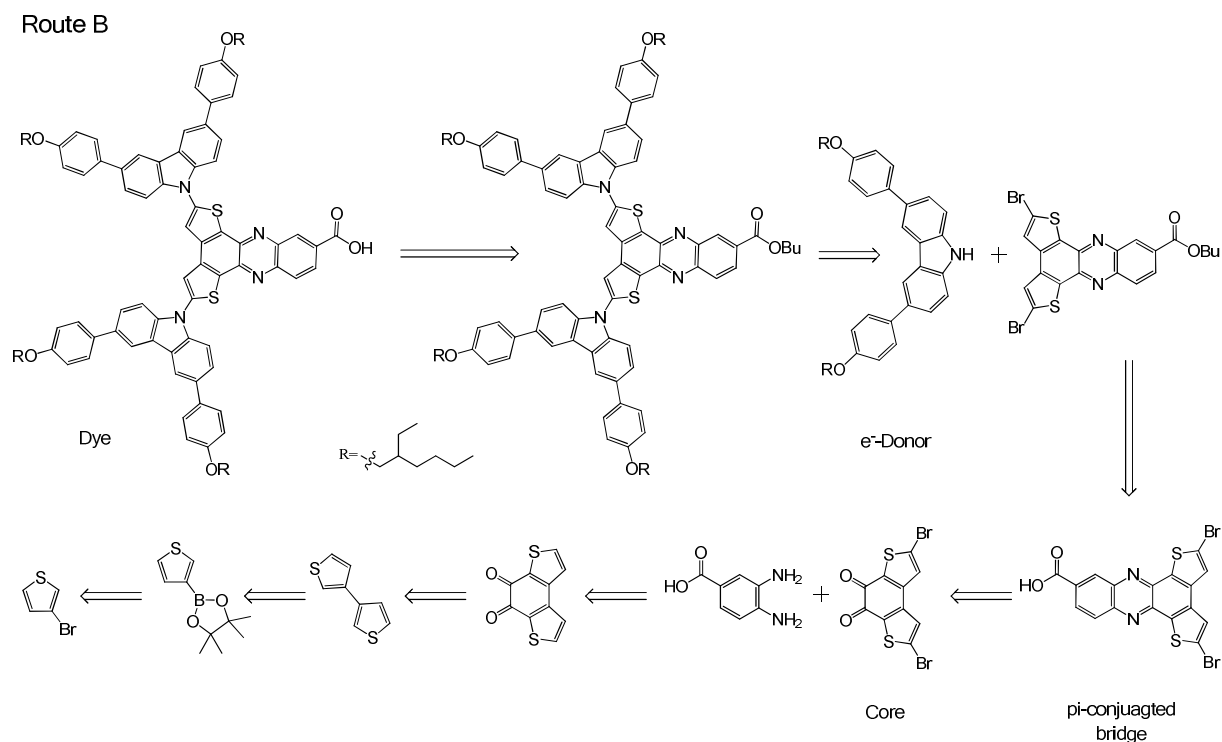
Scheme 2: Retrosynthetic analysis of route B.
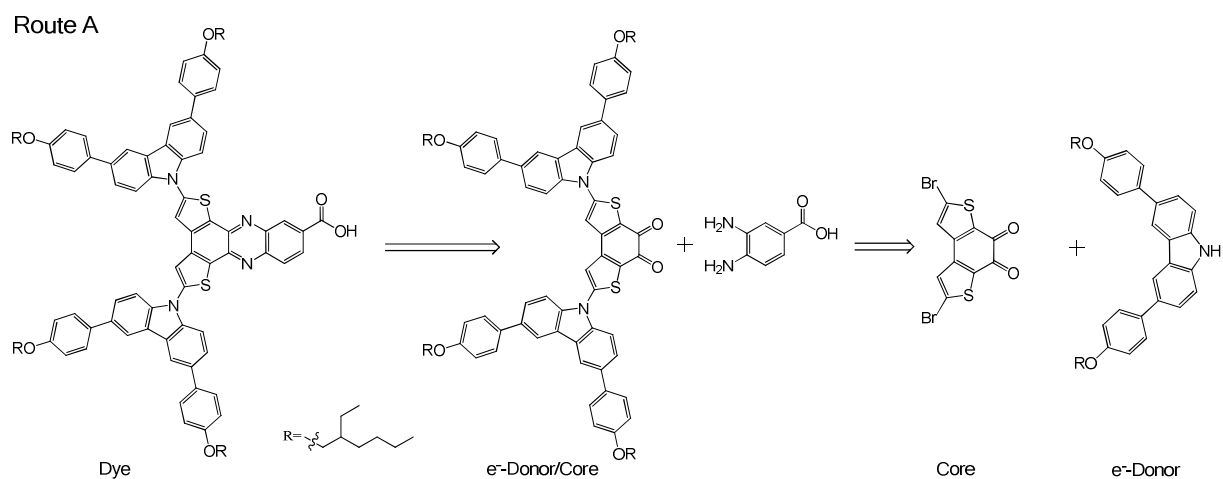
Scheme 3: Retrosynthetic analysis of route A.

2.2 Synthesis of 2-Ethylhexyloxy-carbazole (e⁻-Donor)
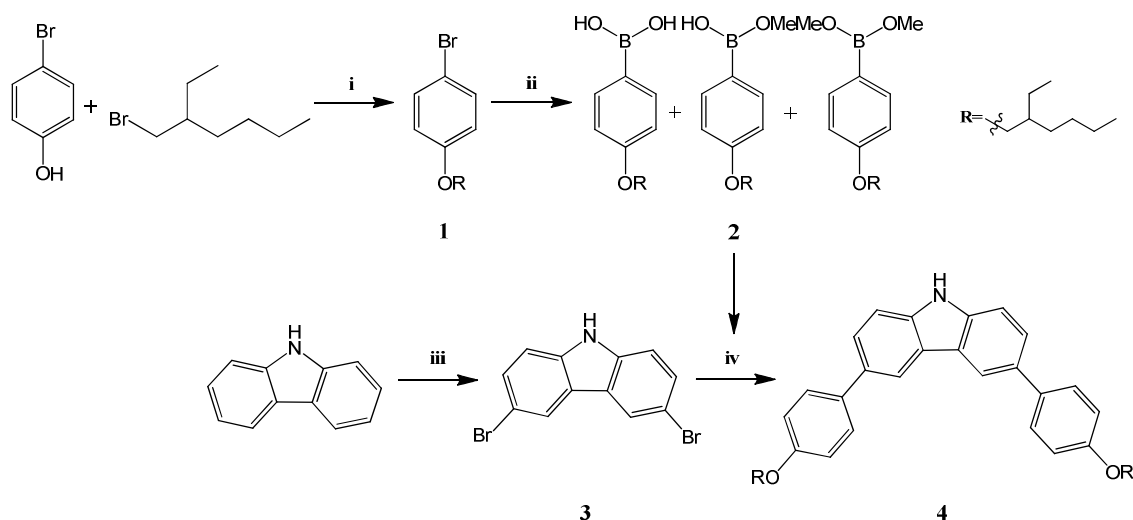
Scheme 4: Synthesis of e⁻-Donor: i. 2-ethylhexyl bromide, KOH, DMSO, r.t., Ar$_{(g)}$, 68 h, 92%. ii. THF, a) *n*-BuLi, -78 °C, 1.6 h, b) B(OMe)$_3$, -78 °C, 2.5 h, c) HCl 3M, r.t., 2 h; Ar$_{(g)}$, 95%. iii. NBS, THF, 30 min, r.t., 74%. iv. Pd(PPh$_3$)$_4$, 2 M Na$_2$CO$_3$, EtOH, toluene, 100 °C, 68 h, Ar$_{(g)}$, 71%.

The synthesis of the electron-donating group **4** of the organic dye was accomplished in 4 steps as depicted in Scheme 4, following literature.[42] The first step towards **4** involved the formation of an ether linkage, whilst the introduction of a 2-ethylhexl moiety provided solubility and decreased stacking of the dye, once adsorbed on the TiO$_2$. 4-Bromophenol and 2-ethylhexyl bromide were used as

reactants in a suspension of potassium hydroxide in DMSO at room temperature. The ether was formed via a simple S_N2 substitution of the aryl alkoxide with the alkyl halide to give the desired product **1**, in an excellent yield of 92%. The product was supported with ^{1}H NMR spectroscopy with a characteristic multiplet at 3.80-3.86 ppm, corresponding to the two protons in the alkyl chain which are closest to the oxygen. To attach **1** onto the carbazole unit, the carbazole moiety firstly had to be dibrominated and **1** had to be transformed into the boronic acid. Double-bromination of carbazole was carried out with *N*-bromosuccinimide in tetrahydrofuran. Since this reaction is exothermic and therefore shows self initiated heating, NBS was added slowly in small portions in order to avoid over-bromination at room temperature to yield **3** in 74 % as a light brown solid. To prepare the boronic acid **2**, bromophenol was first lithiated by *n*-butyllithium in anhydrous tetrahydrofuran at -78 °C and then reacted with trimethyl borate and followed by hydrolysis to form the corresponding boronic acids in excellent yields (~95%). It is important to note that there are a number of boronic species formed after hydrolysis, including triaryl anhydride (triarylboroxin). As all of the isomers are reactive in the following Suzuki coupling reaction purification of the crude yellow oil proved to be sufficient by using a silica plug even though the ^{1}H NMR spectrum of the mixture was complicated. To prepare carbazole **4**, two equivalents of **2** were coupled to dibromocarbazole **3** under Suzuki conditions catalysed by tetrakistriphenylphosphine in the presence of Na_2CO_3 to afford the white solid **4** in a 71% yield. ^{1}H NMR spectrum of **4** (Figure 13) was identical to those reported in literature.[42]

Figure 14 shows the aromatic region ^{1}H NMR spectrum of compound **4** at two different concentrations. What can be seen is that peaks in the upper spectrum (more concentrated) possess decreased resolution which is due to aggregation of this carbazole derivative in solutions of higher concentrations. The best illustration for this effect was found when the doublets at 7.46 ppm of both spectra were compared to each other. Furthermore, the singlet at 8.27 ppm started to split and the doublets at 7.64 and 7.03 ppm showed characteristics of multiplets. Additionally it was found that the multiplet at 7.64 ppm originated from the signals of two carbazole protons and four phenyl protons whereas the muliplet at 7.03 ppm exclusively corresponds to the remaining phenyl protons. The successful preparation of **4** was also supported by low resolution mass spectroscopy (LRMS) with the expected mass peak at 574.4 Da.
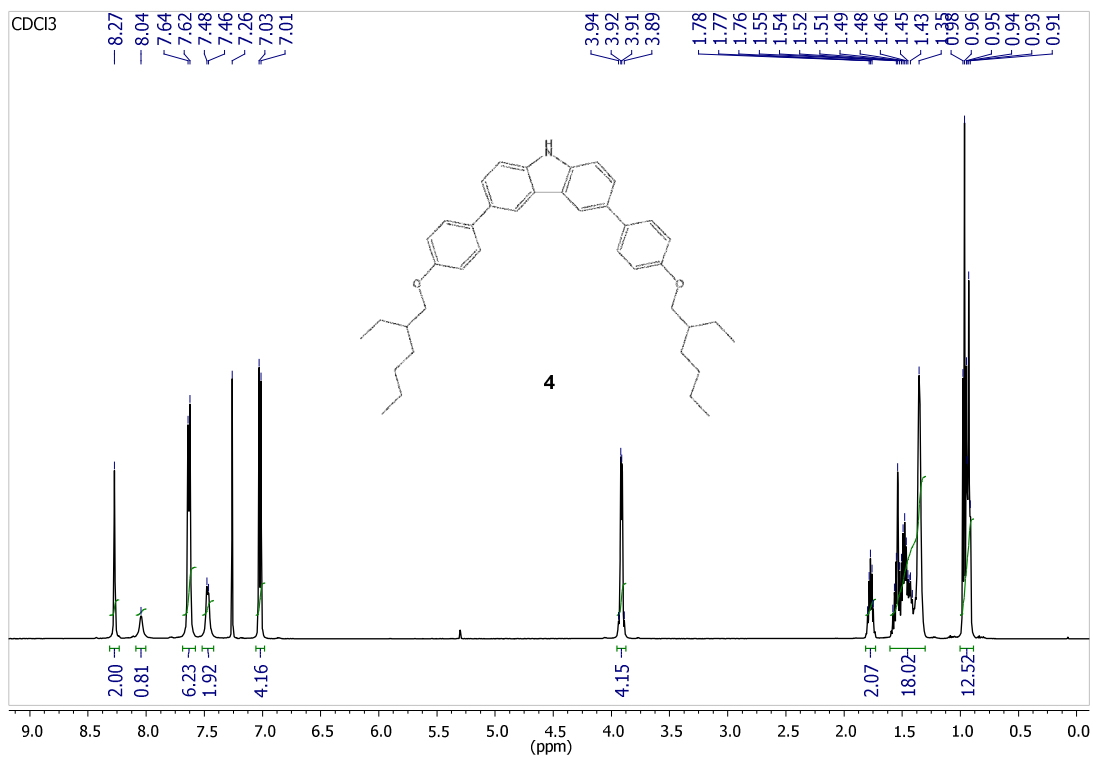
Figure 13: ^{1}H NMR spectrum of **4** in CDCl$_3$.
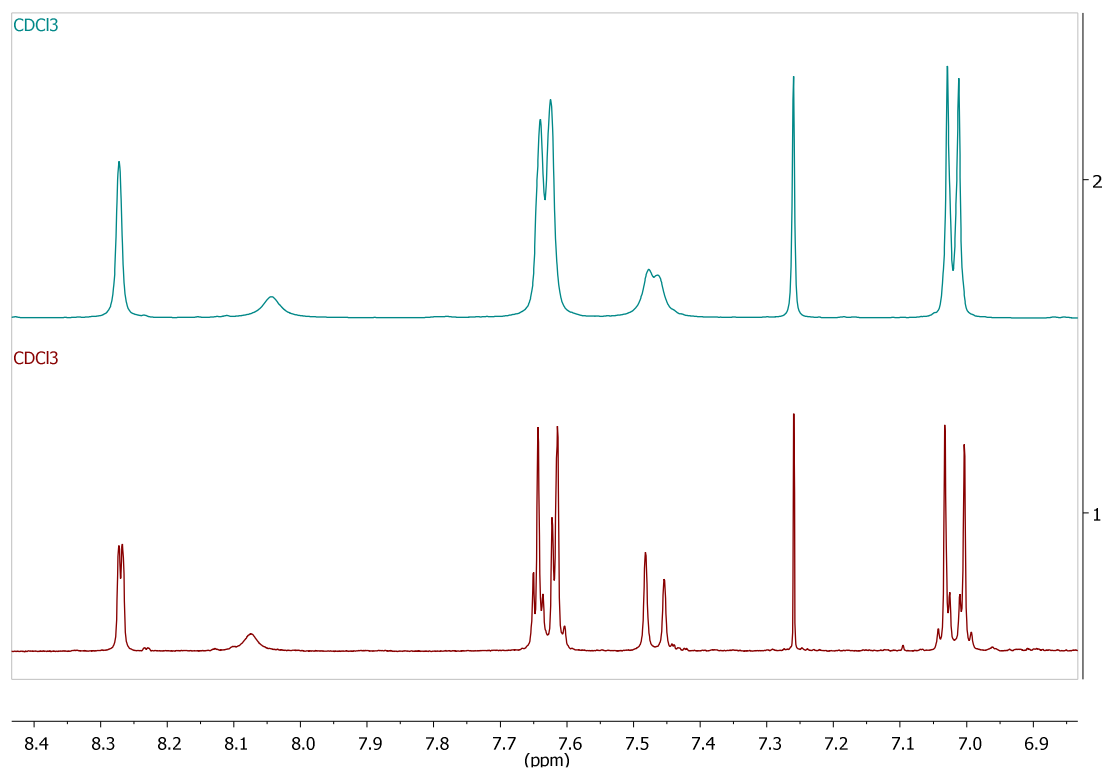
Figure 14: ^{1}H NMR spectrum of **4** in concentrated solution (top) and dilute solution (bottom) in CDCl$_3$.

2.3 Synthesis of dibromo-benzodithiophene-dione (Core)
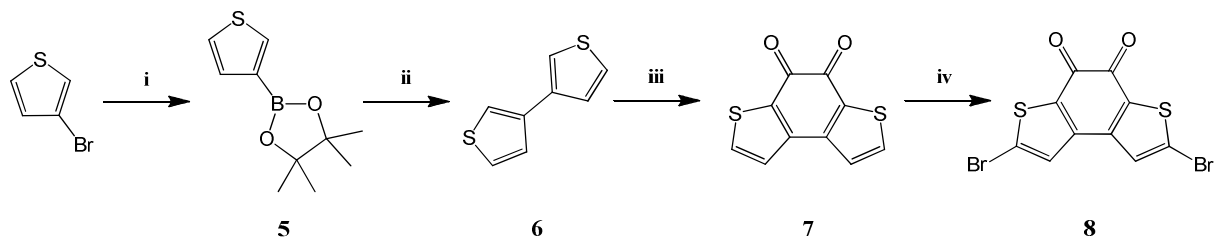
Scheme 5: Synthesis of Core material **8**: i. Pd(dppf)$_2$Cl$_2$, bis(pinacolato)diboron, KOAc, dioxane, 100 °C, 67 h, Ar$_{(g)}$, 73%. ii. Pd(PPh$_3$)$_4$, 3-bromothiophene, 2 M Na$_2$CO$_3$, EtOH, toluene, 100 °C, 20 h, Ar$_{(g)}$, 93%. iii. oxalyl chloride, 1,2-dichloroethane, 70 °C, 10 d, Ar$_{(g)}$, 79%. iv. Br$_2$, CH$_3$COOH, CHCl$_3$, 38 °C, 2h, 69%.

The synthesis of the dibrominated benzodithiophene-dione core **8** was achieved in four steps as shown in Scheme 5. The first step in the synthesis involved boronation of thiophene at 3-position from commercially available 3-bromothiophene in a way that would allow the coupling to the initial starting material and hence the formation of 3,3'-bisthiophene. The initial attempt to achieve **5** involved the formation of the boronic acid by lithiation with *n*-butyllithium of 3-bromo-thiophene in anhydrous tetrahydrofuran at -78 °C. The reaction was then treated with trimethyl borate and followed by hydrolysis to give the corresponding boronic acid. The reaction was carried out under various conditions [43,44] but failed to produce the desired product. In a second effort to create a suitable intermediate for the subsequent Suzuki coupling reaction, the transformation of 3-bromothiophene into the boronic ester was attempted and was carried out using bis(pinacolato)diboron, potassium acetate and dioxane in the presence of a palladium(II) catalyst as shown in Scheme 5. A yellow brown crystalline solid of **5** was prepared in a good yield (73%) but purification over silica had to be handled with care since this material seemed to partially degrade on silica for the acidity of silica.

To proceed to the synthesis of bisthiophene **6**, **5** was coupled with 3-bromothiophen under the same Suzuki coupling conditions as mentioned in Scheme 4. This gave **6**, in an excellent yield of 95%.

To build up the core material onto **6**, the third step was to form diketone **7**, which was achieved by dissolving **6** in anhydrous 1,2-dichloroethane (DCE) and oxalyl chloride was added in portions over 10 days as described in literature.[39] This was found necessary while monitored by thin layer chromatography (TLC). The reason for the slow addition of oxalyl chloride was to prevent over-acetylation of **6**

with an excess of reagent from occurring, thereby facilitating formation of the fused ring system. Upon heating to 70 °C the light yellow colour resulting from the dissolved bisthiophene changed to orange at first. Thereafter, the solution went darker in colour until a red precipitate formed which grew more densely in coming days. When no further change in the amount of **6** or **7** by spotting on TLC plates could be detected, the reaction was stopped, the precipitate filtered off and thoroughly washed with methanol, yielding 79% of a dark red powder.

Having synthesised **7** the next step in line was the halogenation of the second position on the thiophene rings. Before bromination was attempted, iodination procedures were tested on the benzodithiophene-dione core with the aim of being able to achieve superior reactivity in the subsequent Buchwald-Hartwig coupling, when compared to the dibrominated analogue, due to the lower dissociation energy of the C-I bond which facilitates oxidative addition to the Pd^0 centre of the catalyst.[45] As displayed in Scheme 6, iodination reactions were attempted under various conditions.[46,47] Unfortunately, both procedures lead to no conversion and to decomposition of some of the starting material.
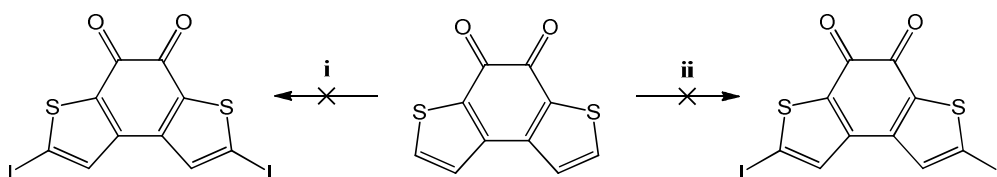
Scheme 6: Failed iodinations: i. I_2, AgOAc, $CHCl_3$, r.t. to 55 °C. ii. I_2, H_5IO_6, aq. EtOH.

While iodination of **7** was not possible, bromination of **7** was attempted, following literature.[39] In the method of Meyer A. *et al.* **7** was dissolved in chloroform ($CHCl_3$) and acetic acid (CH_3COOH) followed by the slow addition of bromine diluted 1:10 (vol.) in $CHCl_3$. After complete addition the reaction mixture was heated to reflux for 5 hours, then cooled, extracted and purified giving **8** in a 95% yield. When the bromination of **7** was attempted, the literature method was followed, which lead to over-bromination in each try while using shorter reaction times and a temperature of 50 °C. Hence the procedure was modified by suspending the starting material in a mixture of $CH_3COOH/CHCl_3$ followed by the slow addition of bromine in $CHCl_3$ (1:18) at 0 °C and subsequent heating at 38 °C for 2 hours. In all reactions performed, a thick bright orange precipitate crushed out within seconds after the first hour. After multiple attempts to raise the yield of 69 % for this reaction to the postulated 97 % by

Meyer A. et al.[39] it was concluded that, the reaction conditions listed above, are most efficient since a raise in reaction temperature as well as the extension of reaction time to 5 hours led to significant over-bromination and the formation of the dark red tribrominated analogue. When kept under a flow of nitrogen to prevent the possible accumulation of HBr in the reaction flask, formation of large amounts of the light red monobrominated product was observed. Due to the low solubility of this compound in common organic solvents, purification proved to be difficult. It was found that the best way to separate the two side products from the target compound was to dissolve 200 mg in about 200 ml of dichloromethane and to pass it through a column with a diameter of 8 cm and a path length of 20 cm using dichloromethane as eluent, yielding the bright orange solid.

^{1}H NMR spectra of compounds **5**, **6**, **7**, **8** were recorded and showed consistency with those reported in literature [39, 42]. ^{1}H NMR spectra of compounds **5**, **6**, **7** and **8** is displayed in Figure 15.
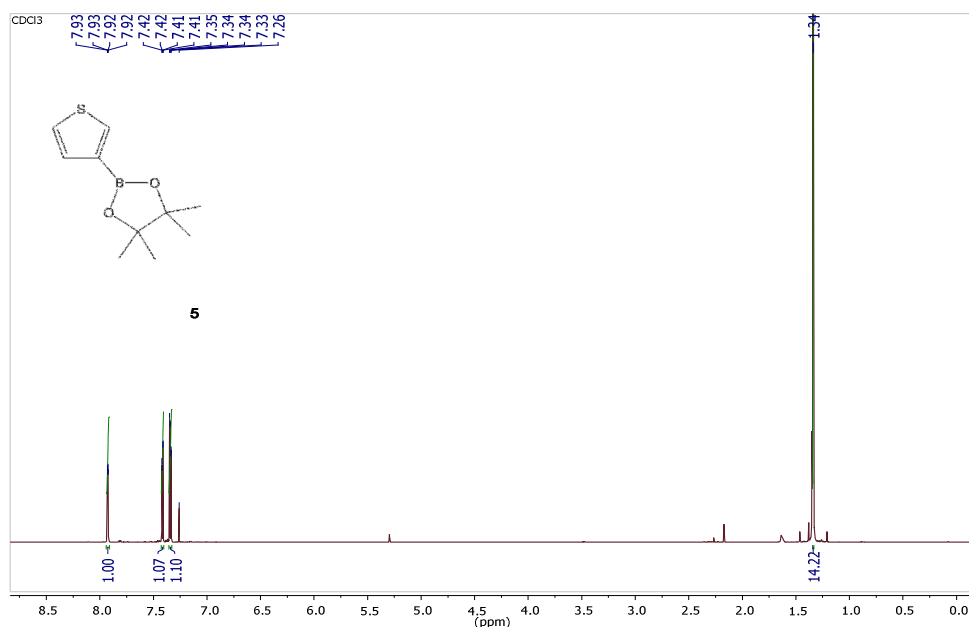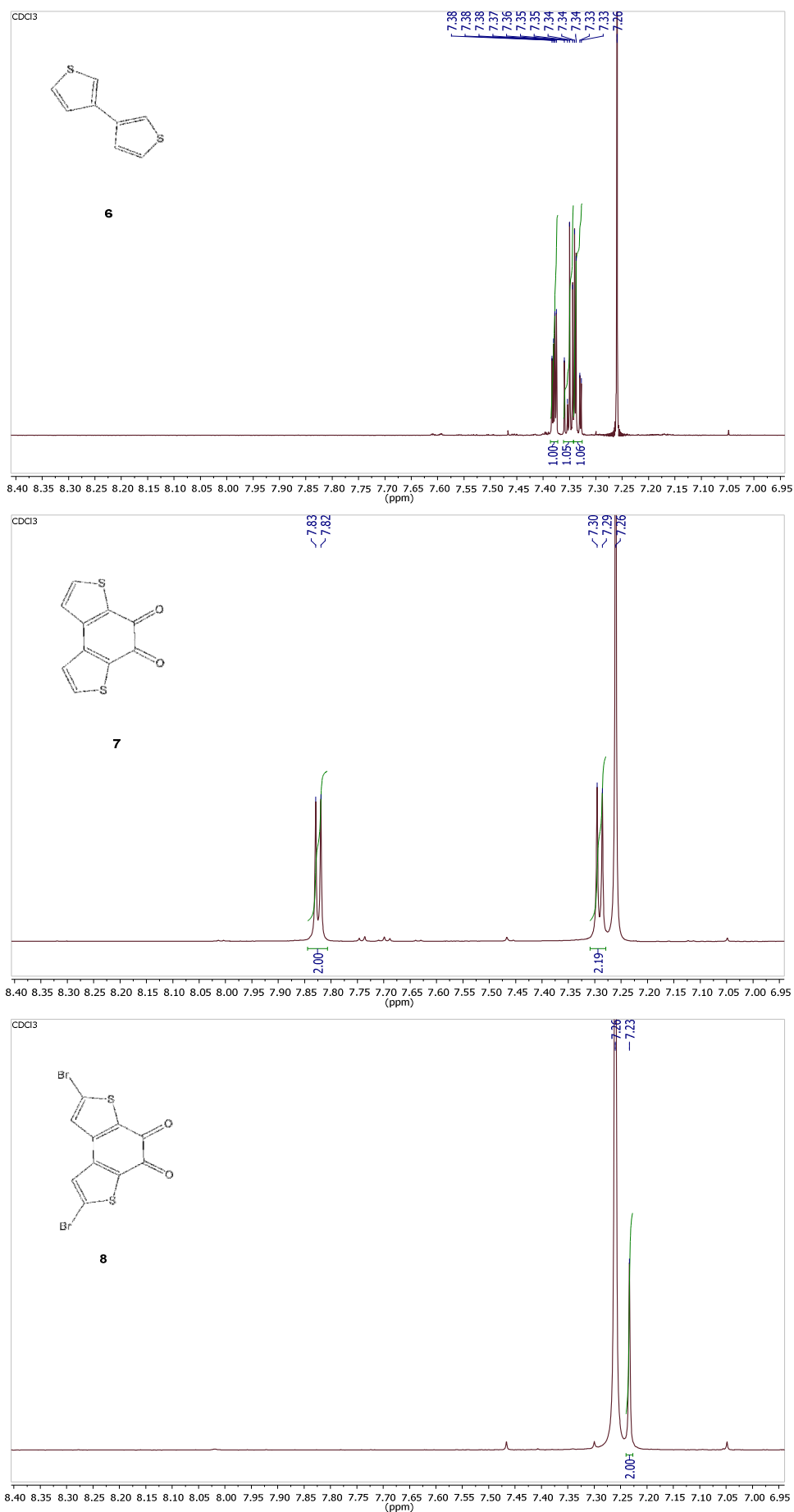
Figure 15: ^{1}H Spectrum of **5**, **6**, **7** and **8** in CDCl$_3$.

2.4 Synthesis of organic dye (e⁻-Donor/Core/e⁻-Acceptor): Route A
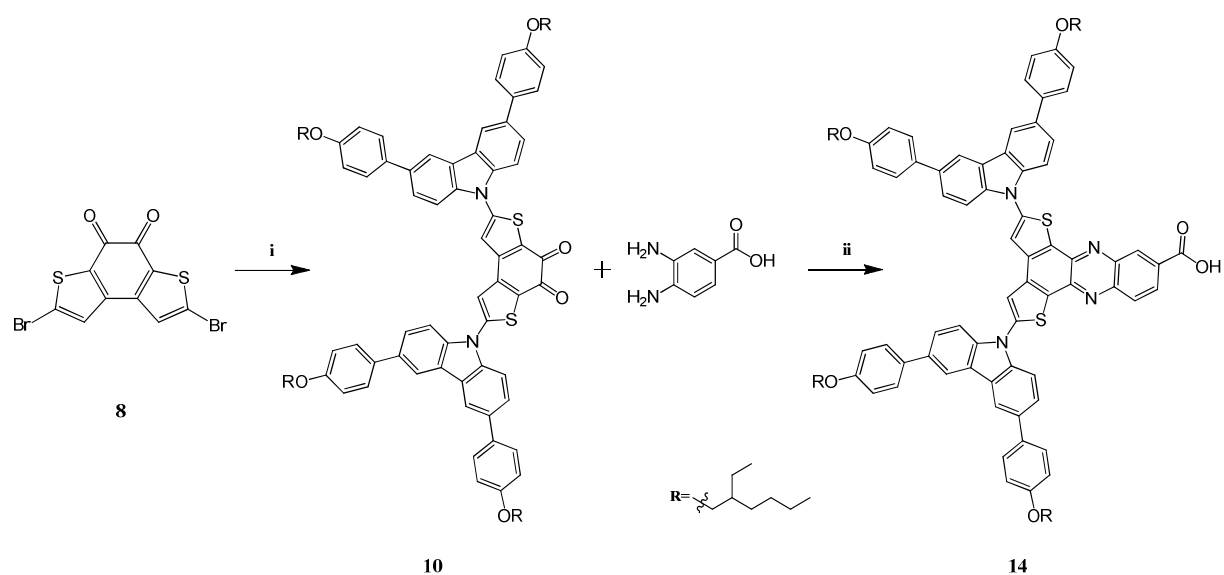
Scheme 7: Synthesis of e⁻-Donor/Core molecule **10**: i. Pd$_2$(dba)$_3$*CHCl$_3$, G$_1$-Carbazole, *t*-BuONa, [(*t*-Bu)PH]BF$_4$, xylene, Ar$_{(g)}$, 130 °C, 2 h, 34%. ii. CH$_3$COOH, 65 °C, Ar$_{(g)}$, 22.5 h.

With the core dibromothiophen diketone **8** in hand, the next step for the synthesis was to proceed to the coupling of the synthesised core **8** with the electron donating carbazole derivative **4**. This was first attempted under Buchwald-Hartwig conditions [48,49] in the presence of a catalyst formed *in situ* from a tris(dibenzylideneacetone)dipalladium(0)*CHCl$_3$ adduct and tri-*tert*-butylphosphonium tetrafluoroborate, in anhydrous xylene, and sodium *tert*-butoxide as a base.

For attempt one, all chemicals were transferred in a Schlenk tube, placed under argon and heated at 130 °C for 19 hours to yield a black-purple target compound **10** in 3% after purification with column chromatography (Table 1, entry1).

The successful synthesis of **10** in the reaction was supported by ¹H NMR spectrum (Figure 16). The ¹H NMR spectrum of **10** appeared to resemble those of the electron donor **4** with the most characteristic carbazole peak at 8.29 ppm corresponding to the proton at 4-position of the carbazole only experiencing a minor downfield shift of 0.02 ppm. Signals corresponding to phenyl rings in this structure were now fully detached from the remaining protons of the carbazole moiety, which lead to the formation of a AA'XX' at 7.03 and 7.63 ppm. Furthermore, the characteristic singlet of the thiophenyl proton had now shifted from 7.23 to 7.53 ppm moving from **8** to **10**. For the purpose of simplicity, only the aromatic region of the

spectrum is displayed below (Figure 16). Figure 17 shows matrix-assisted laser desorption-ionisation time of flight mass spectrometry of compound **10**, which displays desired peaks at 1368.02 and 1390.98 Da corresponding to [M]$^+$ and [M+Na]$^+$, respectively.
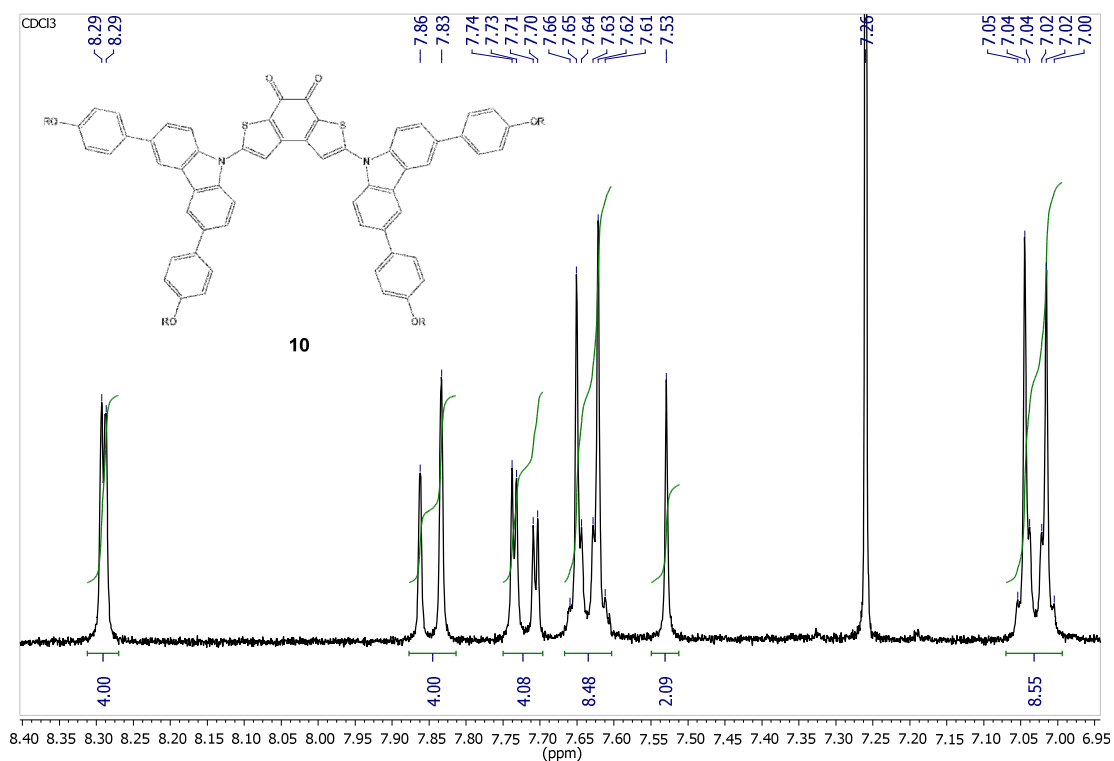
Figure 16: ^{1}H NMR spectrum of **10** in CDCl$_3$ displaying all peaks in the aromatic region.
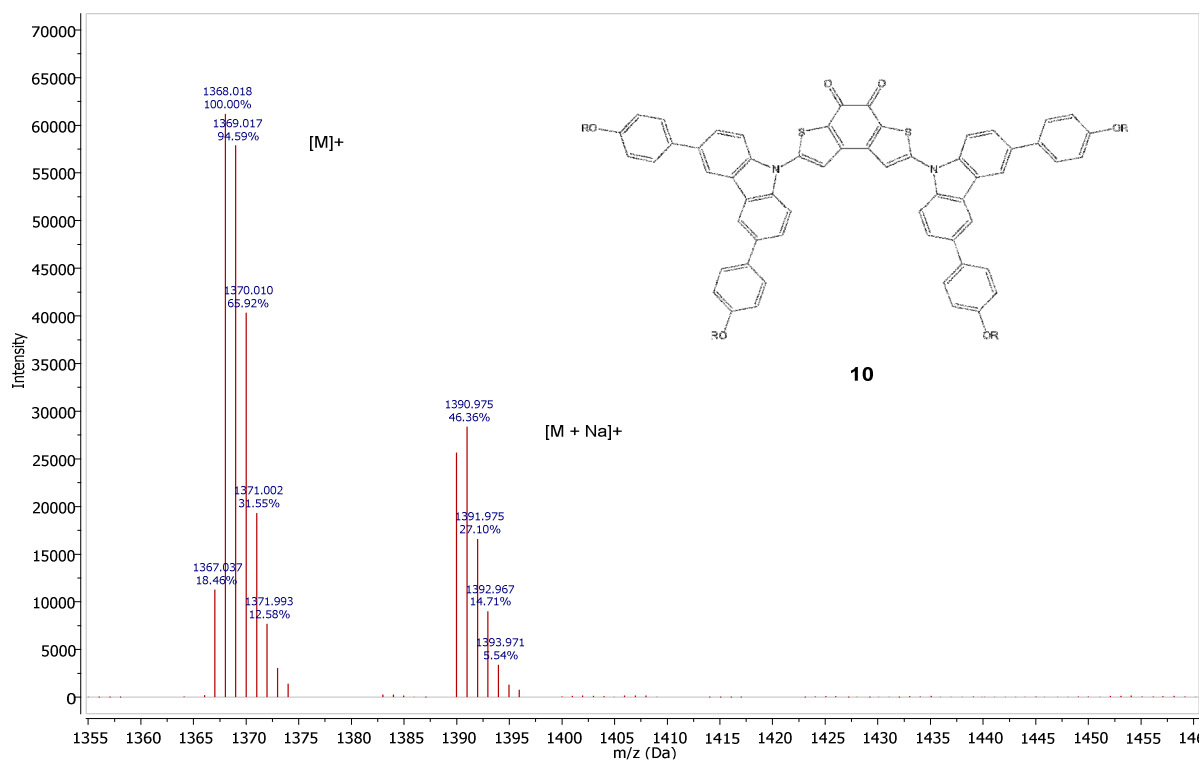
Figure 17: MALDI-TOF spectrum of **10** using DHB as matrix. [MALDI-TOF, DHB] [M]$^+$ calculated: 1367.7 (100%) vs. found: 1368.0 (100%).

This Buchwald-Hartwig coupling reaction was proved problematic while repeating the synthesis of **10** with respect to these particular starting materials. The reactions were repeated multiple times under different conditions and produced differing and inconclusive results, which are summarised in Table 1, displayed below.

Table 1: Summary of attempted synthesis of **10**.

	c (8) [mM]	c (4) [mM]	c (base) [mM]	c (ligand) [mM]	c (cat.) [mM]	xylene [ml]	T [℃]	t [h]	Yield [%]
1	86.7	213.3	346.7	146.7	20.0	1.5	130	66.5	3
2	62.5	150.0	250.0	100.0	12.5	0.8	130	2.0	34
3	61.5	138.5	246.2	100.0	15.4	1.3	130	19.0	0
4	80.0	200.0	330.0	130.0	20.0	1.0	120	2.0	0
5	80.0	200.0	320.0	130.0	20.0	1.0	130	21.5	7
6	65.0	163.0	261.0	106.0	13.0	10.0	130	48.5	n.d
7	61.5	153.8	261.5	100.0	15.4	1.3	110	19.0	0
8	61.5	153.8	246.2	100.0	15.4	1.3	120	19.0	0
9	63.6	150.0	68.2	100.0	13.6	2.2	130	63.0	0

The reaction was repeated under the same conditions but a shorter reaction time was applied giving the target compound **10** in a 34% yield (entry 2). In the third attempt a new batch of the starting material **8** was used with a reaction time of 19 hours, with no further changes made to the experimental procedure. Unfortunately no desired product formed while using a new batch of **8** (entry 3). Since the last attempt to synthesise **10** failed, the reaction was repeated but with heating at 120 ℃ and a reaction time of 2 hours which seemed to be beneficial when compared to the second attempt. Again, no formation of product could be observed (entry 4). Before the reaction was repeated compound **4** and **8** were further pre-dried and purified by column chromatography (entry 5). Product formation was confirmed by spotting on TLC plates after a reaction time of 3 hours. In order to achieve maximum conversion the reaction was extended to 21.5 hours and **10** was isolated by column chromatography in 7% yield. Success of the previous reaction seemed to be related to the additional purification step and hence the reaction was scaled up. Product formation was confirmed for attempt number six, but an increased formation of side

products which appeared to be related to longer reaction times and the strong streaking behaviour of **10** on silica made isolation of the target compound difficult. Hence, no yield was determined for this reaction. In order to systematically rule out temperature dependence of the reaction as well as batch-to-batch variations of compound **4** and the catalyst, the reaction was repeated with heating at 110 °C (entry 7), heating at 120 °C (entry 8) and a new batch of **4**. Both reactions did not affect the progress of this reaction. In attempt seven and eight the order in which the chemicals were added was altered. **8**, **4** and the ligand were transferred into a schlenk tube before xylene was added. The mixture was degassed under vacuum before catalyst and the base were added. A colour change from light yellow to dark brown was observed upon addition of sodium *tert*-butoxide almost instantly for both reaction mixtures. The reaction progress was monitored by spotting on TLC plates but at no point product formation was confirmed. The final attempt to synthesise **10** was made by heating at 130 °C and the use of a freshly synthesised batch of catalyst (entry 9). Unfortunately no change in results was observed.

In summary it can be said that every reaction in Table 1 gave a countless number of side products which complicated purification. Shorter reaction times seemed to give better results in terms of yield as noted for reaction two, while simultaneously a lesser amount of side products was observed, but in no instance remaining starting material could be recovered. This fact could support the observations made regarding the change in colour upon base addition.

To produce more **10** on a larger scale to facilitate the preparation of a wide range of dyes, alternative synthetic approaches were attempted. As noted in Scheme 6 that direct bisiodination of **7** had not been successful, to increase the reactivity of **8**, the two bromines of **8** were converted into di-iodines by using copper(I)iodide and potassium iodide in DMSO at 110 °C. This gave **9** in a 75% yield as a dark red solid with metallic glance. Since **8** and **9** share similar polarity on TLC, ^{1}H NMR spectroscopy was used to monitor the progress of this reaction. The appearance and growth of a downfield singlet (at 7.43 ppm) corresponding to the two thiophene protons of **9**, against the decrease in intensity of those of **8** at 7.23 ppm, could be observed. To investigate the outcome of this reaction further, LRMS was performed to show major peaks at 495 Da $[M + Na]^+$ and 511 Da $[M + K]^+$ which were identified to theoretical mass of **9**.

The synthesised diiodo-substrate was once again subjected to Buchwald coupling conditions. As shown in Scheme 8 the standard Buchwald coupling conditions described previously were first attempted without success. An Ullmann reaction was also carried out under weaker base such as potassium carbonate, which was thought to be favourable for the reaction's outcome. Again, the reaction failed to produce **10**.
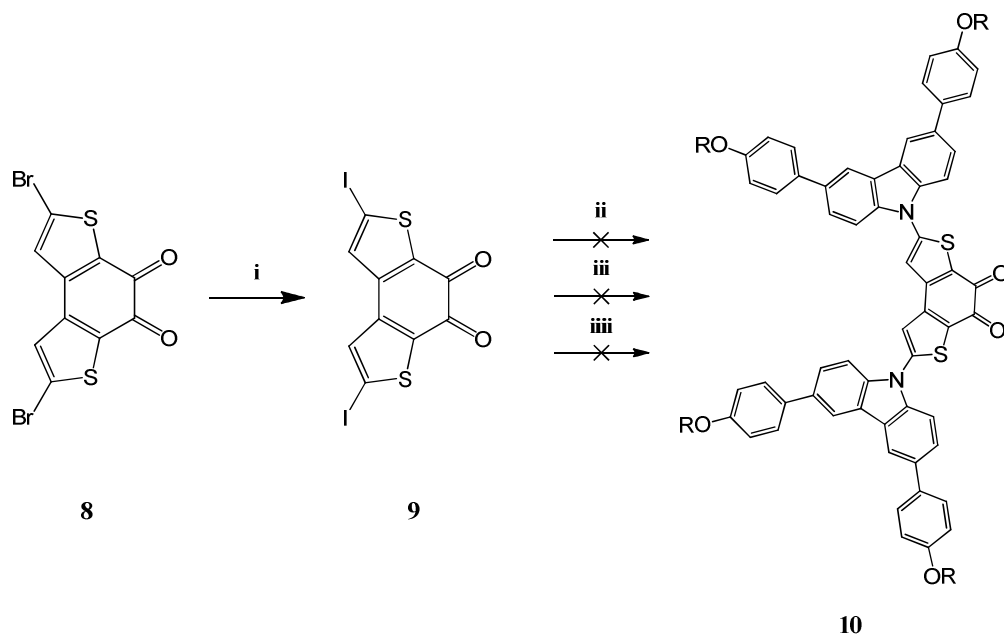
Scheme 8: Halide exchange and failed coupling reactions: i. KI, CuI, DMSO, 110 °C, 28 h, Ar$_{(g)}$, 75%. ii. Pd$_2$(dba)$_3$*CHCl$_3$, **4**, t-BuONa, [(t-Bu)PH]BF$_4$, xylene, 130 °C, 19 h, Ar$_{(g)}$. iii. **4**, Cu$_{(s)}$, K$_2$CO$_3$, NO$_2$Ph, 200 °C, Ar$_{(g)}$, 19 h. iiii. Pd$_2$(dba)$_3$*CHCl$_3$, **4**, K$_2$CO$_3$, 18-Crow-6, [(t-Bu)PH]BF$_4$, xylene, 130 °C, 16 h, Ar$_{(g)}$.

A further attempt to synthesise **10** was conducted using the same Buchwald coupling conditions as mentioned earlier, in the presence of sodium *tert*-butoxide, potassium carbonate as base and crown ether. This unfortunately did not yield **10**. Nevertheless, condensation of a small amount of **10** with 3,4-diaminobenzoic acid in glacial acetic acid at 65 °C for 22.5 h was attempted. The development of a dark red colour could be observed. Due to the small scale of the test reaction and the free carboxylic acid group of the dye, **14** could not be isolated in amounts that would have been sufficient for characterisation. MALDI-TOF mass spectrometry showed a mass peak at 1485.93 Da, which was close to that of (1484.00 g/mol), illustrating **14** was successfully produced (Figure 18).
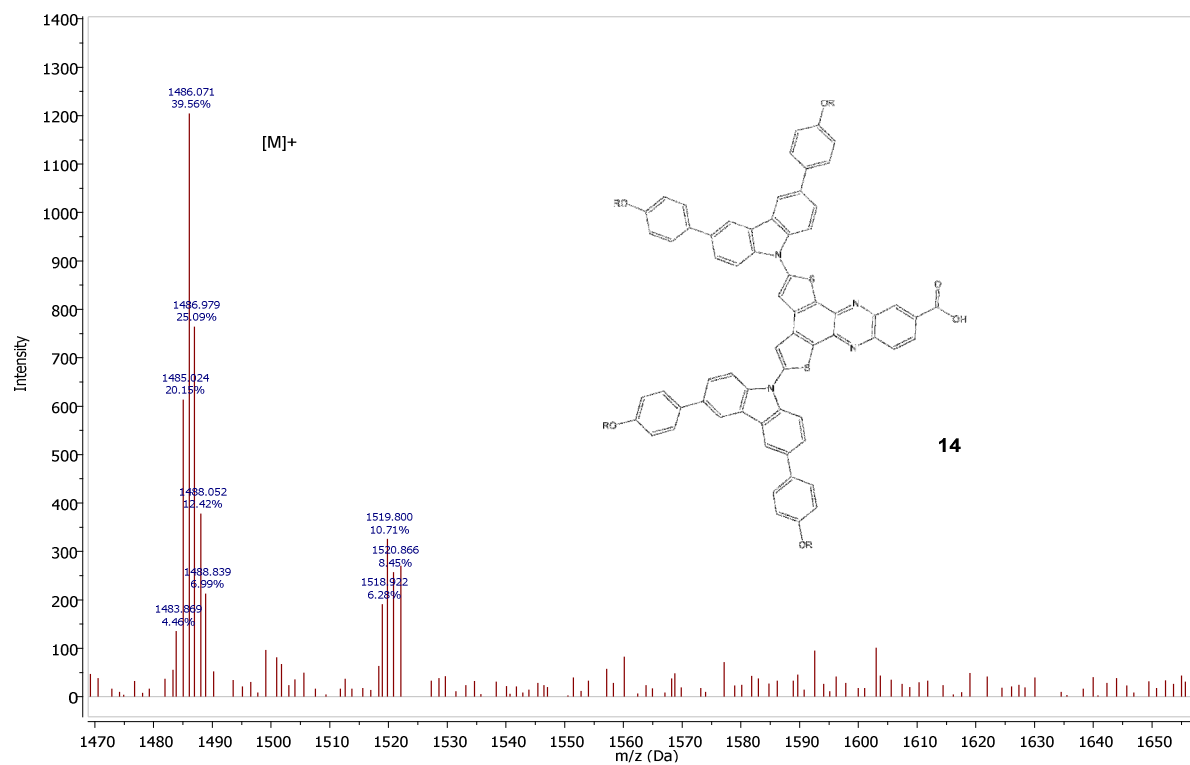
Figure 18: MALDI-TOF spectrum of crude material **14** from condensation reaction using DHB as matrix.

Due to the small scale of the free carboxylic acid group of **14** obtained in the test reaction, it was not sufficient for other characterisation.

2.5 Synthesis of organic dye (e⁻-Donor/Core/e⁻-Acceptor): Route B
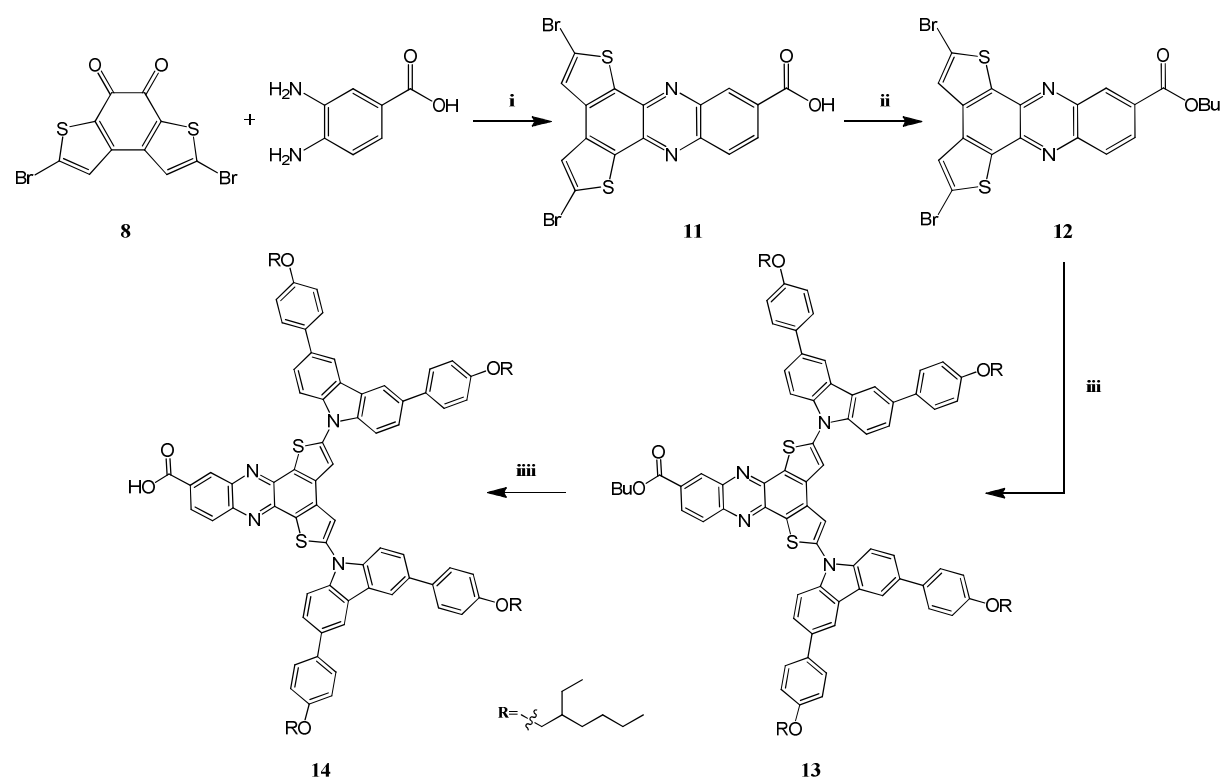
Scheme 9: Synthesis of Dye **14**: i. CH_3COOH, 50 °C, 22 h, $Ar_{(g)}$, 87%. ii. n-BuOH, $H_2SO_{4\ conc.}$, toluene, 130 °C, 42 h, $Ar_{(g)}$, 50%. iii. $Pd_2(dba)_3 \cdot CHCl_3$, **4**, t-BuONa, $[(t$-Bu)PH]BF_4$, xylene, 130 °C, 19 h, $Ar_{(g)}$, 26%. iiii. LiOH, MeOH, THF, H_2O, 65 °C, 14 h, $Ar_{(g)}$, 82%.

As displayed in Scheme 9, a similar synthetic approach to **14** was taken in comparison to route A. The major difference in route B involved a reversed sequence of synthetic steps. It was hoped that firstly conducting the condensation reaction of **8** with the diamino-benzoic acid would allow the creation of a stable core compound that could be subjected to the coupling reaction with the carbazole derivative **4**.

The first step in the new route was the formation of dithienophenazine carboxylic acid **11** by treating the diketone **8** with 3,4-dimaniobenzoic acid under similar conditions as discussed in Scheme 5 to give **11** in an excellent yield of 87% as a yellow-green solid. Compound **11** was found to be quite insoluble in common organic solvents, which made the purification over silica impossible. Furthermore, the low solubility of **11** means that the use of the solvent mixture of DMSO-d₆/CDCl₃ was required for ¹H NMR. This resulted in some broadening of peaks, which was probably due to the poor shimming as shown in Figure 19. The ¹H NMR spectrum showed the characteristic singlet at about 8.13 ppm, which corresponds to the two thiophenyl

protons of **11**. Additionally, two doublets at 8.26 and 8.34 ppm and one singlet at 8.83 ppm could be observed for the dithienophenazine carboxylic acid **11**
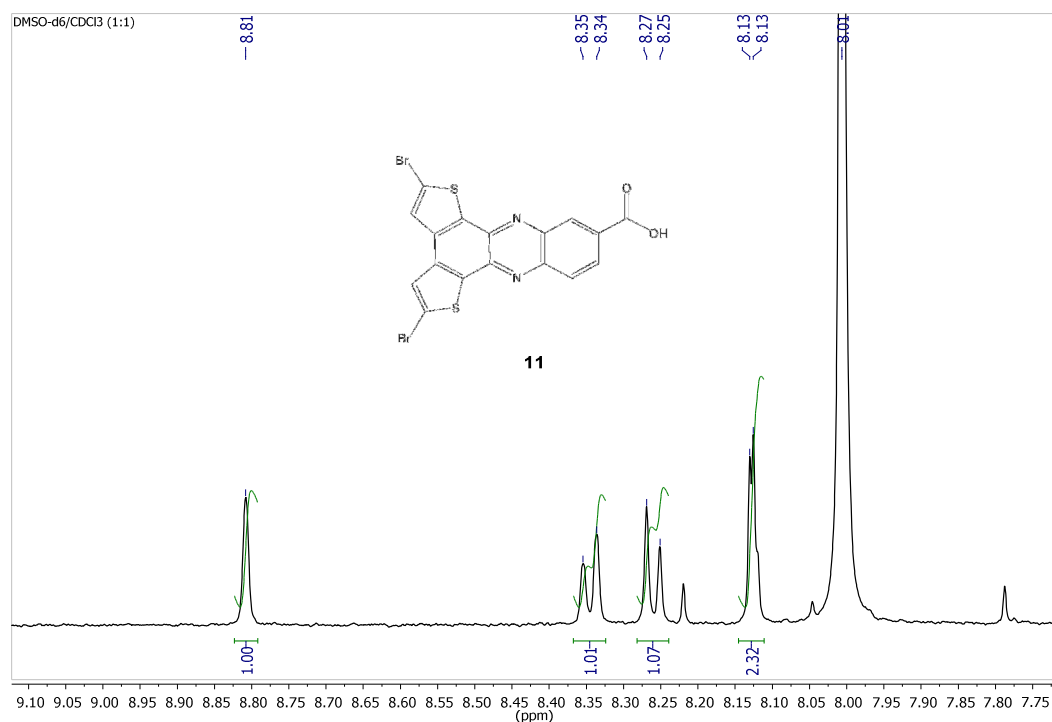
Figure 19: ^{1}H NMR spectrum of **11** in DMSO-d$_6$/CDCl$_3$ (1:1).

. The following esterification of **11** was carried out using *n*-butanol in order to increase the solubility of the materials for readily accessibility in the subsequent reaction but also to protect the free carboxylic acid. The reaction afforded **12** as a bright yellow solid in a mild yield of 50%. Despite the protection of the carboxylic acid and hence the introduction of a butyl group into the molecule, solubility increased only slightly. The slight improvement in terms of solubility gave way to a proton NMR spectrum with better resolved peaks in CDCl$_3$ (Figure 20). The ^{1}H NMR spectrum of **12** gave similar patterns of peaks in the aromatic region as those in **11** with the addition of three characteristic signals of a butyl group in the aliphatic region of the spectrum.

The dibromo-dithieno-phenazine-butyl ester **12** was then coupled to carbazole **4** using the same set of conditions as discussed in section 2.4 (Scheme 6). The dye ester **13**, was isolated using silica column chromatography in a 26% yield as a purple red solid. The low yield of this reaction appeared to be understandable regarding the formation of a number of side products in similar amounts. The eventual success in synthesising a stable core/e⁻-donor molecule was supported by the ^{1}H NMR spectrum of **13** as illustrated in Figure 20. As discussed before the major chemical

shift was experienced by the two-proton singlet originating from the thiophene rings in this structure, which was downfield shifted to 7.93 ppm, compared to **12**. The characteristic singlet at 9.02 ppm and the two doublets at 8.44 and 8.42 ppm that correspond to the dithienophenazine core as well as the presence of all carbazole related peaks observed for the spectrum of **10** supports the synthesis of **13**.
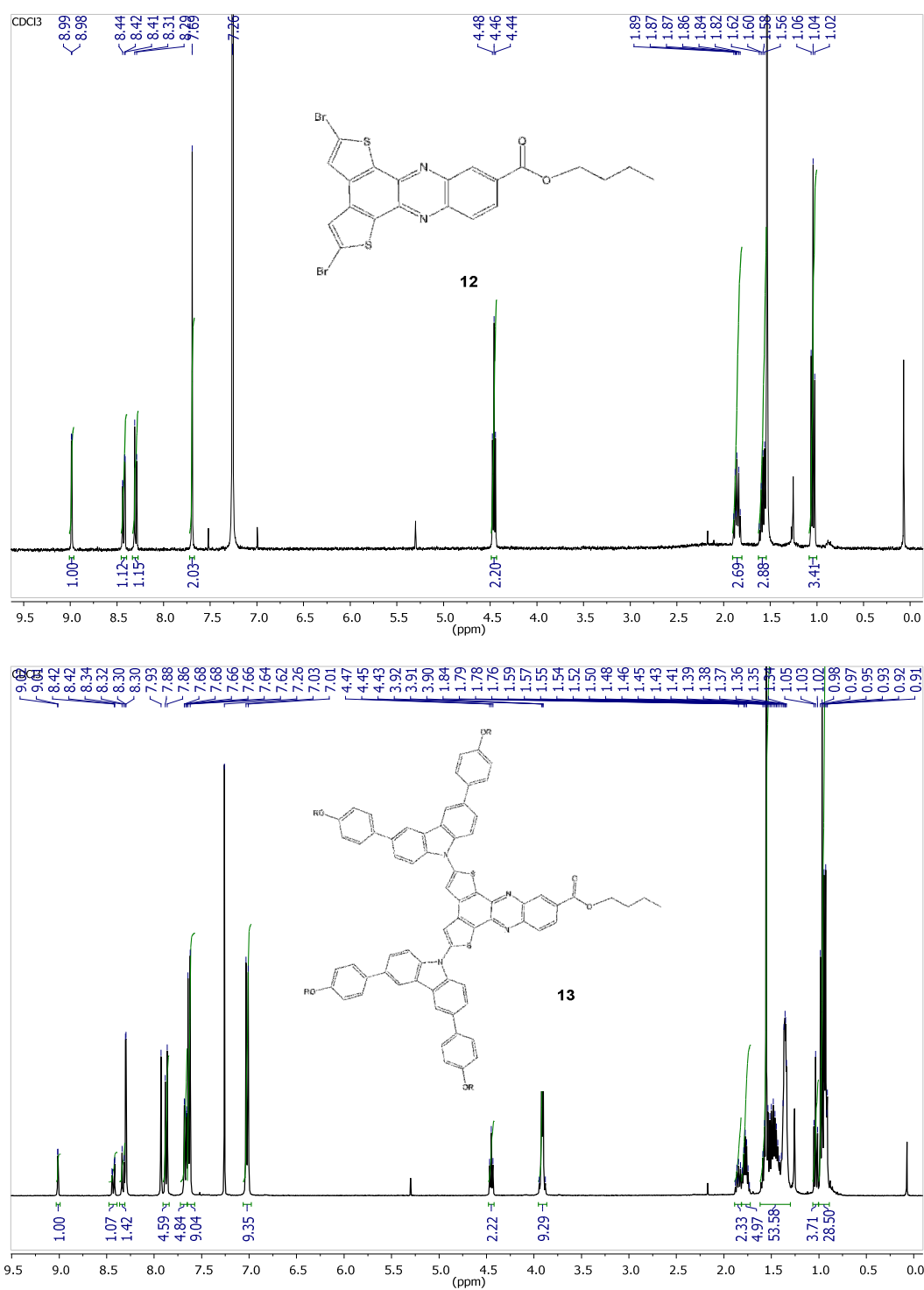
Figure 20: ^{1}H NMR spectrum of **12** and **13** in CDCl$_3$.

The final step in the synthesis of the target dye required the hydrolysis of the ester group in **13** which was carried out by using lithium hydroxide as the base in a solvent mixture of methanol/tetrahydrofuran/water (= 1:5:1). After 14 hours of heating at 65 ℃, a dark red solid was obtained in a good yield of 82%.

Although the material appeared to be soluble in $CDCl_3$, no interpretable ^1H NMR spectrum could be recorded at first. It was found that the broad hump in the aromatic region was due to strong aggregation behaviour of the dye in solution of concentrations as little as 2.0 mg/ml. This distinct broadening of signals is the result of aggregates moving slower in solution than individual molecules, therefore the signal averages over more different environments per proton species resulting in the observed effect.

The effect of different concentrations on the broadening of signals is illustrated in Figure 21. The chemical shift and appearance of observed peaks compared to Figure 22, can be accredited to the use of pure $CDCl_3$ as a solvent.
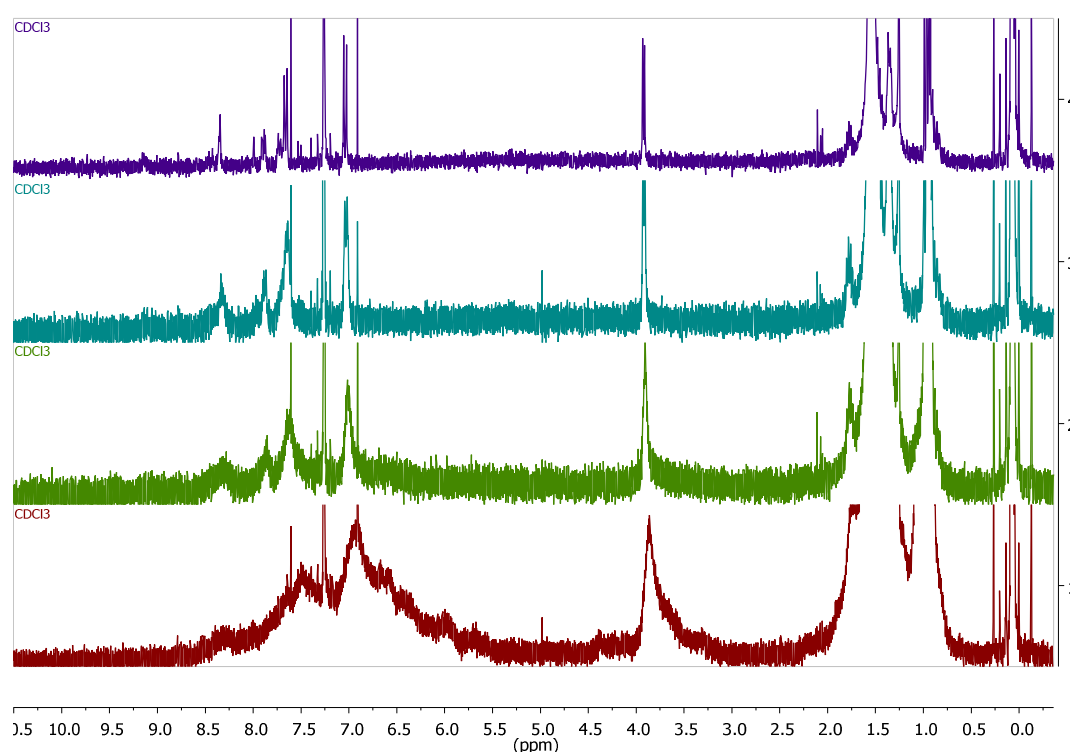
Figure 21: Concentration and solvent effect on the ^1H NMR spectrum of **13** in $CDCl_3$. Spectra are displayed in decreasing order of concentration (1 to 4) and sample solutions were made up accordingly: 1) maroon (4 mg/ml), 2) green (2 mg/ml), 3) blue (0.5 mg/ml) and 4) purple (0.25 mg/ml).

Dilution of the ^{1}H NMR sample and the addition of DMSO-d$_6$ seemed to facilitate the dissipation of aggregates as shown in Figure 22. Once again the ^{1}H NMR spectrum of the dye molecule **14** displayed all peaks that were reported and discussed before for dibromo-dithienophenazine-carboxylic acid **11** and the dye-butyl-ester **13** with the loss of signals related to the butyl group and the addition of a singlet at 10.60 ppm, corresponding to the carboxylic acid proton.
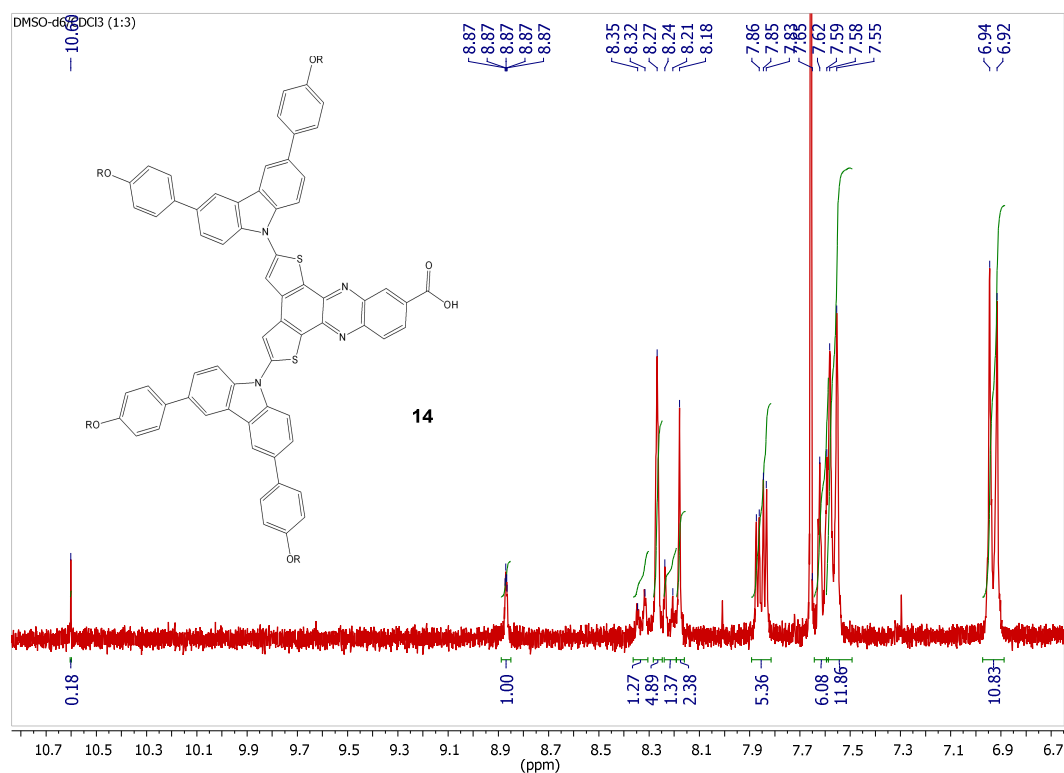
Figure 22: ^{1}H NMR spectrum of **14** in DMSO-d$_6$/CDCl$_3$ (1:3) displaying all peaks in the aromatic region (0.5 mg/ml).

The dye was further characterised with MALDI-TOF mass spectroscopy and the resulting mass spectrum indicated the presence of the expected mass peak at 1484.90 Da, displayed in Figure 23.
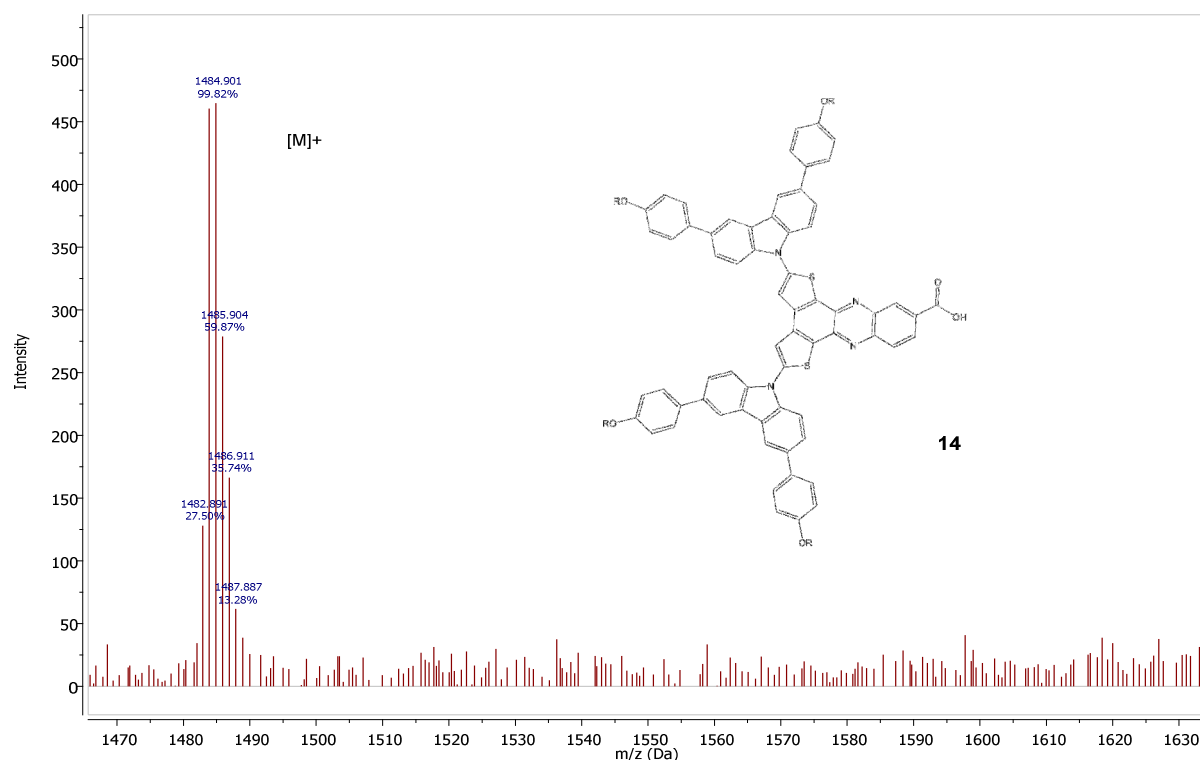
Figure 23: MALDI-TOF spectrum of **14** using DITH as matrix. [MALDI-TOF, DHB] [M]$^+$ calculated: 1483.7 (100%) vs. found: 1483.9 (96%).

From the means of characterisation mentioned above it was concluded that synthesis and isolation of **14** was successful. In addition to the provided mass and proton NMR spectra, elemental analysis of **14** further supported the successful formation of the desired dye **14** (see experimental section).

Chapter 3 - Material properties: Results and Discussion

3.1 Introduction

The novel dye **14** was successfully synthesised as discussed in chapter 2. It is important to study the photophysical, thermal and electrochemical properties of **14** to gain insights into the structure-property relationships and kinetic aspects in photovoltaic cells.

3.2 Photophysical properties

The photophysical properties of **10** to **14** were first studied by using UV-Vis (at concentration of 10^{-6} M). All spectra were measured in dilute solutions of dichloromethane, with the exception of compound **11**, whose inferior solubility in most common organic solvents required the use of acetone. The obtained data is displayed in Figure 24 and related spectral features are summarised in Table 2.

The absorption spectrum of **11** and **12** are essentially the same with minor blue shift in the absorption maxima of the double vibronic transition at 413 and 415 nm of **11** compared to **12**. Acetone exhibits multiple absorption maxima from 335 to 350 nm and is therefore responsible for the missing data below 350 nm in the spectrum of **11**. The UV-Vis spectra of synthesised materials **10**, **13**, and **14** can be divided into two distinct sections. The high energy transition at about 240 to 390 nm can be assigned as $\pi–\pi^*$ electron transitions of the carbazole derived electron-donating moieties [42] as well as the benzodithiophene-dione core. For compounds **10**, **13**, and **14** with carbazole attached, two bands with strong molar absorptivity at approximately 260 and 300 nm are visible. The absorption maximum of **13** and **14** at about 340 nm appears to originate from the condensed phenazine core which is missing in compound **10**. A similar absorption peak of equal intensity at shorter wave lengths (at about 315 nm) in the spectrum of **12** seems to support the latter. This batochromic shift may be ascribed to the coupling of the core material to the carbazole derivative and thereby resulting in the extension of π-conjugation. In this context, it is interesting to note that comparing molecules containing the free

carboxylic acid and their esterified analogues, latter ones exhibit slightly overall higher extinction coefficients.

The second region above 400 nm is marked by significantly weaker absorption bands which can be attributed to intramolecular charge transfer (ICT). [50] In the case of **13** and **14**, charge transfer occurs between the double donating carbazole units and the carboxylic acid electron-accepting anchoring group. However, absorption spectra of **11** and **12** also show the ICT related absorption bands at slightly shorter wavelengths (about 430 nm). This observation can be accredited to an inherent D-π-A character where thiophenes act as the electron rich part of the molecule (D) and the phenazine moiety with the carboxylic acid as the electron deficient one.[39] As expected, it was found that the spectrum of the dye **14** and the dye ester **13** are almost identical. The displayed spectrum of **14** (Figure 24) also shows a desirable red shift of ICT band at about 480 nm when compared to **11** and **12**, while at the same time a decrease in the molar extinction coefficient from 16.661 to 15.311 M^{-1}cm^{-1} could be observed. The red shifts of **13** and **14** is a direct result of the extension of π-conjugation.

Surprisingly, the UV-Vis spectrum of the black-purple solid **10** shows two absorption peaks at 445 and 560 nm which are indicative for a charge transfer process. The absorption maximum at the higher wave length stretches all the way to 755 nm and reaches the edge of the infrared part of the spectrum of light. In this case the diketo-group of the molecule most likely creates a strong electron withdrawing effect and hence generates these favourable absorption properties. These properties appear to be lost upon conducting the reaction between **10** and 3,4-diaminobenzoic acid. However, the condensation with a diamine is an inevitable synthetic step in order to create an extended conjugated system and therefore increase the molar extinction coefficient and red-shift the ICT band of the dye molecule.
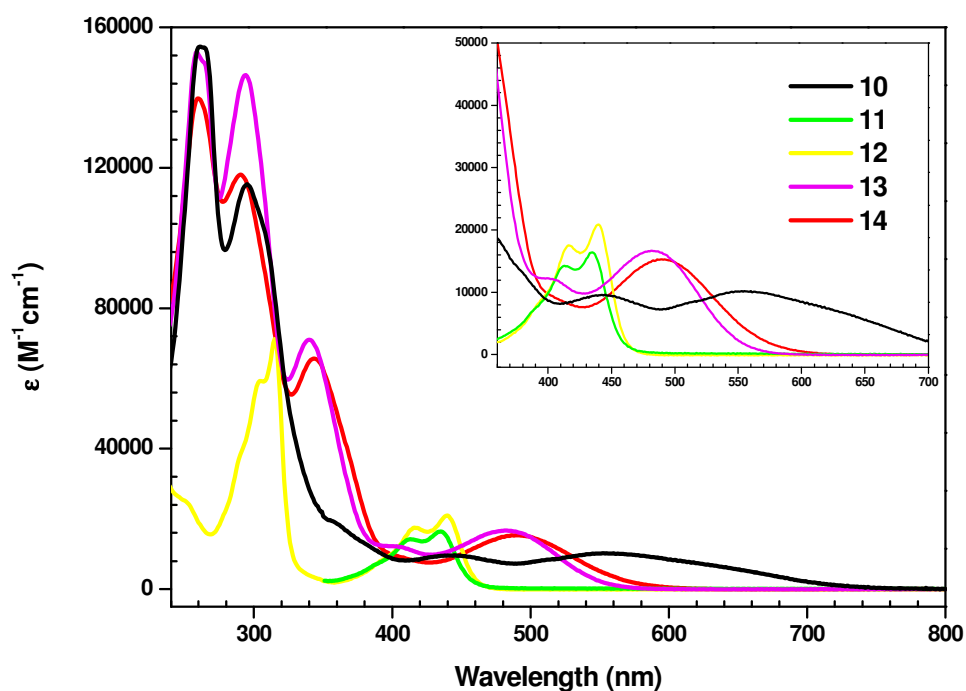
Figure 24: UV-Vis absorption spectra of compounds **10** to **14**.

In order to fully photophysically characterise the synthesised dye **14**, excitation and emission spectra were recorded in dilute dichloromethane solution (10^{-6} M), as shown in Figure 25.
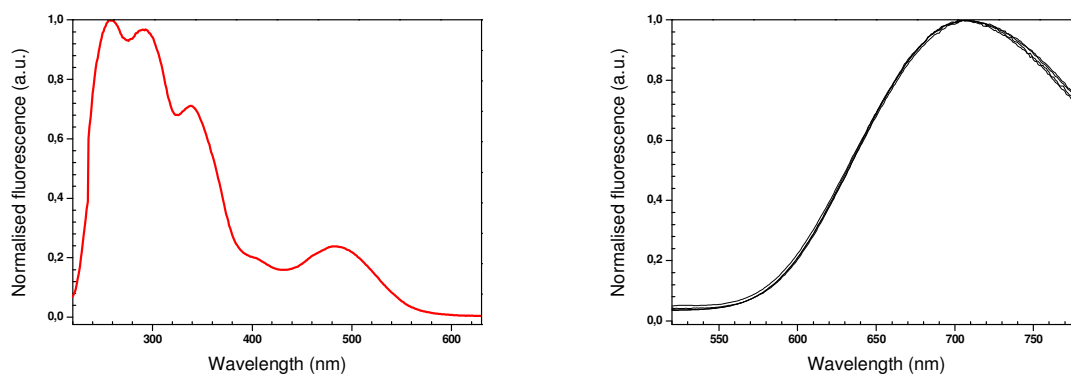
Figure 25: Left: normalised excitation spectrum of **14** in DCM (5 µM); Right: normalised fluorescence spectra of **14** in DCM (2.5 µM).

A 5 µM solution of the dye in DCM was monitored at 650 nm, which gave the emission as shown in Figure 25. All of the four absorption maxima as well as the shoulder at about 404 nm are displayed in good accordance with those in the previously discussed UV-Vis spectrum of **14** in Figure 24. The last step in the

analysis of spectral features of **14** was to examine its emissive properties. Using a 2.5 µM solution of the dye in DCM the compound was excited at wavelengths corresponding to its λ_{max} at 260, 290, 343, 489 nm and the emission spectrum is shown in Figure 25. It was found that excitation of each of the four wavelengths gave emission with maxima at 707 nm.

Table 2: Summary of photophysical properties of compounds **10** to **14**.

Compound	$\lambda^{abs}_{max}{}^a$ [nm]	Log ε^{abs}_{max} [M^{-1}cm^{-1}]	$\lambda^{em}_{max}{}^b$ [nm]
10	261, 295, 355 (sh), 445, 560	5.2, 5.1, 4.3, 4.0, 4.0	n.a.
11	413, 435	4.2, 4.2	n.a.
12	250 (sh), 290 (sh), 305 (sh), 315, 416, 440	4.3, 4.2, 4.8, 4.9, 4.6, 4.4	n.a.
13	259, 294, 340, 400 (sh), 481	5.2, 5.2, 4.9, 4.1, 4.2,	n.a.
14	260, 299, 343, 404 (sh), 489	5.2, 5.1, 4.8, 4.0, 4.2	707

a Values for compounds 10,12,13 and 14 were obtained in dilute DCM solution. Compound 11 was dissolved in acetone (10^{-6} M).
b Excited at the four absorption maxima.

3.3 Thermal properties

Thermal gravimetric analysis (TGA) was carried out with a heating rate of 10 °C/min to determine the decomposition temperatures (TGA$_{(5\%)}$), which were quoted at 5% weight loss. The trend suggests that the structurally related compounds **11** and **12** were thermally stable up to temperatures above 330 °C, while **13** and **14** were found to be stable up to temperatures above 410 °C. The TGA spectrum of **14** is displayed in Figure 26 indicating an occurring weight loss of 5 % at 420 °C.

Melting points of the respective materials were recorded on a Buchi melting point apparatus with a heating rate of 2 °C/min. It should be noted that melting points could only be found for the butyl ester analogues **12** and **13** while the two compounds **11** and **14**, which contain the free carboxylic acid, only possess decomposition points. Recorded melting and decomposition points are summarised in Table 3.
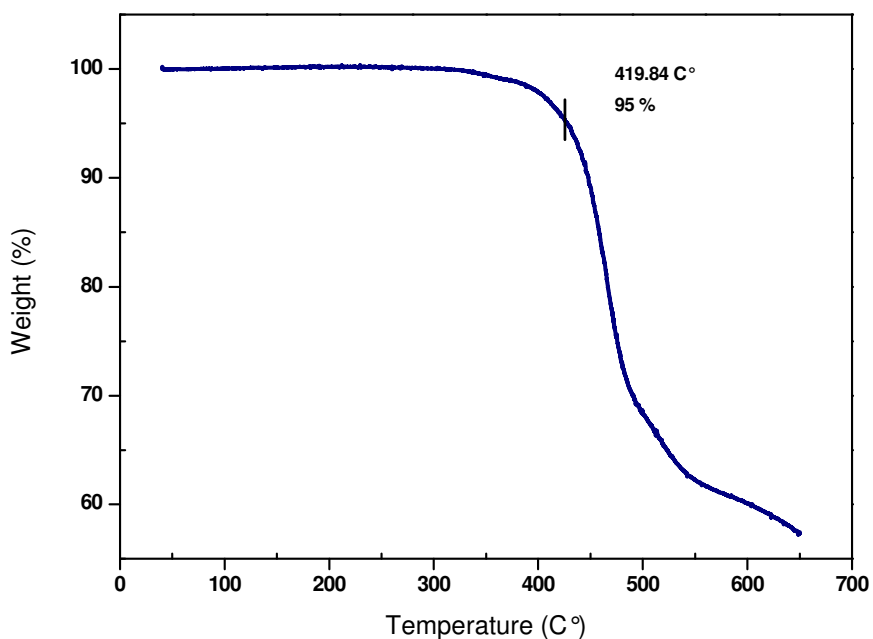
Figure 26: TGA spectrum of **14** quoting TGA$_{(5\%)}$ for 5 % weight loss.

Differential scanning calorimetry was carried out at a heating rate of 100 °C/min, examining two different temperature ranges from -150 to 200 °C (left) and 0 to 250 °C (right) as shown in Figure 27 below. With the experimental set-up only being calibrated up to 250 °C, no transitions could be detected within the observed temperature ranges.
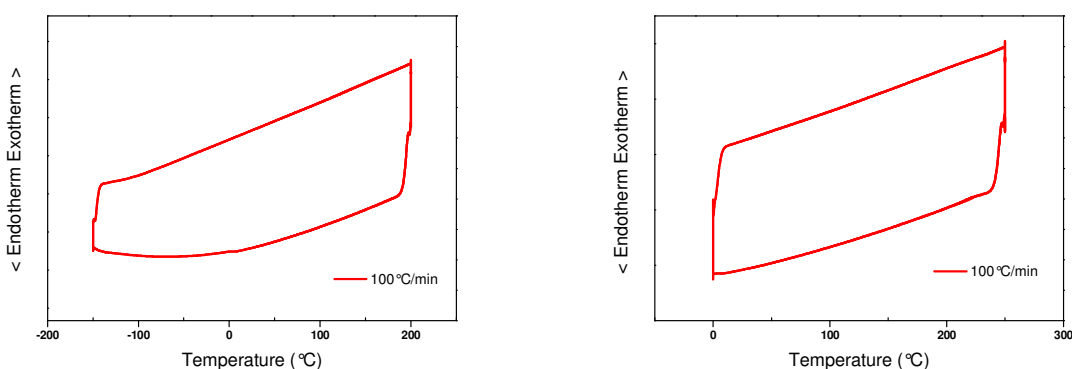
Figure 27: DSC spectrum of compound **14** in a temperature range from -150 to 200 C° (left) and from 0 to 250 C° (right).

Data obtained from TGA and DSC as well as the determined melting points of the synthesised compounds indicate high thermal stability, which makes **14** suitable for operating under standard DSSC conditions.

Table 3: Summary of melting and TGA of compounds **11** to **14**.

Compound	mp [℃] [a]	TGA$_{(5\%)}$ [℃] [b]
11	n.a.	383
12	265.9-266.2	331
13	294.4-296.1	415
14	n.a.	420

[a]   Determined on a Buchi melting point apparatus with a heating rate of 2 C°/min. The range from the start of the melting process to to when they have completely melted was reported.

[b]   Measured in a thermal gravimetric analyser with a heating rate of 10 C°/min. T$_{dec}$ was quoted for 5 % weight decomposition.

3.4 Electrochemistry

The ability to absorb a wide region of the spectrum of light is an essential requirement for a photovoltaic cell, but the following step of charge generation of the closely bound electron-hole pair within an organic molecule has an impact on device performance as well.[52] This process occurs at the interface between the dye and the titanium dioxide displaying a preferred energy level alignment.[53] Hence, cyclic voltammetry was performed to examine the redox properties and estimate the HOMO and LUMO energy levels for the possibility of electron transfer from the excited dye molecule into the conducting band of TiO_2 and regeneration of dye from the electrolyte.

Reduction and oxidation potentials were determined using a standard three-electrode electrochemical cell, where a platinum electrode served as working electrode, platinum wire as counter electrode and $Ag/AgNO_3$ as non-aqueous reference electrode. A solution with a 1 mM sample concentration and 0.1 M electrolyte (tetrabutylammonium tetrafluoroborate) concentration in tetrahydrofuran was prepared for the measurement which was conducted at room temperature and deoxygenated by purging with argon. Calculated half-wave potentials ($E_{1/2}$) were referenced externally to the ferricenium /ferrocene (Fc^+/Fc) redox couple which has a potential of $E_{0(Fc+/Fc)} = 0.802$ V vs. NHE (in THF).[54] HOMO and LUMO energy levels were calculated from the determined $E_{1/2}$s and based on the standard energy level of ferrocene (4.8 eV below the vacuum level, which per definition is set as zero).[51]

$$E_{HOMO\ (CV)} = -[E_{1/2,\ ox} - E_{(Fc/Fc+)} + 4.8\ V]\ eV$$

$$E_{LUMO\ (CV)} = -[E_{1/2,\ red-1} - E_{(Fc/Fc+)} + 4.8\ V]\ eV$$

For the new dye **14**, only a single oxidation process was observed in tetrahydrofuran. The found oxidative cycle appeared to be chemically reversible under the applied conditions, as shown in Figure 28. Oxidation half-wave potentials were calculated by averaging the anodic and cathodic peak potentials to give a value of 0.53 V (vs. Fc^+/Fc) for $E_{1/2,ox}$.

Regarding the reduction potentials, the dye was found to exhibit one chemically reversible reduction profile in tetrahydrofuran (Figure 29). Again, the reduction half-wave potential was calculated by averaging the anodic and cathodic peak potentials. This gave a value of –1.76 V (vs. Fc^+/Fc) for $E_{1/2,red}$. Along with these observations, energy levels of HOMO and LUMO could be estimated by using the equation stated above, to give -5.33 eV and -3.04 eV for HOMO and LUMO, respectively. This also gave a band gap$_{(CV)}$ of 2.28 eV for the dye as summarised in Table 4. The occurrence of the observed first oxidation and reduction peak was further validated by the use of differential pulse voltammetry (DP).
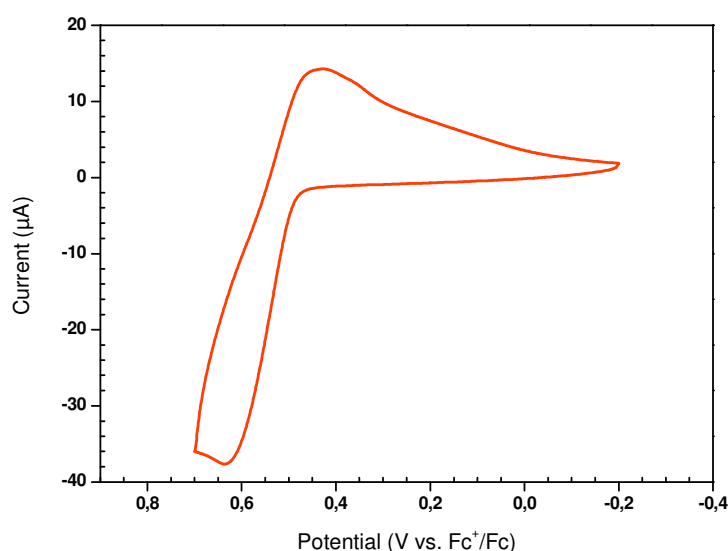
Figure 28: CV of **14** in THF showing the oxidative cycle vs. Fc^+/Fc. (Pt working electrode, scan rate = 100 Vs^{-1}).
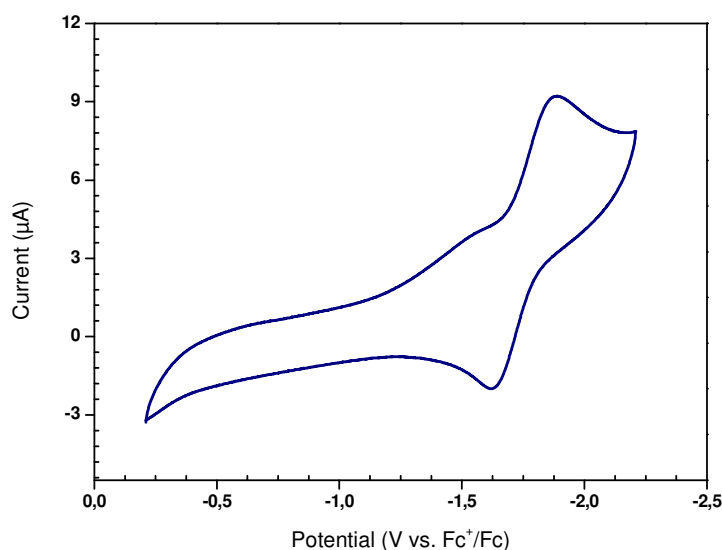
Figure 29: CV of **14** in THF showing the reductive cycle vs. Fc$^+$/Fc. (Pt working electrode, scan rate = 500 Vs^{-1}).

Using the Planck distribution stated in the equation below, the optical band gap energy can be estimated with λ being the absorption onset wavelength of the ICT band of the dye in solution and h*c corresponding to a value of 1240 [eV*nm].

$$\text{Band gap Energy (E)} = h^*c/\lambda \text{ [55]}$$

The band gap deduced from the UV-VIS spectrum of the material (with onset at 580 nm) gave a value of 2.14 eV which is 0.14 eV lower when compared to the band gap received from the CV experiment.

Table 4: Summary of electrochemical data.

$E_{1/2, ox}$ [V] [a]	$E_{1/2, red1}$ [V] [a]	E_{HOMO} [eV] [b]	E_{LUMO} [eV] [b]	Band gap$_{(CV)}$ [eV] [c]	λ_{ONSET} [nm]	Band gap$_{(UV)}$ [eV] [d]
0.53	-1,76	-5.33	-3.04	2.28	580	2.14

[a] Values are referenced externally against Fc$^+$/Fc by adding 0.21 V.
[b] E_{HOMO} and E_{LUMO} were determined by referencing $E_{1/2, ox}$ and $E_{1/2, red}$ against the external standard Fc/Fc$^+$ and based on the standard energy level of ferrocene (+ 4.8 V).
[c] Determined by $E_{HOMO} - E_{LUMO}$
[d] Determined by the onset of the UV-Vis ICT absorption band of **14** and calculated via equation for Planck distribution.

At this point it is worth noting that at least 100 to 200 mV in terms of a potential gradient between the dye's HOMO energy level and the conduction band edge energy level of TiO_2 as well as between the dye's LUMO energy level and the energy level of the electrolyte is needed as the thermodynamic driving force to facilitate electron transfer reactions in a photovoltaic cell.[56] With the HOMO level of the new dye being more positive than the iodide/triiodide redox couple (I^-/I_3^- ~0.42 V vs NHE) enough driving force for the efficient regeneration of the oxidized dye can be expected.[53,57] Furthermore, the excited state oxidation potential of the sensitizer is more negative than the conduction band edge of TiO_2 (-0.5 V vs NHE) indicating that electron injection is energetically favourable.[58] Energy levels (referenced to NHE) of related materials such as TiO_2, the N3 standard reference dye and the I^-/I_3^- redox mediator are displayed for comparison in Figure 30 (taking -4.5 eV vs. vacuum level corresponding to 0 V vs. NHE).[59] A schematic representation of the dye's working principle in a DSSC is displayed in Figure 31.
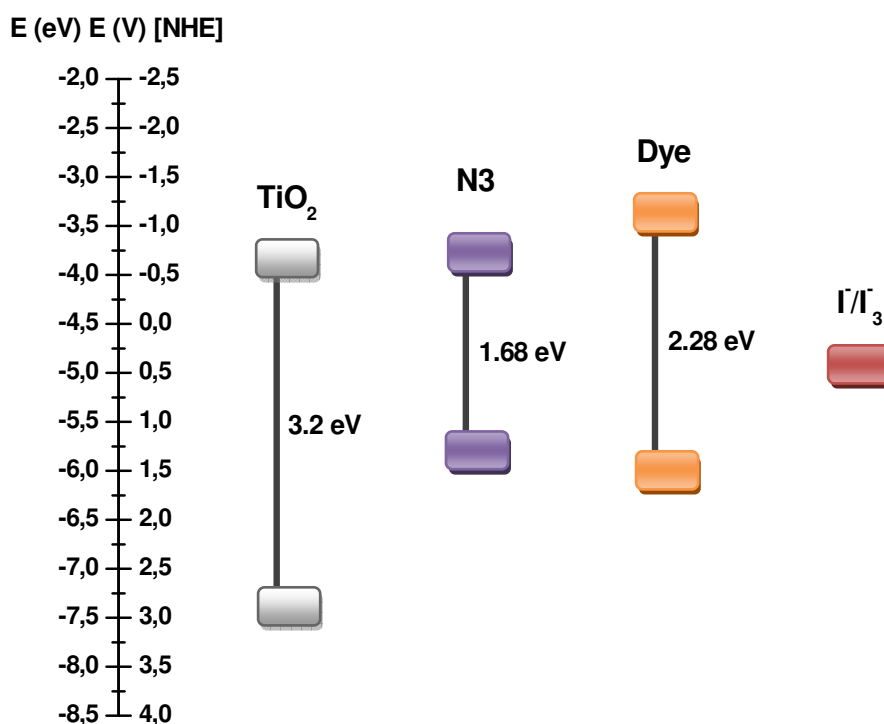
Figure 30: Energy levels and band gaps of dye **14** and related materials.
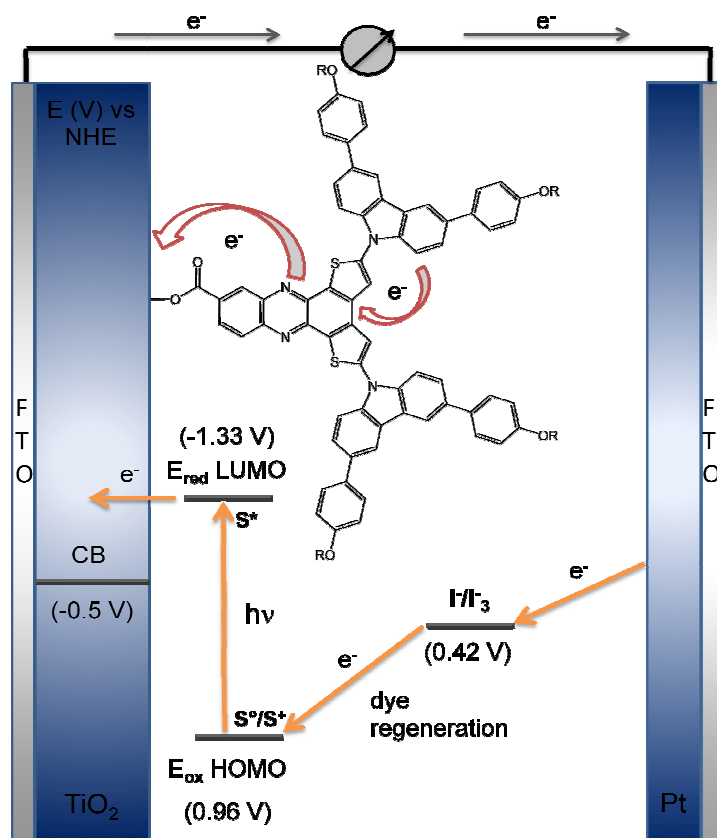
Figure 31: Scheme of e⁻-injection and dye regeneration in a DSSC according to the energy levels of **14** and related materials.

3.5 Adsorption characteristics and kinetics

Dyes can be adsorbed onto titanium oxide from a whole range of organic solvents. In order to make a statement on the amount of dye molecules being adsorbed onto TiO_2 in the process of cell preparation as well as the order of adsorption kinetics thereof, dye adsorption measurements were performed following literature.[60] The use of different solvents for the sensitisation of the photoanodes can lead to diversified interactions between dyes and the solvent, ultimately changing properties existing between the dye and the semiconductor surface, which makes the choice of solvent important in order to obtain high conversion efficiencies.[61,62] While solvents with higher dielectric constants seem to be favourable for dye adsorption, it is speculated that the solvent-specific solvation state of the molecule determines whether a dye exists in its monomer or aggregate state, with the latter resulting in a decrease of device performance.[63]

Due to time constraints it was not possible to optimize solvent compositions for adsorption. The experiments were conducted in distilled N,N-dimethylformamide (DMF) due to its high boiling point which would ensure minimal solvent loss through evaporation during the experiment and under the assumption that the high dielectric constant ($\varepsilon_r = 38$) of the solvent would facilitate dye adsorption. Firstly, absorption spectra of solutions of the dye at concentrations ranging from 1×10^{-4} molL^{-1} to 2.5×10^{-5} molL^{-1} were recorded on a Cary 5000 UV-Vis-NIR spectrophotometer to establish the linear correlation between concentration and absorption according to the Beer-Lambert law, as shown in Figure 32.

Equation	y = a + b		
Adj. R-Squa	0,99993		
		Value	Standard Err
B	Intercept	0	--
B	Slope	0,0140	4,68162E-5
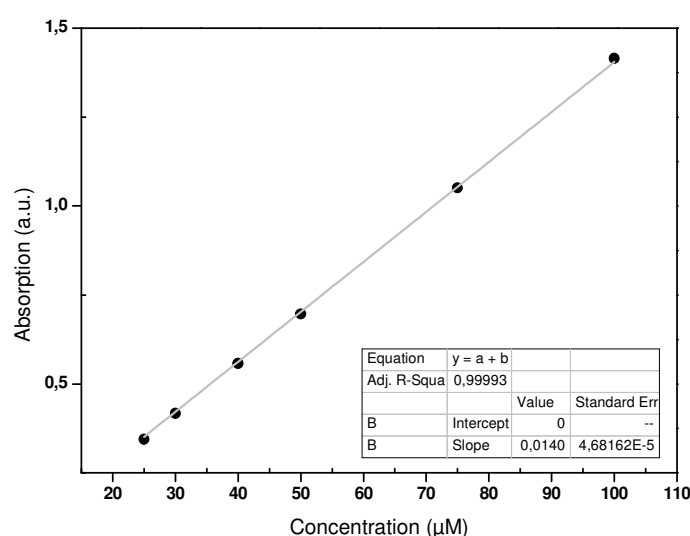
Figure 32: Absorption data of the organic dye at 6 different concentrations (solid line represents the linear regression fit).

Secondly, a dye solution in DMF with the initial concentration of 5×10^{-5} molL^{-1} was prepared and its absorption spectrum measured. The TiO$_2$ substrates were baked at 450 °C for 40 minutes and then kept at 80 C° before immersion into the prepared dye solution in a UV cuvette with the dimensions of 1 cm x 1 cm. After the initial dipping the change in absorbance of the longest wavelength band at λ_{max} (467 nm) over time (Figure 33) was monitored every 30 min for the first 2 h, hourly up to 10 h and then hourly from 23 h to 30 h.

This method allows for the *in situ* determination of the decrease in dye concentration as a function of time. The method poses several advantages over more commonly used procedures that use strong bases such as tetrabutylammonium hydroxide to desorb the dye from TiO$_2$ after the uptake experiment which neither

guarantees the stability nor the full desorption of the dye and therefore its full recovery.[64]
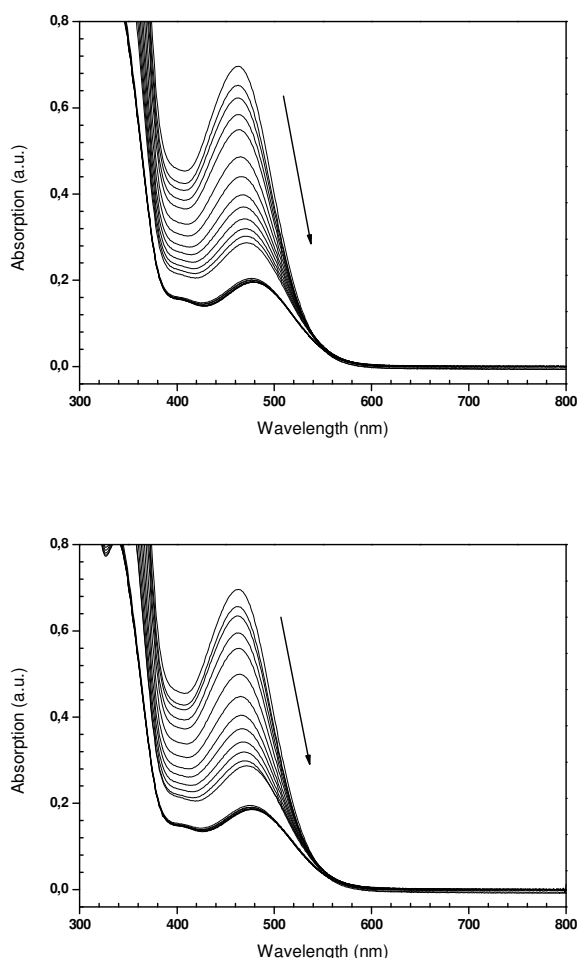
Figure 33: Decrease in absorption of dye solution (initial conc.: 5×10^{-5} molL^{-1}) upon adsorption onto TiO$_2$ substrate 1 (top) and 2 (bottom) measured over a period of 30 h (0 min, 30 min, 60 min, 90 min, 2h, 3 h, 4 h, 5 h, 6h, 7 h, 8 h, 9h, 10 h, 23 h, 25h, 26 h, 27 h, 28 h, 29 h, 30 h).

The active area of the photoanodes (purchased from Dyesol) was determined by using the ImageJ software package and were determined to be 0.806 cm^2 (Substrate 1) and 0.821 cm^2 (Substrate 2), respectively. Consecutively, the amount of adsorbed dye was then determined by comparison with the standard solutions of know concentrations and the equation received from the linear regression fit in Figure 32. The dye uptake profiles (N$_t$) as a function of time are displayed in Figure 34. It was found that the rate of dye adsorption is initially rapid and reaches a plateau after 28 to 30 h which represents the equilibrium value associated with maximum dye uptake.[60]
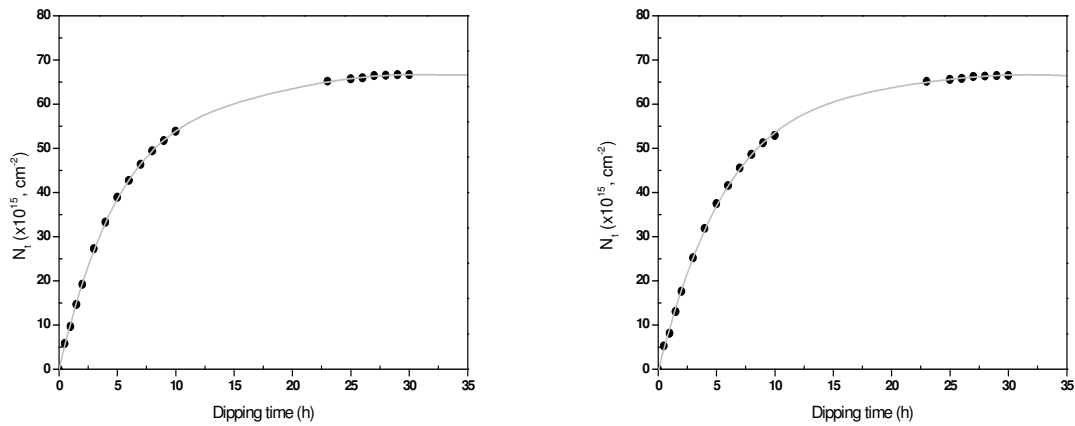
Figure 34: Adsorption data for the organic dye onto TiO_2 substrate 1 (left) and 2 (right) measured over a period of 30 h (solid line represents the numerical regression fit).

Taking into account different active surface areas of substrate 1 and 2, the amount of dye molecules on the surface of both substrates was almost identical (Table 5) with an average of 65.79 x 10^{15} [cm^{-2}] molecules being adsorbed.

It was recently suggested by B.-K. An et al.[60] that the molecular volume of a dye determines the amount of dye being adsorbed onto TiO_2 in the dipping process. The paper states that the amount of dye uptake at equilibrium is controlled by steric hindrance. While the overall rate-limiting step in such nano-porose inorganic matrices is due to chemisorption, kinetic hindrance also controls the initial uptake rate.[60, 65] The effect of the molecular volume on dye uptake as well as the molar extinction coefficient of a dye can therefore both be seen as first order parameters and hence are directly related to conversion efficiencies in terms of device performance.[60] With respect to the size of the sensitizer molecule a satisfactory amount of dye was adsorbed onto TiO_2, which should provide good initial results in terms of device performance.

Table 5: Amount of dye molecules adsorbed.

	N [cm^{-2}]
Substrate 1	65.84 x 10^{15}
Substrate 2	65.73 x 10^{15}
Average	65.79 x 10^{15}

The mechanism of the dye adsorption process can be investigated by the use of kinetic models. Dye adsorption onto to titanium oxide tends to follow the pseudo-

second-order rate law and hence was analysed using the equation expressed as [65,66].

$$\frac{1}{c_t} = \frac{1}{c_e} + k_{ads}t$$

where t stands for dipping time in hours, c_t for the concentration of soluted sorbent (dye) on the surface of the sorbent (TiO$_2$) at any time t in $(\mu M*L)^{-1}$, c_e for the concentration of soluted sorbant (dye) at equilibrium in $\mu M*L^{-1}$ and k_{ads} for the rate constant of adsorption in $(\mu M*h)^{-1}$.

The rate constant (k_{ads}) of the adsorption process can be determined from the slope of the linear progression of the curve obtained by plotting c_t^{-1} as a function of time, which is shown in Figure 35. It was found that a linear correlation is only given for the first 10 h of the adsorption process. The flattening of the adsorption curve after 10 h indicates a change in kinetic processes and may be related to aggregation of the dye on the TiO$_2$ surface which would significantly alter the conditions for further adsorption. The averaged k_{ads} for substrate 1 and 2 was found to be 0.00293 $(\mu M*h)^{-1}$ as summarised in Table 6.
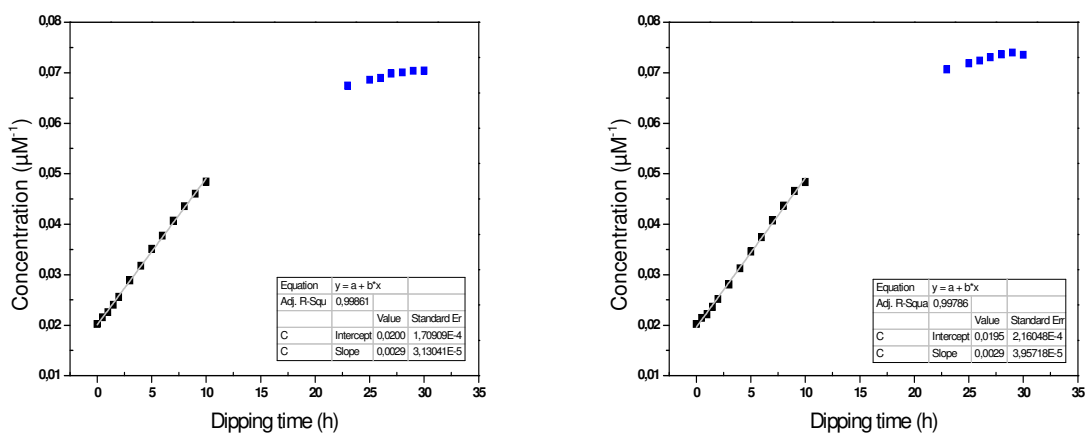
Figure 35: Data for the determination of the adsorption rate constant (k_{ads}) (solid line represents the linear regression fit).

Table 6: Adsorption rate constants and correlation factors for substrate 1 and 2.

	k_{ads} [μMh^{-1}]	R^2
Substrate 1	0.00290	0.9986
Substrate 2	0.00296	0.9979
Average	0.00293	

3.6 Device fabrication and charaterisation

DSSCs were fabricated using **14** as the sensitiser, with the cells having an effective area of 0.20 cm^2 (determined by using the ImageJ software package). TiO$_2$ electrodes were purchased from Dyesol Pty. Ltd. (Queanbeyan, NSW Australia) and consisted of a 11-12 µm thick film of 20 nm anatase particles randomly interspersed with 400 nm scattering centers (10% by weight) with a specific surface area of approximately 70-80 m^2/g deposited onto 15 Ω^2 fluorine doped tin-oxide (FTO) coated glass. Prior to dye sensitisation, the titania substrates were heated to ~ 450 °C for 40 min, then transferred into a freshly made solution of 0.04 M titanium tetrachloride and kept at 70 °C for 30 min. The TiO$_2$ films were then washed with distilled water and subsequently baked in a muffle furnace at 500 °C for 30 min before being allowed to cool to 80 °C. The prepared substrates were immersed in the dye solution (1.5 x 10^{-4} molL^{-1}) which was made up from 5.65 mg of the dye in 26 ml of distilled THF and kept in the dye bath for 3 days in order to allow dye adsorption to reach its equilibrium. After the sensitisation process, excess dye was removed by rinsing with THF and the photoanodes were dried under a gentle stream of N$_2$ before cell assembly. Platinum (Pt) counter electrodes on fluorine doped tin oxide (FTO) glass substrates (purchased from Dyesol Pty. Ltd.) were heated to 450 °C for 30 min before being allowed to cool to room temperature and subsequent cell assembly. A few drops of the electrolyte (EL-HSE purchased from Dyesol) in 3-methoxypropionitrile, which uses I$_3^-$/I$^-$ as the redox mediator, were placed on the dye coated TiO$_2$ and the photoanode and the Pt counter electrode were assembled immediately into a sealed sandwich type cell. For the sealing of the cell a hot-melt ionomer film (Surlyn 1702, 25 µm thickness, Solaronix), which serves as a spacer between the electrodes, was used.

As mentioned earlier, the sensitisation step was carried out in tetrahydrofuran because of superior solubility of the compound in the respective solvent. Dye aggregation on the surface of TiO$_2$, which would negatively affect the cell's performance, can most possibly be neglected due to the solvents weak dielectric constant (ε_r = 7.5).

Device efficiencies were measured with an ABET technologies Sun 2000 solar simulator under AM 1.5 conditions. Prior to each measurement, the solar simulator illumination intensity was measured using a reference silicon photodiode with white

light filter (with respect to an N3 DSSC response). The exact white light illumination intensity was used for the power conversions. The J-V curves were measured with a Keithley 2400 source measure unit and an appropriate photomask was used to illuminate only the cell area. The value of the overall power conversion efficiency (η) was calculated from the short current density (J_{SC}), the open circuit voltage (V_{OC}), the fill factor of the cell (ff) and the intensity of the incident light (P_{IN}) as follows:

$$PCE = \frac{V_{OC} * J_{SC} * ff}{P_{IN}} * 100\%$$

Figure 36 shows the current density-voltage (J-V) characteristics of the best performing device based on **14**. The J-V curve for the N3 standard reference cell is displayed in Figure 37 for direct comparison. The sensitised cell exhibits photovoltaic performance with a short-circuit photocurrent density of 5.14 mA/cm^2, an open circuit voltage of 0.60 V, a fill factor of 0.59 and a corresponding power conversion efficiency of (PCE) of 2.27%. PCE of 2.27% is high as the standard reference N3 cell was assembled and characterised under the same conditions reaching an efficiency of 3.18%.

Once more, due to the time constraints the data reported above only represents unoptimised values obtained for the cell prototype. Nevertheless, this result could indicate the potential of the dye system discussed within this work and justifies the choice of intended structural architecture of **14**.
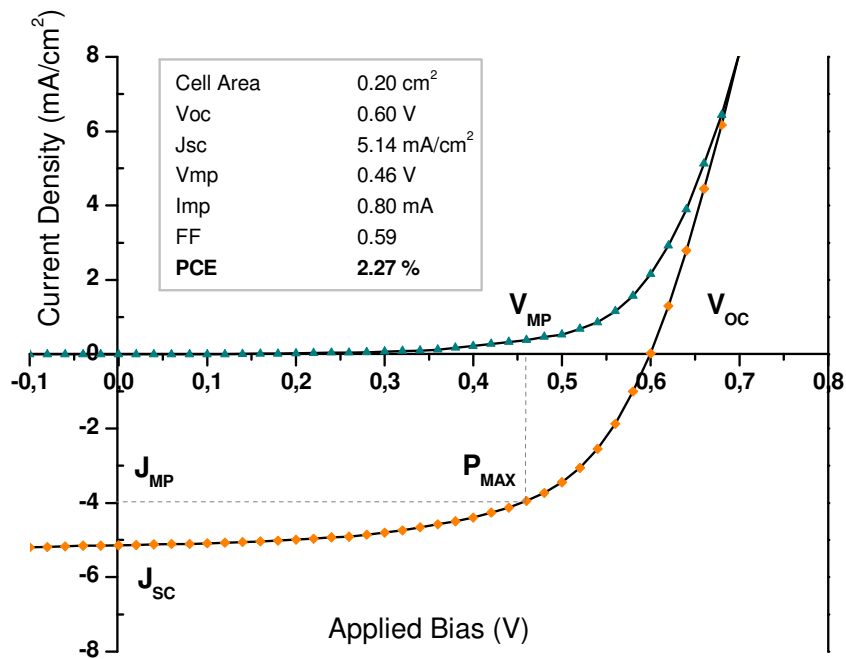
Figure 36: Light J-V (orange), and dark J-V (cyan) of device constructed from compound **14**. Note that the result shown represents the highest efficiency obtained.
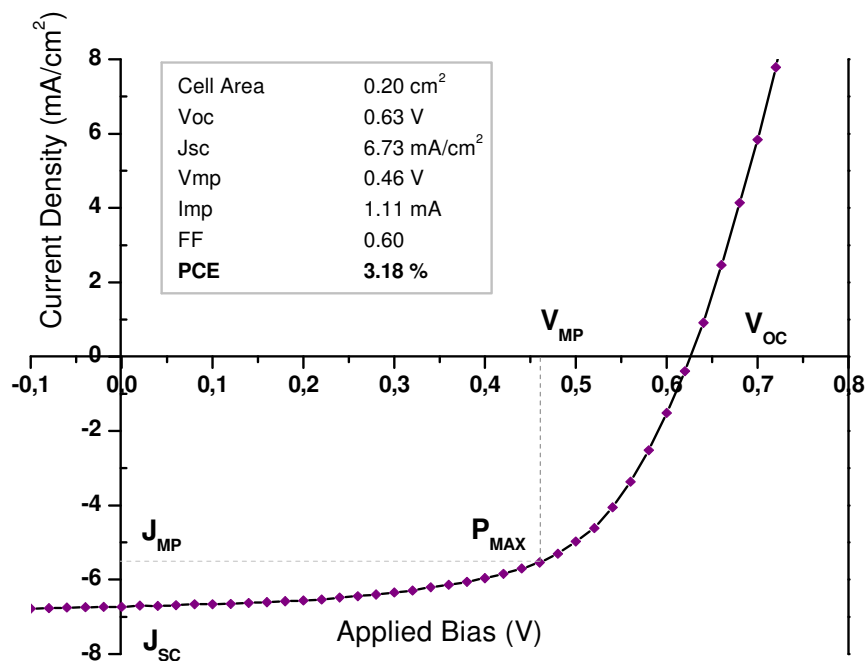
Figure 37: Light J-V (purple) of device constructed from standard **N3** reference cell.

Chapter 4 - Conclusion and Outlook

4.1 Conclusion

The novel sensitiser dye **14** and its precursors were synthesised and all new compounds were successfully characterised by means of ^{1}H NMR, UV-Vis spectroscopy, FT-IR spectroscopy, mass spectrometry and elemental analysis.

In terms of synthesis a facile way to obtain the e[-]-donating carbazole derivative **4** in high yield has been outlined. The dibromo-dithieno-dione core **8** could be prepared following a four step synthesis, where formation of the desired dibrominated product was hard to control due to the strong tendency towards over-bromination of the dithieno-dione substrate **7**. Nevertheless, optimised reaction conditions gave **8** in a yield of 69 %. With the two building blocks **4** and **8** at hand, synthesis of the dye **14** was attempted via route A. The preparation of the core/e[-]-donor compound **10** via Buchwald-Hartwig cross-coupling succeeded but repeated attempts to reproduce the initial result failed. It was concluded that starting material **8** may not be stable under basic conditions leaving the initial product formation unexplained. Consequently a different synthetic approach was taken via route B. Condensation of **8** with diamino-benzoic acid created a stable core compound that could be subjected to the coupling reaction with the carbazole derivative **4**. This route proved to be working and lead to the successful synthesis of the target molecule **14**.
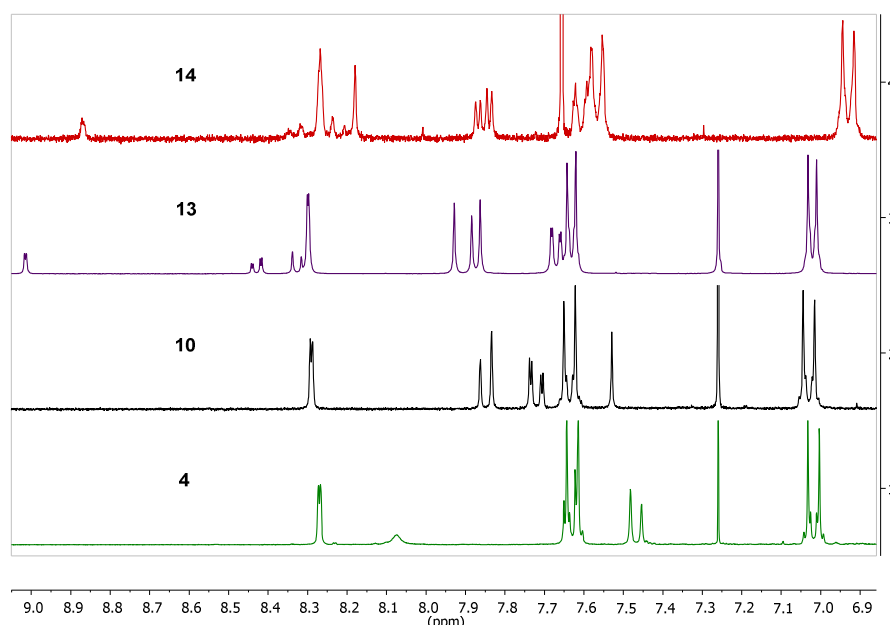
Figure 38: Comparsion of ^{1}H NMR spectra of compounds **4**, **10**, **13**, and **14**.

With the N-C coupling reaction giving the lowest yields the synthesis of the dye and its intermediates in overall good yields was demonstrated. A comparision between the ^{1}H NMR spectra of compounds **4**, **10**, **13** and **14** is displayed in Figure 38.

The photophysical properties of the dye and its intermediates were thoroughly characterised with UV-Vis as well as fluorescence spectroscopy for the new dye **14**. Absorption spectra of the recorded dye precursors (**10**-**13**) and the dye itself demonstrated comprehensibly the change in spectral features with subsequent steps in synthesis. UV absorption spectra of the π-conjugated bridge materials **11** and **12** showed ICT related absorption bands from 416 to 440 nm. This observation can be accredited to an inherent D-π-A character where thiophenes act as the electron rich part of the molecule (D) and the phenazine moiety with the carboxylic acid as the electron deficient one. Compound **10** was found to exhibit superior absorption properties with an absorption onset of 755 nm. The diketo-group of this molecule has to create a strong electron withdrawing effect and hence generates these favourable absorption properties. However, these properties appear to be lost upon conducting the reaction between **10** and 3,4-diaminobenzoic acid. Furthermore, the new dye exhibits an ICT transition band at 489 nm with high molar extinction coefficient (15.311 $M^{-1}cm^{-1}$) in DCM, showing good visible light absorption in such short π-conjugated system.

The target molecule was further examined with cyclic and differential pulse voltammetry to show the presence of one oxidation and reduction process. Both electrochemical processes exhibited chemical reversibility. The ionisation potential and electron affinity were found to be at 0.53 V (vs. Fc^+/Fc) and -0.76 V (vs. Fc^+/Fc), respectively. This gives HOMO and LUMO energy levels of about -5.33 and -3.04 eV, showing the dye has a deeper HOMO than that of I^-/I_3^- electrolyte and higher LUMO than that of TiO_2. This also suggests that the dye has correct energy levels that would allow for efficient electron injection into the conducting band of TiO_2 after photoexcitation as well as dye regeneration through the redox mediator I^-/I_3^-. Figure 39 summarises e^--transfer processes in a DSSC according to determined energy levels of dye **14**.
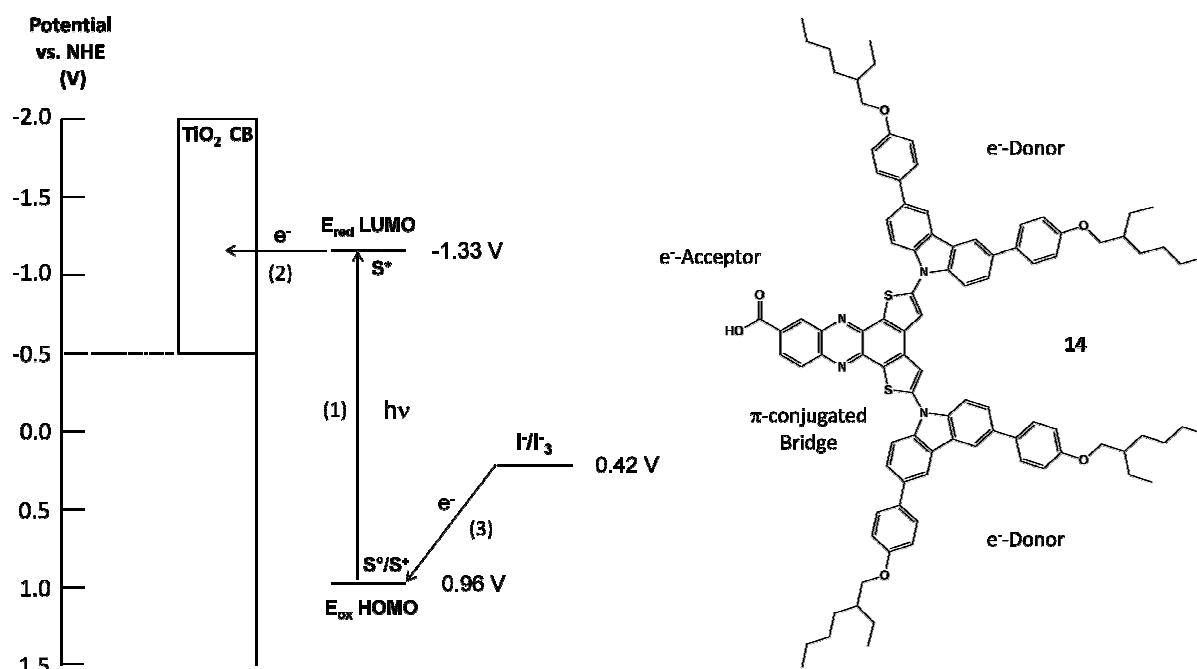
Figure 39: Electron-transfer processes: (1) Excitation, (2) e⁻-injection, (3) dye regeneration and dye structure.

Thermal properties of the synthesised compounds revealed high thermal stability with the dyes $TGA_{(5\%)}$ reaching a value of 420 °C with 5% weight loss. Melting points were only found for compounds **12** and **13**, containing the butyl ester group. Dye **14** showed no T_g within the observed temperature range.

The sensitisation process of the TiO_2 photoanode in a dye bath (5×10^{-5} molL⁻¹) was investigated by monitoring the decrease in dye concentration as a function of time. As a result, a characteristic adsorption profile that reached equilibrium after 28 to 30 h was obtained. With the data received from the adsorption experiment, it was shown that the adsorption process only follows the pseudo second order rate law for the first 10 hours by plotting the amount of the adsorbed dye concentration as a function of time. After 10 hours the curve flattens which indicates a change in kinetic processes. It was theorised that a change in adsorption kinetic may be related to aggregation of the dye on the TiO_2 surface, especially due to the strong tendency of **14** to aggregate in solution, which would significantly alter the conditions for further adsorption. Due to the initially linear correlation a rate constant (k_{ads}) of 0.00293 $(\mu Mh)^{-1}$ could be determined.

Finally, preliminary photovoltaic devices using the novel dye **14** as a sensitiser were constructed with the best performing device yielding an overall power conversion efficiency of 2.27% relative to the 3.18% for a standard reference cell that

were achieved under the same conditions, showing the promising potential. In summary, a novel organic DSSC dye **14**, was successfully synthesised, with overall good yields. Evaluation of the photopysical, electrochemical and adsorption properties as well as device performance outlined the possible use and the future potential of the prepared di-carbazole-dihtienophenazine system in DSSCs.

4.2 Outlook

Future work will focus on the optimisation of parameters for cell assembly such as the quantification of effects of the adsorption solvent on device performance as well as the optimum amount of dye adsorbed on the TiO_2 photoanode. Further work will also include a more detailed characterisation of the device's photovoltaic performance and molecular orbital calculations to elucidate the structure-properties relationship. With respect to results obtained from synthetic work, emphasis has to be placed on optimising the conditions for the N-C cross-coupling reaction between the carbazole moiety and dithieno-phenazine compounds. Due to the promising results obtained for **14** the possible modification of the di-carbazole-dihtienophenazine system with respect to molecular volume, conjugation length and a stronger electron accepting moiety, which in return would result in desired red shifted absorption properties and an increase in the molar extinction coefficient, can be investigated in the future.

Chapter 5 - Experimental

5.1 General Procedures

^{1}H NMR and ^{13}C NMR spectra were recorded on a Bruker Avance 300 (300 MHz), 400 (400 MHz) or 500 (500 MHz) spectrometer. Chemical shifts (δ) are reported in parts per million (ppm) relative to the residual deuterium solvent peaks. Multiplicities are reported as singlet (s), doublet (d), doublet of doublets (dd), triplet (t), multiplet (m) and broad (b). Coupling constants (J) are quoted in Hertz (Hz). Assignment of peaks where appropriate as follows: Carb = Carbazole; Thioph = thiophene; Ph = phenazine; Ar = aryl; CH, CH$_2$, CH$_3$ = aliphatic protons.

UV-Vis spectra were recorded on a Varian Cary 5000 UV-Vis-NIR spectrophotometer with dicholoromethane (spectroscopic grade), acetone (spectroscopic grade) and *N,N*-dimethylformamide (dried and distilled) solutions in 10 x 10 mm quartz or optical glass cuvettes (as indicated). Absorption maxima (λ) and peaks from 225-800 nm were recorded and molar extinction coefficients (ε) were determined by Beer-Lambert law. Infrared spectra were recorded on a Perkin Elmer Spectrum 100 FT-IR Spectrometer as a powder and the absorption quoted in wavenumbers (cm^{-1}), where the strength of absorption was denoted as weak (w), medium (m) or strong (s).

Fluorescence spectra were recorded on a Horiba Jobin Yvon Fluoromax-4 Spectrometer using a Kodak 411 nm long pass gelatin filter no. 2B with dimensions of 75 x 75 x 1 mm. Sample solutions were prepared in dichloromethane (spectroscopic grade) and 10 x 10 mm quartz cuvettes were used to record emission and excitation spectra.

MALDI-TOF mass spectra were recorded on an Applied Biosystems Voyager-DE STR instrument with a matrix-assisted laser-desorption ionisation (MALDI-TOF) setup in reflectron mode. Samples were prepared by dissolution of the respective compounds in tetrahydrofuran and loading onto a 96 well plate using a 'sandwich' technique. 1,8-dihydroxy-9,10-dihydroanthracen-9-one (Dith) and 2,5-dihydroxy benzoic acid (DHB) served as matrices. High resolution mass spectra were recorded on a BRUKER MicrOTof-Q instrument in ESI mode, low resolution mass spectra on a

BRUKER HCT 3D Ion Trap instrument in ESI mode via looped injection. Mass units (m/z) are reported in Daltons and intensities quoted relative to the base peak.

DSC spectra for the determination of glass transition temperatures (T_g) were recorded on a Perkin Elmer Diamond DSC Differential Scanning Calorimeter calibrated to an indium standard. DSC samples were analysed in a temperature range of -150 °C to 250 °C using aluminium crucibles. TGA samples were analysed under a nitrogen atmosphere and heated from 40 °C to 600 °C at 10 °C/min using a ceramic crucible. TGA temperatures ($TGA_{(5\%)}$) are quoted at 5% weight loss using a Perkin Elmer STA 6000 Simultaneous Thermal Analyser.

Melting points of synthesised materials were determined on a Buchi B-545 melting point apparatus with a heating rate of 2 °C/min. The range from the start of the melting process of the respective compounds to when they have completely melted was reported.

Elemental Analysis (EA) was carried out at the Centre for Microscopy and Microanalysis, by Mr. George Blazak, using a Carlo Erba NCHS Analyser Model NA 1500 instrument at the University of Queensland.

Thin layer chromatography (TLC) was carried out with Merck aluminium plates coated with fluorescent P_{254} indicating silica and visualised with long (364 nm) and short (254 nm) wave UV irradiation where applicable. Column chromatography was performed using the gravity feed as well as the flash chromatography technique. The Silica gel used ranged from 30 - 40 µm in size. Silica plug refers to a short path of silica column chromatography, with wet-packed silica, loaded in a sintered glass funnel to which the adsorbed compound was eluted under reduced pressure using two solvents of very different polarities. All solvents used in chromatographic methods were distilled prior to use and solvent mixtures were quoted by volume.

Centrifugal thin layer chromatography (Chromatotron) was carried out using a Chromatotron Silica Plate of either 1 or 2 mm in thickness freshly prepared with Merck silica gel 60 PF_{254} containing gypsium. Preparative TLC was carried out with Analtech Uniplates coated with silica gel GF_{254} where the silica layer possessed a thickness of 500 µm and the plate dimension was 20 x 20 cm.

Electrochemistry was performed in a Bioanalytic System, Inc. Cell Stand C3 instrument. The electrochemical setup consisted of the Inc. Cell Stand C3 instrument using a glassy carbon or platinum electrode (as indicated) as working electrode, platinum wire as counter electrode and an $Ag/AgNO_3$ reference electrode. The

sample solution contained tetrabutylammonium tetrafluoroborate as the electrolyte and the synthesised dye in freshly distilled tetrahydrofuran. Calculated half-wave potentials ($E_{1/2}$) were referenced externally to a ferricenium/ferrocene (Fe^+/Fe) couple. The more detailed procedure is listed under 3.3.

5.2 Experimental Procedures

(1) *1-Bromo-4-(2-ethylhexyloxy)benzene*

A suspension of potassium hydroxide pellets (27.8 g, 495 mmol) in dimethyl sulfoxide (131 ml) was deoxygenated under vacuum and purged with argon three times. 4-bromophenol (20.0 g, 116. mmol) and 2-ethylhexyl bromide (28.8 ml, 162 mmol) were added to the suspension causing a colour change from the initial pinkish orange to brown. The reaction mixture was degassed under vacuum and purged with argon for another three times. The mixture was kept stirring at room temperature under argon for 63 hours. The mixture was slowly added to a separating funnel containing 300 ml of ice water and extracted with hexane (3 x 200 ml). The organic layers were combined, washed with brine (200 ml), dried over anhydrous magnesium sulfate and filtered. The filtrate was collected and the solvent was removed by vacuum. Excess 2-ethylhexyl bromide was removed from the crude material by using a Kugelrohr distillation apparatus to give **1** a yellow oil (30.3 g, 92%). ^{1}H NMR (400 MHz, CDCl$_3$) δ 0.98-0.93 (m, 6H, CH$_3$), 1.58-1.31 (m, 8H, CH$_2$), 1.79-1.70 (m, 1H, CH), 3.86-3.80 (m, 2H, ArOCH$_2$), 6.82-6.78 (m, 2H, ArH), 7.40-7.36 (m, 2H, ArH), which had an identical ^{1}H NMR spectrum to an authentic sample.[42]

(2) *(4-(2-Ethylhexyl)oxyphenyl)boronic acid*

1-Bromo-4-(2-ethylhexyloxy)benzene (30.3 g, 106mmol) was dissolved in freshly distilled tetrahydrofuran (380 ml). The solution was deoxygenated under vacuum and purged with argon for three times. The mixture was cooled down to -78 ℃ with a dry ice - acetone bath. *N*-butyllithium (1.60 M, 114 ml, 182 mmol) was added drop wise to the stirred solution via pressure equalizing dropping funnel under argon. After

complete addition, the mixture was stirred for 1.6 hours at -78 °C under argon. Timethyl borate (64 ml, 574 mmol) was added slowly via syringe to the cool mixture, was stirred for another 2.5 hours at -78 °C under Argon. The dry-ice bath was removed, the mixture allowed to warm up to room temperature and stirred at latter over night (to give a cloudy solution with pale yellow colour on the second day). The reaction was cooled down to 0 °C using an ice bath. 3M aqueous hydrochloric acid (46 ml) was added to the reaction, which was stirred for another 2 hours at room temperature. Water (200 ml) was added and the two layers were separated. The aqueous phase was extracted with diethyl ether (2 x 200 ml). The organic layers were combined, dried over anhydrous magnesium sulfate and filtered. The filtrate was collected and concentrated under vacuum. The yellow oily crude was purified over a silica plug (300 ml) using diethyl ether as eluent. The solvent was removed to give **2** as alight yellow oil (25.1 g, 95%). The product was used in the next reaction without further purification.

(3) *3,6-Dibromo-9H-carbazole*

9H-Carbazole (1.02 g, 6.07 mmol) was suspended in tetrahydrofuran (5 ml) under stirring in the dark. *N*-Bromosuccinimide (2.11 g, 11.9 mmol) was added in small portions to the mixture over 30 minutes at room temperature. After complete addition the orange solution was stirred for another 10 minutes at room temperature. Water (5 ml) was added to the solution and the two layers were separated. The aqueous layer was extracted with dichloromethane (2 x 10 ml). The organic layers were combined, washed with brine (10 ml), dried over anhydrous magnesium sulfate and filtered. The filtrate was collected and the solvent was removed under reduced pressure.The crude was purified by recrystallisation from ethanol and the product **3** was obtained as a light brown solid (1.46 g, 74%). ^{1}H NMR (300 MHz, CDCl$_3$) δ 7.33 (dd, *J* = 8.6, 0.5, 2H, CarbH), 7.54 (dd, *J* = 8.6, 2.0, 2H, CarbH), 8.11 (bs, 1H, NH), 8.14-8.13 (m, 2H, CarbH), which had an identical ^{1}H NMR spectrum to an authentic sample.[42]

(4) 3,6-Bis(4-((2-ethylhexyl)oxy)phenyl)-9H-carbazole

A mixture of 3,6-dibromo-9H-carbazole **3** (4.32 g, 13.3 mmol), (4-(2-ethylhexyloxy)phenyl)boronic acid (10.2 g, 40.7 mmol), sodium carbonate (30.7 g, 0.290 mmol), water (145 ml), ethanol (110 ml) and toluene (115 ml) was deoxygenated through bubbling with nitrogen and vigorous stirring for 2 hours. Tetrakis(triphenylphosphine)palladium(0) (891 mg, 0.800 mmol) was added to the reaction in one portion to give a light orange colour. The reaction was heated at reflux (100 °C) for 68 hours under a constant flow of nitrogen (to produce colour change from orange to yellow). The mixture was allowed to cool to room temperature and filtered through some cotton wool to remove solids. Dichloromethane (100 ml) was added and the layers were separated. The aqueous phase was extracted with dichloromethane (2 x 100 ml). The organic layers were combined, washed with brine (100 ml), dried over anhydrous magnesium sulfate and filtered. The filtrate was collected and concentrated under reduced pressure. The residue was purified by column chromatography over silica using dichloromethane-hexane mixture (1:5 to 1:3) as eluent to give **4** as a white solid (5.41 g, 71%). ^{1}H NMR (500 MHz, CDCl$_3$) δ 0.99-0.89 (m, 12H, CH$_3$), 1.63-1.30 (m, 16H, CH$_2$), 1.83-1.73 (m, 2H, CH), 3.96-3.87 (m, 4H, ArOCH$_2$), 7.04-6.99 (m, 4H, sp H), 7.48 (d, J = 8.4, 2H, CarbH), 7.65-7.60 (m, 6H, CarbH and sp H), 8.07 (bs, 1H, NH), m 8.27 (d, J = 1.5, 2H, CarbH), which had an identical ^{1}H NMR spectrum to an authentic sample.[42] ESI LRMS: m/z [M - H]$^-$ (calcd: 574.37 g/mol) found: 574.4.

(5) 4,4,5,5-Tetramethyl-2-(thiophen-3-yl)-1,3,2-dioxaborolane

Bis(pinacolato)diboron (1.87 g, 7.38 mmol), potassium acetate (1.75 g, 17.9 mmol) and [1,1'-Bis(diphenylphosphino)ferrocene]dichloropalladium(II) (170 mg, 0.230 mmol) were loaded in a two-neck round-bottom flask under nitrogen. Distilled 1,4-dioxane (15 ml) was added to the reaction via syringe and followed by the addition of 3-bromothiophene (0.58 ml, 6.13 mmol). The mixture was deoxygenated through bubbling with nitrogen and vigorous stirring for 25 minutes before being replaced with argon. A colour change of the suspension from light red to dark brown occurred upon degassing. The reaction was heated at 100 °C for 67 hours under argon. The mixture was allowed to cool to room temperature and filtered through cotton wool to remove

solids. Diethyl ether (100 ml) and water (100 ml) were added to the filtrate and the two layers were separated. The aqueous layer was extracted with diethyl ether (3 x 50 ml), and the organic layers were combined, washed with brine (150 ml), dried over anhydrous magnesium sulfate and filtered. The filtrate was collected and the the solvent was completely removed. The residue was purified by column chromatography over silica using dichloromethane-hexane mixture (1:4 to 1:2) as eluent to give **5** as a light brown solid (946 mg, 73%). ^{1}H NMR (500 MHz, CDCl$_3$) δ 1.33 (s, 12H, CH$_3$), 7.34 (dd, J = 4.9, 2.7 Hz, 1H, ThiophH), 7.41 (dd, J = 4.8, 1.0, 1H, ThiophH), 7.93 (dd, J = 2.7, 1.0, 1H, ThiophH), which had an identical ^{1}H NMR spectrum to an authentic sample.[39]

(6) *3,3'-Bithiophene*

3-Bromothiophene (0.21 ml, 2.22 mmol), 4,4,5,5-tetramethyl-2-(thiophen-3-yl)-1,3,2-dioxaborolane (550 mg, 2.62 mmol), sodium carbonate (1.39 g, 13.1 mmol), water (3.8 ml), ethanol (3.8 ml) and toluene (11 ml) were added in a Schlenk tube. The mixture was deoxygenated through bubbling with nitrogen and vigorous stirring for 20 minutes. Tetrakis(triphenylphosphine)palladium(0) (83 mg, 74.6 µmol) was added to the bright yellow reaction mixture in one portion, the tube was sealed, placed under argon and heated at 100 °C for 20 hours. The colour of the reaction turned into light brown. The mixture was allowed to cool to room temperature, filtered through cotton wool to remove solids and dichloromethane (50 ml) and water (40 ml) were added to the filtrate. The two layers were separated and the aqueous layer was extracted with dichloromethane (2 x 30 ml). The organic fractions were combined, washed with water (2 x 100 ml), saturated aqueous sodium bicarbonate solution (100 ml) and brine (100 ml), then dried over anhydrous magnesium sulfate, and filtered. The filtrate was collected and the solvent was removed under reduced pressure. The crude product was purified by column chromatography over silica using dichloromethane-hexane (1:5) as eluent to give **6** as a white solid (343 mg, 93%). mp: 131.6-134.2 °C. ^{1}H NMR (500 MHz, CDCl$_3$) δ 7.34 (dd, J = 5.0, 1.4, 2H), 7.36 (dd, J = 5.0, 2.9, 2H), 7.38 (dd, J = 2.9, 1.4, 2H), which had an identical ^{1}H NMR spectrum to an authentic sample.[39]

(7) Benzo[1,2-b:4,3-b']dithiophene-4,5-dione

3,3'-Bithiophen (4.70 g, 28.2 mmol) was loaded in a Schlenk tube under positive argon pressure and dissolved in anhydrous 1,2-dichloroethane (40 ml) to give a pale yellow solution. Oxalyl chloride (1.45 ml, 17.1 mmol) was added to the solution which was then placed under a continuous flow of argon to prevent hydrochloric acid gas from accumulating in the reaction flask. The mixture was heated at 70 ℃. Upon heating an orange colour could be seen. The reaction was kept at this temperature for 10 days. More oxalyl chloride (2.4 ml, 28.4 mmol) was added in small portions over 10 days in compliance with the progress of the reaction as indicated by TLC. After 10 days a thick red precipitate formed. The reaction was allowed to cool to room temperature and stored under argon in the dark over night. The suspension was filtered through a G4 sintered glass funnel and the red precipitate was collected and thoroughly washed with n-hexane (50 ml) and warm ethanol (50 ml) to give the **7** as a red powder (4.89 g, 79%). ^{1}H NMR (500 MHz, CDCl$_3$) δ 7.29 (d, J = 5.0, 2H), 7.83 (d, J = 5.0, 2H), which had an identical ^{1}H NMR spectrum to an authentic sample.[39] ESI LRMS: m/z (M+H)$^+$ (calcd: 219.97 g/mol) found: 221.0.

(8) 2,7-Dibromobenzo[1,2-b:4,3-b']dithiophene-4,5-dione

Benzo[1,2-b:4,3-b']dithiophene-4,5-dione **7** (501 mg, 2.28 mmol) was suspended in acetic acid (12 ml) and chloroform (11 ml). The bright red suspension was stirred and cooled to 0-2 ℃ (with an ice-bath). A solution of bromine (0.24 ml, 4.68 mmol) in 2.4 ml of chloroform was slowly added to the reaction mixture over 1.5 hours. After complete addition the ice-bath was removed and the mixture was allowed to warm to room temperature. The suspension was stirred at room temperature for 1 hour and was then heated at 38 ℃ for 2 hours. (After approximately 1 hour a bright thick orange precipitate crashed out.) The reaction was cooled to room temperature and a 10 w/w% aqueous sodium metabisulfite solution (15 ml) was added. Water (300 ml) was then added to the mixture and extracted with dichloromethane (400 ml). The orange looking spongy solid at the interphase between aqueous and organic solvent layer was dissolved and extracted through washing with dichloromethane (300 ml, 200 ml, 100 ml). The organic extracts were combined, washed with saturated aqueous sodium bicarbonate solution (700 ml), brine (700 ml), dried over anhydrous

magnesium sulfate, and filtered. The filtrate was collected and concentrated under reduced pressure. The crude material was purified by column chromatography over silica using dichloromethane as eluent to give **8** as an orange solid (592 mg, 69%). ^{1}H NMR (500 MHz, CDCl3) δ 7.23 (s, 2H), which had an identical ^{1}H NMR spectrum to an authentic sample.[39]

(9) 2,7-Diiodobenzo[1,2-b:4,3-b']dithiophene-4,5-dione

2,7-Diiodobenzo[1,2-b:4,3-b']dithiophene-4,5-dione **8** (82 mg, 0.22 mmol), potassium iodide (443 mg, 2.67 mmol) and copper(I) iodide (338 mg, 1.77mmol) were suspended in deoxygenated dimethyl sulfoxide (18 ml). The light orange suspension was degassed under a vacuum (~ 12 mbar) and backfilled with argon. This was repeated for four times. The reaction was heated at 110 °C and kept at this temperature for 28 hours under argon. The colour of the solution continuously went darker and turned black after several hours of heating. The progress of the reaction was monitored via ^{1}H NMR. When no further change in educt conversion could be observed (28 h) the mixture was allowed to cool to room temperature. The reaction flask was further cooled in an ice bath which was found to facilitate precipitation from DMSO and facilitate subsequent extraction. 200 ml of water and 100 ml of dichloromethane were added to the crude following the separation of layers. The dark red precipitate which had formed at the interphase between the two layers was further extracted with dichloromethane (100 ml, 2 x 50 ml). The organic extracts were combined, washed with brine (150 ml), dried over anhydrous $MgSO_4$ and filtered. The filtrate was collected and the solvent was completely removed under reduced pressure. The resulted dark red residue was purified by column chromatography over silica using dichloromethane as eluent to give **9** as an dark red solid with metallic glance (76 mg, 75%). ^{1}H NMR showed evidence of a small amount (~ 8%) of the mixed halide molecule contained within the product fraction. Since both compounds should yield the same product in subsequent reaction no further purification was necessary. ^{1}H NMR (500 MHz, CDCl3) δ 7.43 (s, 2H). ESI LRMS: m/z [M][+] (calcd: 471.76 g/mol) found: 495 [M+Na][+], 511 [M+K][+].

(10) 2,7-Bis(3,6-bis(4-(2-ethylhexyl)oxyphenyl)-9H-carbazol-9-yl)benzo[1,2-b:4,3-b']dithiophene-4,5-dione

2,7-Dibromobenzo[1,2-b:4,3-b']dithiophene-4,5-dione **9** (18 mg, 48.4 µmol), 3,6-bis(4-(2-ethylhexyloxy)phenyl)-9H-carbazole (67 mg, 0.12 mmol), sodium *tert*-butoxide (19 mg, 0.20 mmol), tri-*tert*-butylphosphonium tetrafluoroborate (23 mg, 80.3 µmol) and tris(dibenzylideneacetone)dipalladium(0)-chloroform adduct (10 mg, 9.8 µmol) were loaded in a Schlenk tube under positive argon pressure. Anhydrous xylene (0.8 ml) was added to the reaction mixture, which was deoxygenated through bubbling with argon for 6 minutes with vigorous stirring to produce a dark brown solution. The tube was then sealed with a stopper and parafilm and heated at 130 °C for 2 hours. Upon cooling to room temperature water (25 ml) and dichloromethane (15 ml) were added to the mixture. The two layers were separated and the aqueous was extracted with dichloromethane (3 x 15 ml). The organic fractions were combined, washed with brine (25 ml), dried over anhydrous magnesium sulfate and filtered. The filtrate was collected and the solvent was completely removed under reduced pressure. The residue was purified by column chromatography over silica using dichloromethane-hexane (1:1 to 3:1) as eluent leaving a purple-black solid (23 mg, 34%). ^{1}H NMR (300 MHz, CDCl3) δ 0.98-0.90 (m, 24H, CH_3), 1.63-1.23 (m, 32H, CH_2), 1.81-1.73 (m, 4H, CH), 3.96-3.87 (m, 8H, $ArOCH_2$), 7.05-7.00 (m, 8H, ArH), 7.53 (s, 2H, ThiophH), 7.66-7.61 (m, 8H, ArH), 7.74 (dd, J = 8.6, 1.8, 4H, CarbH), 7.86 (d, J = 8.7, 4H, CarbH), 8.29 (d, J = 1.8, 4H, CarbH). λ_{max} (DCM)/nm 560 (log ε/$M^{-1}cm^{-1}$ 4.0), 445 (4.0), 355 sh (4.3), 295 (5.1), 261 (5.2). ν_{max}/cm^{-1} 3076-3035 (=C-H, w), 2957-2858 (-CH_3, -CH_2, -C-H, m), 1637 (Ar-C=O, s), 1608 (-C=C-, s), 1220 (-Ar-O-C-, s). m/z ([MALDI-TOF, DITH] $[M]^+$ calculated 1366.7 (96%), 1367.7 (100%), 1368.7 (61%), 1369.7 (27%), 1370.7 (10%), 1371.7 (3%), found 1367.0 (19%), 1368.0 (100%), 1369.0 (95%), 1370.0 (66%), 1371.0 (32%), 1372.0 (13%). Found: C 78.7, N 3.2, H 7.5, S 4.3. $C_{90}H_{98}N_2O_6S_2$ requires C 79.0, N 2.1, H 7.2, S 4.7.

(11) 2,5-Dibromodithieno[2,3-a:3',2'-c]phenazine-9-carboxylic acid

A mixture of 2,7-dibromobenzo[1,2-b:4,3-b']dithiophene-4,5-dione **10** (559 mg, 1.48 mmol), 3,4-diaminobenzoic acid (229 mg, 1.51 mmol) was loaded in a Schlenk tube under positive argon pressure and suspended in acetic acid (50 ml). The bright

orange suspension was deoxygenated by using vacuum (~ 20 mbar) and purged with argon. This was repeated for three times. The tube was sealed under argon and heated at 50 °C for 22 hours. Upon heating the colour of the precipitate slowly changes to yellow. The mixture was allowed to cool to room temperature and dichloromethane (100 ml) was added to the tube and stirred for another 10 minutes in order to dissolve the remaining starting material. The reaction mixture was filtered through a G4 sintered glass funnel and the precipitate was collected and was thoroughly washed with n-hexane (100 ml) and dichloromethane (200 ml) to give **11** in pure form as a yellow powder (633 mg, 87%). $TGA_{(5\%)}$: 383 C°. ^{1}H NMR (500 MHz, DMSO-d_6/ $CDCl_3$ 1:1) δ 8.13 (s, 2H, ThiophH), 8.27 (d, 2H, J = 8.9, PhH), 8.35 (d, J = 9.2, 2H, PhH), 8.81 (s, 1H, PhH). λ_{max} (acetone)/nm 435 (log ε/$M^{-1}cm^{-1}$ 4.2), 413 (4.2). ν_{max}/cm^{-1} 3270-2300 (-OH, br), 1695 (C=O, s), 1624 (-C=C-, m), 1281 (-COOH, m). ESI HRMS m/z [M - H]$^-$ (calc: 490.8159 g/mol) found: 490.8165. m/z [MALDI-TOF, DITH] [M]$^+$ calculated 491.8 (49%), 492.8 (10%), 493.8 (100%), 494.8 (21%), 495.8 (57%), 496.8 (12%), 497.8 (6%), 498.8 (1%), found 492.5 (57%), 493.5 (34%), 494.5 (100%), 495.5 (51%), 496.5 (66%), 497.5 (31%), 498.5 (18%), 499.5 (11%). Found: C 41.3, N 5.6, H 1.2, S 13.2. $C_{17}H_6Br_2N_2O_2S_2$ requires C 41.3, N 5.7, H 1.2, S 13.0.

(12) *Butyl 2,5-dibromodithieno[2,3-a:3',2'-c]phenazine-9-carboxylate*

2,5-Dibromodithieno[2,3-a:3',2'-c]phenazine-9-carboxylic acid **11** (226 mg, 0.46 mmol) was suspended in anhydrous toluene (150 ml) and followed by the addition of *n*-butanol (6.0 ml, 65.6 mmol) and a catalytic amount of concentrated sulfuric acid (6 drops). The reaction mixture was deoxygenated using vacuum (~ 450 mbar) and purged with argon. This was repeated for four times. The reaction was then heated at reflux (130 °C) under argon for 42 hours. The yellowish light brown suspension was allowed to cool to room temperature and the remaining precipitate (starting material) was recovered through filtration using a G4 sintered glass funnel. The filtrate was collected and transferred into a separating funnel and water (1 x 150 ml) was added. The two layers were separated and the organic fraction was dried over anhydrous magnesium sulfate, filtered and the filtrate was collected. The solvent was completely removed under reduced pressure. The yellow/brown crude material was purified by

column chromatography over silica using dichloromethane as eluent to give a bright yellow solid (125 mg, 50%). mp: 265.9-266.2 °C. TGA$_{(5\%)}$: 331 C°. ^{1}H NMR (400 MHz, CDCl$_3$) δ 1.04 (t, J = 7.4, 3H, CH$_3$), 1.62-1.53 (m, 2H, CH$_2$), 1.89-1.82 (m, 2H, CH$_2$), 4.46 (t, J = 6.6, CH$_2$), 7.69 (s, 2H, ThiophH), 8.31 (d, J = 8.9, 1H, PhH), 8.44 (dd, J = 8.9, 1.9, 1H, PhH), 8.99 (d, J = 1.5, 1H, PhH). λ$_{max}$(DCM)/nm 440 (log ε/M^{-1}cm^{-1} 4.3), 416 (4.2), 305 sh (4.8), 315 (4.9), 290 sh (4.6), 250 sh (4.4). ν$_{max}$/cm^{-1} 3087 (=C-H, m), 2957-2846 (-CH$_3$, -CH$_2$-, -CH-, m), 1704 (-C=O, s). m/z [MALDI-TOF, DITH] [M]$^+$ calculated 547.9 (48%), 548.9 (13%), 549.9 (100%), 550.9 (26%), 551.9 (56%), 552.9 (14%), 553.9 (6%), 554.9 (1%), found 547.5 (18%), 548.5 (65%), 549.5 (30%), 550.5 (100%), 551.5 (43%), 552.5 (66%), 553.5 (27%), 554.5 (22%). Found: C 45.9, N 5.0, H 2.6, S 11.4. C$_{21}$H$_{14}$Br$_2$N$_2$O$_2$S$_2$ requires C 45.8, N 5.1, H 2.6, S 11.7.

(13) *Butyl 2,5-bis(3,6-bis(4-(2-ethylhexyloxy)phenyl)-9H-carbazol-9-yl)dithieno[2,3-a:3',2'-c]phenazine-9-carboxylate*

Butyl 2,5-dibromodithieno[2,3-a:3',2'-c]phenazine-9-carboxylate **12** (147mg, 0.27 mmol), bis(4-(2-ethylhexyloxy)phenyl)-9H-carbazole (385 mg, 0.67 mmol) and sodium *tert*-butoxide (99 mg, 1.03 mmol) were loaded in a Schlenk tube under positive argon pressure. Anhydrous xylene (4.5 ml) was added to the reaction to produce a green solution and the mixture was deoxygenated under vacuum (~ 15 mbar) and purged with argon. This was repeated for three times before and after the addition of tri-*tert*-butylphosphonium tetrafluoroborate (23 mg, 80.3 μmol) and tris(dibenzylideneacetone)dipalladium(0)-chloroform adduct (63 mg, 61.1 μmol). The reaction vessel was placed under argon, sealed with a septum and heated at 130 °C for 19 hours to give a dark red colour solution upon heating. After cooling to room temperature water (50 ml) and dichloromethane (30 ml) were added to the mixture and the two layers were separated. The aqueous phase was extracted with dichloromethane (4 x 10 ml) and the organic layers were combined. The combined fractions were washed with brine (1 x 100 ml), dried over anhydrous magnesium sulfate and filtered. The filtrate was collected and the solvent was removed under reduced pressure. The crude material was initially purified by column chromatography over silica using dichloromethane-hexane (2:1) as eluent and further purified by silica (plate with a thickness of 1 mm) Chromatotron silica using

dichloromethane-hexane (1:2 to 1:1) as eluent and finally being loaded on preparative TLC plates with a thickness of 500 μm using dichloromethane-hexane (3:2 to 1:1) as eluent to give **13** as a purple red solid (104 mg, 26%). mp: 294.4-296.1 °C. $TGA_{(5\%)}$: 415 °C. ^{1}H NMR (500 MHz, $CDCl_3$) δ 0.87-0.80 (m, 24H, CH_3), 0.93 (t, J = 7.4, 3H, CH_3), 1.49-1.23 (m, 32H, CH_2), 1.70-1.63 (m, 4H, CH), 1.77-1.71 (m, 2H, CH_2), 3.83-3.78 (m, 8H, $ArOCH_2$), 4.36 (t, J = 6.6, 2H, CH_2), 6.93-6.90 (m, 8H, ArH), 7.55-7.52 (m, 8H, ArH), 7.59 (dd, J = 8.6, 1.8, 4H, CarbH), 7.78 (d, J = 8.5, 4H, CarbH), 7.84 (s, 2H, ThiophH), 8.21 (d, J = 1.4, 4H, CarbH), 8.25 (d, J = 8.9, 1H, PhH), 8.34 (dd, J = 9.0, 1.9, 1H, PhH), 8.93 (d, J = 1.8, 1H, PhH). λ_{max} (DCM)/nm 481 (log $\varepsilon/M^{-1}cm^{-1}$ 4.2), 400 sh (4.1), 340 (4.9), 294 (5.2), 259 (5.2). ν_{max}/cm^{-1} 3038 (=C-H, w), 2957-2859 (-CH_3, -CH_2-, -CH-, m), 1719 (C=O, m), 1608 (-C=C-, m). m/z [MALDI-TOF, DHB] $[M]^+$ calculated 1538.8 (86%), 1539.8 (100%), 1540.8 (66%), 1541.8 (32%), 1542.8 (12%), 1543.8 (4%), found 1538.8 (24%), 1539.9 (71%), 1540.9 (100%), 1541.9 (84%), 1542.9 (48%), 1543.9 (10%). Found: C 78.8, N 3.7, H 7.2, S 4.0. $C_{101}H_{110}N_4O_6S_2$ requires C 78.8, N 3.6, H 7.2, S 4.2.

(14) *2,5-Bis(3,6-bis(4-(2-ethylhexyloxy)phenyl)-9H-carbazol-9-yl)dithieno[2,3-a:3',2'-c]phenazine-9-carboxylic acid*

Butyl 2,5-bis(3,6-bis(4-(2-ethylhexyloxy)phenyl)-9H-carbazol-9-yl)dithieno[2,3-a:3',2'-c]phenazine-9-carboxylate **13** (69 mg, 44.6 μmol) was dissolved in methanol (2 ml) and distilled tetrahydrofuran (10 ml) to give a dark red clear solution. Lithium hydroxide (100 mg, 4.18 mmol) was dissolved in water (2 ml) and slowly added to the above solution, resulting in the instant formation of a dark red precipitate. The mixture was degassed using vacuum (~ 450 mbar) and purged with argon. This was repeated for three times. The reaction vessel was placed under argon and heated at 65 °C for 14 hours. The mixture was allowed to cool to room temperature and was then quenched with aqueous 3M hydrochloric acid (4 ml). The suspension was filtered through a G4 sintered glass funnel. The dark red precipitate was collected and washed with water (20 ml) and methanol (20 ml) before being blow-dried using a gentle stream of nitrogen. The dark red solid was dissolved in chloroform and was then purified in two steps by column chromatography over silica using; first, pure dichloromethane and followed by a mixture of acetic acid-dichloromethane (1:20) as

eluent to give **14** as a dark red solid (55 mg, 82%). $TGA_{(5\%)}$: 420 °C. ^{1}H NMR (300 MHz, DMSO-d_6/ CDCl$_3$ 1:3) δ 0.91-0.83 (m, 24H, CH$_3$), 1.52-1.25 (m, 32H, CH$_2$), 1.73-1.64 (m, 4H, CH), 3.84 (d, J = 6.0, 8H, ArOCH$_2$), 6.94 (d, J = 8.5, 8H, ArH), 7.58 (d, J = 8.6, 8H, ArH), 7.62 (d, J = 8.7, 4H, CarbH), 7.87 (dd, J = 8.6, 3.57 Hz, 4H, CarbH), 8.18 (s, 2H, ThiophH), 8.24 (d, J = 9.3, 1H, PhH), 8.27 (s, 4H, CarbH), 8.35 (d, J = 8.8, 1H, PhH), 8.87 (s, 1H, PhH), 10.60 (s, 1H, COOH). λ_{max}(DCM)/nm 489 (log ε/M^{-1}cm^{-1} 4.2), 404 sh (4.0), 343 (4.8), 299 (5.1), 260 (5.2). ν_{max}/cm^{-1} 3035 (=C-H, w), 2958-2858 (-CH$_3$, -CH$_2$-, -CH-, m), 1717 (C=O, w), 1608 (-C=C-, m). m/z [MALDI-TOF, DHB] [M]$^+$ calculated 1482.7 (89%), 1483.7 (100%), 1484.7 (65%), 1485.7 (30%), 1486.7 (11%), 1487.7 (4%), found 1482.9 (39%), 1483.9 (96%), 1484.9 (100%), 1485.9 (61%), 1486.9 (46%), 1487.9 (26%). Found: C 78.4, N 3.9, H 7.0, S 4.1. $C_{97}H_{102}N_4O_6S_2$ requires C 78.5, N 3.8, H 6.9, S 4.3.

References

[1]   J. Xue, *Polymer Reviews* **2010**, 50, 411.

[2]   C. A Wolden, J. Kurtin, J. A. Baxter, I. Repins, S. E. Shaheen, J. T. Torvik, A. A. Rockett, V. M. Fthenakis, E. S. Ayidil, *J. Vac. Scl. Techol. A* **2011**, 29, 1.

[3]   A. Hagfeldt, G. Boschloo, L. Sun, L. Kloo, H. Pettersson, *Chem. Rev.* **2010**, 110, 6595.

[4]   A. Henze & W Hillebrand, 'Strom von der Sonne', *Ökobuchverlag*, **1999**.

[5]   http://ssis.arts.unsw.edu.au/tsw/LIMITS.htm, 'THE LIMITS TO GROWTH ANALYSIS OF OUR GLOBAL SITUATION', acessed 5th December 2011.

[6]   T.M. Razykov, C.S. Ferekides, D. Morel, E. Ullal, H.S. Stefanakos, H.S. Upadhyaya, *Solar Energy* **2011**, 85, 1580.

[7]   International Energy Agency, 'World Energy Outlook 2011', *IEA/OECD*, Paris, 2011.

[8]   L.M. Gonçalves, V. Z. Bermudez, H. A. Ribeiro, A. M. Mendes, *Energy and Environmental Science* **2008**, 1, 655.

[9]   M. Grätzel, *Pure Appl. Chem.* **2001**, 73, 459.

[10]   H. Spangaard, F.C. Krebs, *Solar Energy materials & Solar Cells* **2004**, 83, 125.

[11]   J. Preat, D. Jacquemin, E. A. Perpète, *Energy & Environmental Science* **2010**, 3, 891.

[12]   B. Parida, S. Iniyan, R. Goic, *Renewable and Sustainable Energy reviews* **2011**, 15, 1625.

[13]   A. Goetzberger, J. Luther, G. Willeke, *Solar Energy Materials and Solar Cells* **2002**, 74, 1.

[14]   F. Dimroth, S. Kurtz, *MRS Bull*. **2007**, 32, 230.

[15]   J. Weickert, R. B. Dunbar, H. C. Hesse, W. Wiedemann, L. Schmidt-Mende, *Advanced Materials* **2011**, 23, 1810.

[16]   D.J. Milliron, I. Gur, P. A. Alivisatos, *MRS Bull.* **2005**, 30, 41.

[17]   P. Sonar, J.P.F. Lim, K.L. Chan, *Energy & Environmental Science* **2011**, 4, 1558.

[18]   M. Grätzel, *Nature* **2001**, 414, 338.

[19]   J.N. Clifford, E. Martínez-Ferrero, A. Viterisi, E. Palomares, *Chem. Soc. Rev.* **2011**, 40, 1635.

[20]   Y. Ooyama, Y. Harima, *Eur. J. Org. Chem.* **2009**, 2009, 2903.

[21]   X. Zhang, J.-J. Zhang, Y.-Y. Xia, *Journal of Photochemistry and Photobiology* **2008**, 194, 167.

[22]   J.-K. Lee, M. Yang, *Materials Science and Engineering B* **2011**, 176, 1142.

[23]   B. O'Regan, M. Grätzel, *Nature* **1991**, 353, 737.

[24]   K.D. Benkstein, N. Kopidakis, J. Lagemaat, A. J. Frank, *J. Phys. Chem. B* **2003**, 107, 7759.

[25]   R. Katoh, A. Furube, T. Yoshihara, K. Hara, G. Fujihashi, S. Takano, S. Murata, H. Arakawa, M. Tachiya, *J. Phys. Chem. B* **2004**, 108, 4818.

[26]   A. Mishra, M.K.R. Fischer, P. Bäuerle, *Angew. Chem. Int. Ed.* **2009**, 48, 2474.

[27]   H. Ozawa, M. Awa, T. Ono, H. Arakawa, *Chemistry an Asian Journal* **2011**, 00, 1.

[28]   H. Lund, R. Nilsen, O. Salomatova, D. Skåre, E. Riisem, 'Solar Cells', 2008, http://org.ntnu.no/solarcells/pages/Chap.2.php, acessed 12th December 2011.

[29]   E. Bundgaard, F.C. Krebs, *Solar Energy Materials & Solar Cells* **2007**, 91, 954.

[30] M.K. Nazeeruddin, A. Kay, I. Rodicio, R. Humpbry-Baker, E. Miller, P. Liska, N. Vlachopoulos, M. Gratzel, *J. Am. Chem. Soc.* **1993**, 115, 6382.

[31] Md.K. Nazeeruddin, P. Péchy, M. Grätzel, *Chem. Commun.* **1997**, 18, 1705.

[32] M. Grätzel, *Journal of Photochemistry and Photobiology C* **2003**, 4, 145.

[33] S.M. Zakeeruddin, M. K. Nazeeruddin, R. Humphry-Baker, P. Péchy, P. Quagliotto, C. Barolo, G. Viscardi, M. Grätzel, *Langmuir* **2002**, 18, 952.

[34] D. P. Hagberg, J.-H. Yum, HJ. Lee, F. De Angelis, T. Marinado, K. M. Karlsson, R. Humphry-Baker, L. Sun, A. Hagfeldt, M. Grätzel, Md. K. Nazeeruddi, *J. Am. Chem. Soc.* **2008**, 130, 6259.

[35] S. Hwang, J. H. Lee, C. Park, H. Lee, C. Kim, M. H. Lee, W. Lee, J. Park, K. Kim, N. G. Park, *Chem. Commun.* **2007**, 4887.

[36] D. Liu, R. W. Fessenden, G. L. Hug, P.V. Kamat, *J. Phys. Chem. B* **1997**, 101, 2583.

[37] Z.S. Wang, Y. Cui, C. Dan-oh, C. Kasada, A. Shinpo, K. Hara, *J. Phys. Chem. C* **2007**, 111, 7224.

[38]   S. Ito, H. Miura, S. Uchida, M. Takata, K. Sumioka, P. Liska, P. Comte, P. Pechy, M. Grätzel, Chem. Commun. **2008**, 5194.

[39] A. Meyer, E. Sigmund, F. Luppertz, G. Schnakenburg, I. Gadaczek, T. Bredow, S.-S. Jester, S. Höger, *Beilstein J.Org. Chem* **2010**, 6, 1180.

[40] D. Kim, J. K. Lee, S. O. Kang, J. Ko, *Tetrahedron* **2007**, 63, 1913.

[41] Y.-J. Cheng, S.-H. Yang, C.-S. Hsu, *Chemical Reviews* **2009**, 109, 5868.

[42] S.-C. Lo, E. B. Namdas, C. P. Shipley, J. P.T. Markham, T.D. Anthopolous, P. L. Burn, I. D.W. Samuel, *Organic Electronics*, **2006**, 7, 85.

[43] T. T. Denton, X. Zhang, J.R. Cashman, *J. Med. Chem.* **2005**, 48, 225.

[44] M. Sandberg, S. Hellström, 'Waterbased compositions for casting and printing', E.P. Office, Sweden, 8, **2010**.

[45] A.F Littke, C. F. Gregory, *Angew. Chem. Int. Ed.* **2002**, 41, 4176.

[46] M. Iglesias, O. Schuster, M. Albrecht, *Tetrahedron Letters* **2010**, 51, 5423.

[47] M. Sosnowski, L. Skulski, Molecules **2005**, 10, 401.

[48] J.P. Wolfe, S. Wagaw, J.-F. Marcoux, S. L. Buchwald, *Acc. Chem. Res*. **1998**, 31, 805.

[49] J.F. Hartwig, *Acc. Chem. Res.* **1998**, 31, 852.

[50] S. Roquet, A. Cravino, P. Leriche, O. Alévêque, P. Frere, J. Roncali, *JACS Articles* **2006**, 128, 3461.

[51] C.-H. Yang, W.-C. Lin, T.-L. Wanga, Y.-T. Shieha, W.-J. Chena, S.-H. Liaoa, Y.-K. Suna, *Materials Chemistry and Physics* **2011**, 130, 638.

[52] M. Pope, C.E. Swenberg, 'Electronic Processes in Organic Crystals and Polymers', *Oxford University Press*, Oxford, 1999.

[53] P. Shen, X. Liu, S. Jiang, Y. Huang, L. Yi, B. Zhao, S. Tan, *Organic Electronics* **2011**, 12, 1997.

[54] N. G. Connelly, W. E. Geiger, Chem. Rev. **1996**, 96, 877.

[55] P. Atkins, J.D. Paula, 'Atkin's Physical Chemistry', *Oxford University Press*, Oxford, 2006.

[56] A. Hagfeldtt, M. Grätzel, *Chem. Rev.* **1995**, 95, 61.

[57] K. Hara, T. Sato, K. Ryuzi, A. Furube, Y. Ohga, A. Shinpo, S. Suga, K. Sayama, H. Sugihara, H. Arakawa, *J. Phys. Chem.* **2003**, 107, 602.

[58] A.C. Onicha, K. Panthi, T.H. Kinstle, F. N. Castellano, Journal of Photochemistry and Photobiology A **2011**, 223, 57.

[59]   J.Y. Kim, A.J. Bard, *Chemical Physics Letters* **2004**, 383, 11.

[60]   B.-K. An, R. Mulherin, B. Langley, P. Burn, P. Meredith, *Organic Electronics* **2009**, 10, 1356.

[61]   R. Chen, G. Zhao, X. Yang, X. Jiang, J. Liu, H. Tian, Y. Gao, X. Liu, K. Han, M. Sun, L.J. Sun, J. *Mol. Struct.* **2008**, 876, 102.

[62]   H. Tian, X. Yang, R. Chen, R. Zhang, A. Hagfeldt, L. Sun, *J. Phys. Chem*. **2008**, 112, 11023.

[63]   T. Ono, T. Yamaguchi, H. Arakawa, *J. Sol. Energ. Eng*. **2010**, 132, 21101.

[64]   S. Kajiyama, Y. Uemura, H. Miura, K. Hara, N. Koumura, *Dyes and Pigments* **2012**, 92,1250.

[65]   Y.S. Ho, G. McKay, *Process Biochemistry* **1999**, 34, 451.

[66]   J. Fan, W. Cai, J. Yu, *Chem. Asian J.* **2011**, 6, 2481.